To the Graduate Council:

I an submitting herewith a dissertation written by Paul A. Westbrook entitled "Deformation of Glassy Polymers." I have examined the final copy of this dissertation for form and content and recommend that it be accepted in partial fulfillment of the requirements for the degree of Doctor of Philosophy, with a major in Polymer Engineering.

John F. Fellers

John F. Fellers, Major Professor

We have read this dissertation
and recommend its acceptance:

J E. Spruiell

Walter F. Jones

Jan-Chyong Lin

Edward S. Clark

Accepted for the Council:

C W Minkel

Vice Provost
and Dean of the Graduate School

DEFORMATION OF GLASSY POLYMERS

A Dissertation

Presented for the

Doctor of Philosophy

Degree

The University of Tennessee, Knoxville

Paul A. Westbrook

August 1985

To Margaret

ACKNOWLEDGEMENT

The author wishes to express appreciation to his major professor, Dr. J. F. Fellers, for his help during the course of this work. Dr. J. S. Lin was also an extremely helpful consultant concerning the operation of the National Center for Small-Angle Scattering Research equipment, and small-angle x-ray scattering data analysis.

The author appreciates the financial support given him by The Department of Materials Science, The Polymer and Textiles Research Association, The National Science Foundation and E. I. duPont de Nemours.

Characterized samples were graciously provided by Dow Chemical Company, The Bayer Company of Germany, General Electric and The Union Carbide Corporation.

The author appreciates discussions with fellow students, especially those who participated in small-angle scattering research during the course of this study: Dr. M. Y. Tang, J. S. Lee, G. C. Rice, and D. E. Warner. Further, the technical help provided by the departmental machine and electronic shops, and the departmental office.

Finally, the author thanks his committee, Professors J. F. Fellers, J. E. Spruiell, E. S. Clark, J. S. Lin and W. F. Jones.

ABSTRACT

Two aspects of the mechanical deformation of polymers in the glassy state are investigated in this dissertation. The glassy polymers investigated in this work include polystyrene, polycarbonate, poly(methyl methacrylate) and polysulfone, with several different molecular weights of the polycarbonate and polysulfone.

First, stress relaxation is modelled using a nonlinear viscoelastic constitutive equation which is based upon the Williams and Watts relaxation element. The resulting four-constant model is shown to fit the relaxation behavior of these materials over several orders of magnitude in time. Thus the stress-strain behavior of glassy polymers can be described with constant material parameters for several deformation kinematics. The material parameters which govern the time dependent character of the mechanical deformation are tau and n. The classical interpretation for tau, being a relaxation time, is valid in this analysis. However, n is an exponent acting on the time variable and accounts for what has previously been treated as a spectrum of relaxation times. The magnitude of log(tau[minutes]) is shown to be in the range of six to thirty, and generally increases with molecular weight parameters and decreases with temperature. Conversely, the magnitude of n is shown to be in the range of 0.02 to 0.2, and generally decreases with molecular weight parameters and increases with temperature. The behavior of n can be correlated to some behavioral aspects of the glass. For example materials with relatively high impact resistance display lower values of n, while

materials which exhibit more active creep behavior have higher values for n. Thus an understanding of n from a conceptual viewpoint may provide an important link between structure and properties of a deformed glass.

Second, a small-angle x-ray scattering study of the crazing phenomenon in glassy polymers is performed. It is reported that the crazed matter of polycarbonates contains comparatively fewer crack-like defects and less void fraction than the crazed matter of polystyrene. Polysulfone and poly(methyl methacrylate) show intermediate behavior. Therefore the polycarbonate crazes contain more stress supporting microfibrils. These observations are proposed to account for the observed superior ultimate mechanical properties exhibited by the polycarbonates.

TABLE OF CONTENTS

LIST OF TABLES

TABLE PAGE

LIST OF FIGURES

FIGURE PAGE

FIGURE PAGE

LIST OF SYMBOLS

Chapter II

English

a	Instantaneous deformation fit parameter.
E	Young's modulus.
L	Gauge length of deforming material.
N	Reduced Deborah Number.
t	Laboratory time boundary condition.
t'	Laboratory time integration variable.
T	Dimensionless time boundary condition.
T'	Dimensionless time integration variable.
Y	Yield stress.

Greek

δ_{ij}	Kroneker delta.
$\varepsilon, \varepsilon_i, \varepsilon_y$	Strain, Initial strain, Yield strain.
$\dot{\varepsilon}$	Strain rate.
η	Viscosity.
θ	Elastic-viscoelastic transition stress.
σ_{ij}, σ	Rheological tensile stress.
σ^o	Instantaneous rheological stress.
σ_i	Initial rheological stress.
τ_{ij}	Total stress.
τ	Relaxation time constant.

Chapter III

English

A	Area of craze.
D	Hausdorff dimension.
D_f	Diameter of fibrils.
$\mathfrak{F}$	Fourier transform.
G	Surface correlation function.
I,i	Scattered intensity.
i_a	Anomalous scattered intensity.
J_1	Bessel function of order one.
K_v,K_s	Volume and surface invariant.
l_c	Width of craze.
l	Volume correlation distance.
N_c	Number of crazes.
P	Incident x-ray power.
q,q_o	Components of wave vectors perpendicular to the surface.
r	Electron fluctuation distance.
$\vec{r}_p$	Position vector.
$\vec{s}$	Scattering vector.
t	time.
T_m	Transmission coefficient.
V_f	Volume fraction of fibrils.
W_v	Volume fraction of voids in sample.

Greek

γ	Volume correlation function.
η_{12}	Difference in index of refraction between interfaces.
θ	Scattering angle.
λ	Wavelength of electromagnetic radiation.
μ	Linear absorption coefficient.
$\Delta\rho$	Electron density difference between phases.
τ	Surface correlation distance.
$\phi, \hat{\phi_o}$	Polar angles.
χ	Azimuthal angle.
Ω	Solid scattering angle.

CHAPTER I

INTRODUCTION

Glassy polymers are an important class of engineering resins whose applications span a wide market. The utility of these materials is a result of their high modulus and ultimate strength at room temperature as well as optical quality and relatively low cost. Four major resins in this class include polystyrene, poly(methyl methacrylate), polycarbonate and polysulfone. These materials are easily processed by melt and foam extrusion, injection molding and thermoforming.

The nature of these glasses, being non-crystal forming and having a high softening temperature, is a result of the chemical structure of the repeat unit of the polymer. Typically they have large, bulky side groups and/or non-flexible main chains which inhibit stereoregular packing and low temperature mobility. The chemical repeat monomers for the polymers studied in the present work are given in Figure 1.1. Polystyrene and poly(methyl methacrylate) are polymerized by addition, whereas polycarbonate and polysulfone (also a polycarbonate) are polymerized by condensation.

Applications for polystyrene range from simple household items to more sophisticated engineering products. Injection molded products emphasize disposable serviceware. Consumer electronics such as audio/visual equipment represent a growing market. Foam extrusion in the area of packaging includes egg cartons and meat trays, as well as

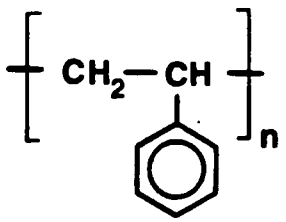

Polystyrene

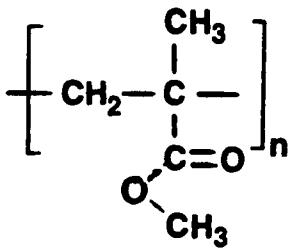

Poly(methyl methacrylate)

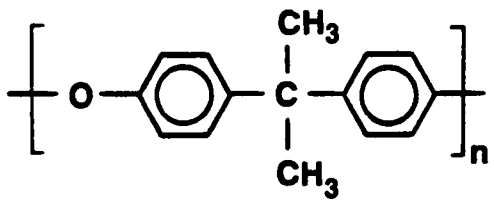

Polycarbonate

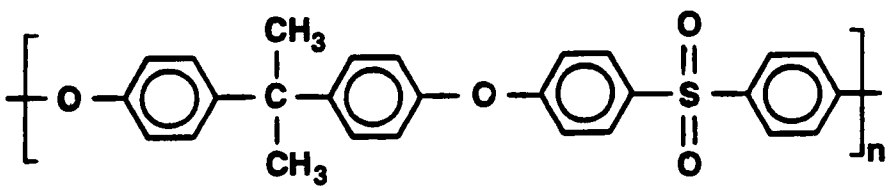

Polysulfone

Figure 1.1 Chemical repeat units for the polymer glasses used in this work.

applications for thermal insulation. The superior optical transmittance of poly(methyl methacrylate) gives it numerous applications for lighting fixtures. Automobile, marine and aviation uses include instrument panels, lenses, mirrors, canopies and windows. The impact properties of polycarbonate meet crash requirements for automotive instrument panels. In construction it is used for door and window components as well as hardware fixtures such as tubing connectors and filter housings. Polysulfone's high glass transition temperature gives it wide applicability in medical instrumentation and trays to hold objects during sterilization. FDA approval allows it to be used in food handling applications, microwave dinnerware and beverage dispensers. Glassy polymers have also seen applications in composites and blends. For example, fiber reinforced polycarbonate is used in football and motorcycle helmets. The impact resistance of polystyrene can be greatly enhanced by the addition of rubber; this material is commonly used in toys.

Because of their commercial importance as engineering thermoplastics, it is very important to understand the mechanical performance characteristics of glassy polymers. These materials are interesting in that they can deform in a variety of modes. Under proper conditions, they can deform homogeneously or inhomogeneously in the form of macroscopic necking and shear banding, or microscopic crazing. In practice, these materials are rarely applied in situations where loading exceeds the macroscopic yielding stress, and there are adequate predictive yield criteria to design against this

kind of failure. Crazing can often occur in a part which has not otherwise failed.

Crazing is a microscopic deformation phenomenon which is subject to fatigue. Crazing (or stress whitening) can be detrimental because the optical quality of the part is lost. Further, the cracks which ultimately fail the part initiate and propagate through crazed matter. Thus the ultimate properties of the glass depend heavily on the morphology of the craze.

The deformation behavior of glassy polymers is often modelled by Hooke's law which is time independent. But the fatigue problem referred to above also manifests itself in mechanical stress relaxation or creep. These time dependent effects may become more pronounced at elevated temperatures. Thus, under prolonged exposure to stress, a glass may irreversibly deform out of the original design specification.

Therefore, in order to improve engineering designs for a part made from a polymer glass for application in an adverse stress or thermal environment, it is necessary to better understand the time dependent mechanical deformation behavior and the craze morphology of these materials. In Chapter II the glassy materials are theoretically treated as homogeneously deforming solids, and a new nonlinear viscoelastic constitutive equation is used to describe the stress strain behavior in various kinematics. Chapter III deals with the inhomogeneous deformation crazing behavior of these materials. The morphology of crazes is studied using small-angle x-ray scattering,

with the goal of a better understanding of why different polymer glasses exhibit various ultimate properties. Chapter IV summarizes the conclusions obtained from the present work, and puts the results into perspective such that recommendations can be made for further study in this field.

CHAPTER II

MODELLING OF DEFORMATION BEHAVIOR IN THE GLASSY STATE

2.2. Introduction to Glassy Deformation

The mechanical deformation of high modulus materials is very often described by the generalized Hooke's Law. This linear relationship between stress and strain provides a simple constitutive equation which is used to solve many solid mechanics problems in closed form. Moreover, Hooke's law may be a good approximation to observed deformation behavior, especially under conditions of moderate to high rates of strain. Thus Hooke's law enjoys wide utility for these applications.

However, Hookean deformation behavior is not observed in all solid materials. Nonlinear deformation may result as a strain softening and/or a stress relaxation phenomenon. The latter effect is amplified under conditions of slow deformation. Although generally regarded as high modulus solids, noncrystalline polymers in the glassy state are examples of materials exhibiting such behavior. Their loss component of the dynamic modulus is large enough to allow stress relaxation to occur. Consequently, a large deviation from Hooke's law may be observed over time.

Considering that actual product applications may involve stress histories of extended duration, the ability to model such non-Hookean solid deformation is of great importance. Under such conditions, nonlinear deformation behavior becomes more pronounced even for the

most brittle of polymers. Therefore, a viscoelastic model for long term solid deformation must be employed as a constitutive relationship.

The following chapter will briefly discuss some previous efforts to describe nonlinear deformation. This discussion is not meant to be an exhaustive review of the literature, but to justify a new approach to solid deformation. Then a new nonlinear viscoelastic model suitable for describing the stress-strain behavior of noncrystalline polymers in the glassy state will be proposed. Material parameters based on the model will be measured for several polymers. The model will then be demonstrated for simplified kinematics in one dimensional deformation. Finally, correlations between rheological parameters, thermal conditions and material parameters such as molecular weight and entanglement molecular weight will be made.

2.2. Background and Theory of Constitutive Equations

The state of stress in a polymeric material depends upon both the state of strain and the strain history. Polymers are thus termed viscoelastic because, phenomenologically, their deformation behavior lies between that of a classical elastic solid (Hookean) and a classical viscous liquid (Newtonian). This complex deformation behavior has precipitated one of the basic problems in rheology, that is, to describe the relationship between stress, strain and time in a deforming viscoelastic material (2-1). These relationships are called

constitutive equations, and they are usually based on some kind of physical model.

To describe the time dependent deformation behavior of glassy polymers, a nonlinear viscoelastic model is required as a constitutive equation. In this section a brief justification for a new approach to solid state viscoelasticity is offered. A detailed description and analysis for a new approach to a nonlinear Maxwell element follows. Finally, a brief discussion of the applications and limitations of the proposed model is given.

The classical treatment of viscoelasticity assumes a general constitutive equation in which the total stress is divided into the hydrostatic and deviatoric stresses

$$\tau_{ij} = -p\delta_{ij} + \sigma_{ij} \qquad 2.1$$

where "p" is determined from the boundary conditions. The deviatoric stress (σ_{ij}) is associated with material deformation and must be modelled from the kinematics. To formulate a physically meaningful relationship for the deviatoric stress, many treatments begin by using a Maxwell Model (2-2) which consists of a spring and dashpot connected in series. The governing differential equation for this type of model in elongation is:

$$\sigma + \tau\frac{d\sigma}{dt} = E\tau\dot{\varepsilon}(t) \qquad 2.2$$

where σ is the tensile stress, and E is Young's modulus. Commonly, this equation is integrated using the Boltzman superposition principle (2-3) to obtain an explicit expression for stress. This integration assumes that the total strain can be represented as a series of infinitesimal strains which are linearly additive and mathematically independent.

$$\sigma(t) = \int_{-\infty}^{t} E\dot{\varepsilon}(t')\exp(-(t-t')/\tau)dt' \qquad 2.3$$

The function for strain rate ($\dot{\varepsilon}(t')$) is defined by the kinematics. The shortfall of such a formulation is that it is a linear model in strain and time, while observed mechanical behavior is nonlinear.

Historically, sophisticated viscoelastic models have been proposed which are perturbations of the simple spring and dashpot model. There are three classes of such perturbations: namely, using nonlinear time derivatives in the differential model, using a nonlinear function for the relaxation time constant (τ), or using a more complicated linear combination of Maxwell or Voight (parallel) elements. Thus, nonlinear viscoelastic theory is well developed.

Generally, nonlinear viscoelastic models have been developed to describe the flow of polymer melts or solutions under large strains. They meet with varying success in predicting the unusual properties of non-Newtonian fluids. For the example of differential models, the convected time derivatives of Zaremba (2-4) and Oldroyd (2-5) as well as other generalizations (2-6 through 2-9) allow for the translation,

rotation and deformation of material coordinates relative to the observer. Thus material and not absolute strains are considered.

Integral theories extend the Boltzman Principle (2-3) for large strains. Typically these theories (2-5,2-6,2-10 through 2-14) make use of a memory function which consists of a summation of exponential decay terms which become active at various times. Each memory function thus has its own characteristic spectrum of relaxation time constants. A material which possesses a spectrum of relaxation time constants can be justified by the shear thinning effect of polymeric fluids. For example, the degree of molecular orientation causes viscosity ($E \cdot \tau$) to be directionally dependent.

Unfortunately, these efforts seem unsuitable for modelling the deformation of glassy polymers. That is to say, prefracture strains in polymeric glasses are typically less than ten percent such that nonlinear strain tensors and convected coordinate systems are unnecessary. Also, well annealed glasses contain uniform molecular configuration which lessens the need for multiple relaxation constants. Further, it is experimentally difficult to determine a large number of rheological parameters for a material. Thus it seems that existing viscoelastic theory is not suitable for the modelling of solid state deformation.

Earlier attempts to describe the nonlinear deformation behavior of polymeric solids predominately employed some form of plasticity theory rather than the viscoelastic models as outlined above. These developments may have resulted from the inability of existing

viscoelastic theory to describe nonlinear behavior at small strains. Further, the ability to use the principles of birefringence and the stress optical law (2-15) in transparent materials led naturally to studies of plasticity. Polycarbonate was used primarily as the model photoelastic-plastic material for these studies (2-16,2-17,2-18). These incremental theories generally used some form of a plastic potential function which is considered analogous to the strain energy functions used for elastomeric materials (2-19). The major disadvantage of these plasticity theories alone is that they have no mechanism to describe the rate effects of deformation. Therefore, the results were limited to constant deformation rates. Plasticity theories are also well developed, and a more detailed discussion of them can be found elsewhere (2-20).

In order to incorporate rate effects, there have been some attempts to characterize solid deformation behavior utilizing a combination of both plasticity and viscoelasticity theory (2-21,2-22,2-23). Typically these attempts to unify two theories result in a superposition of the two effects. Usually a linear viscoelastic model for creep is employed. As indicated above, the linear theory is not adequate.

Brinson has also extensively studied the inelastic deformation behavior of glassy polymers (2-24 through 2-28). Brinson however, was the first to solely employ a viscoelastic model to fit deformation behavior of polycarbonate (2-27,2-28). Apparently motivated by Reiner (2-29), Brinson used a modified Bingham model which is a linear

viscoelastic-plastic constitutive equation, and is described by four material constants: a modulus (E), an elastic-viscoelastic transition stress (theta), a viscoelastic-plastic transition stress (Y), and a viscosity (mu). Brinson denotes the value of "Y" as the yield stress of the material. Mathematically, the differential model which Brinson (2-27,2-28) used can be expressed as:

$$\begin{aligned} \sigma &= E\varepsilon \\ \mu &= E\tau \\ (\sigma - \Theta) + \frac{\mu d\sigma}{E dt} &= \mu\varepsilon(t) \end{aligned} \qquad 2.4$$

Using this model, Brinson was able to fit individual stress-strain curves for polycarbonate quite well, but various deformation rates required different rheological parameters. This difficulty is again a result of the application of a linear viscoelastic theory. Brinson himself disclaims, "To obtain a single equation representative of all (rate dependent) strain data would require the use of multiple elements to provide a spectrum of relaxation times. (2-27)" He further correlates the observed yield stress "Y" to the initial strain rate of the material using an empirical logarithmic fit (2-27,2-28).

More recently, Brinson (2-30) has investigated the nonlinear viscoelastic behavior of composite materials with the goal of developing accelerated mechanical tests using shift factors and the superposition principle. He employed a nonlinear method due to Schapery (2-31,2-32) which was developed using irreversible

thermodynamics. For the case of uniaxial loading at constant temperature for an isotropic homogeneous nonlinearly elastic material, Schapery's theory reduces to the following:

$$\varepsilon(t) = g_0 D_0 \sigma + g_1 \int_0^t D'(\psi - \psi') \frac{d(g_2\sigma)}{dt} dt \qquad 2.5$$

This constitutive model is remarkably similar in form to the single Maxwell element integral model where g_0, g_1 and g_2 are nonlinearizing stress parameters and ψ and ψ' are shift factors. The major difference is that here one integrates over the stress history to obtain the strain instead of vice-versa. Brinson (2-30) illustrates how this model can be used to predict long term mechanical performance at low temperatures using accelerated testing at elevated temperatures.

A different and simple approach to nonlinear viscoelasticity was given by Matsuoka (2-33). He applied the Williams- Watts (3-30) relaxation element to describe the relaxation behavior of polymeric solids in tension, shear and compression. This approach can be summarized mathematically as the following:

$$\sigma = E(t)\varepsilon$$
$$E(t) = E_0 \exp(-(t/\tau)^{\beta}) \qquad 2.6$$

where beta is a factor which ranges between zero and one and accounts for a spectrum of relaxation time constants. When beta equals one

there exists only one characteristic relaxation time, tau; but as beta approaches zero the effective relaxation time spectrum becomes broader. This approach is novel to viscoelasticity; however, these types of nonlinear relaxation elements have enjoyed success in modelling dielectric, magnetic as well as other types of relaxation in materials (2-34,2-37 through 2-42). Matsuoka found for mechanical stress relaxation in polymers, that both tau and beta are functions of temperature and that tau scales with an Arrhenius type equation (2-33,2-35). The use of this type of relaxation element for solid state viscoelasticity seems appropriate. It defines a simple usable framework to describe complex behavior. However this application of the Williams-Watts theory is limited in its empericism. That is, a fundamental constitutive equation based on a physical model from which stress-strain relationships can be calculated for diverse deformation kinematics has yet to be developed. For example, the stress relaxation element of Matsuoka (2-33) would be one solution to a generalized theory, while the theory would be capable of handling more complicated kinematics by formulating other solutions. A development and demonstration of such a theory will be the subject of the remainder of this chapter.

It now seems clear that to describe the rate dependent deformation behavior of glassy polymers, some form of viscoelastic model is necessary. It is also evident that simple linear theories do not adequately model the relaxation processes which are active in a material under load. Further, the classical attempts at

nonlinearization of viscoelastic theory are either not applicable to small strain systems or are cumbersome to apply in practice. Therefore, a new approach to nonlinear viscoelastic theory for the application to solid state rate dependent deformation is needed.

Since models based on the Maxwell element are widely understood, it is desirable to construct new constitutive relations within that general framework. The proposed formulation incorporates a nonlinear strain softening function in the elastic element as well as a nonlinear time derivative in the viscous element of a single Maxwell construction. Consider Equations 2.7a and 2.7b.

$$\sigma = E(\varepsilon)\varepsilon \qquad 2.7a$$

$$\sigma = E(\varepsilon)\tau\frac{d\varepsilon}{dt}\left[\frac{1}{\tau}\frac{dt}{dT}\right] \qquad 2.7b$$

Equation 2.7a is capable of describing elastic strain softening behavior by an unspecified function $E(\varepsilon)$. Similarly, Equation 2.7b describes a viscous stress relaxation behavior in terms of a nonlinear dimensionless time T(t). The time derivative in brackets is a statement of relativity which describes how the laboratory time clock (t) varies with the material time clock (T). Notice that both these generalizations are independent of the previous notions of nonlinearity because the ability to use nonlinear strain tensors and time constants is preserved. Further, complex constructions of springs and nonlinear dashpots may also be used; however, only the Maxwell construction is considered here. As yet no assumption as to

the forms of the dimensionless time function T(t) or the strain softening function E(ε) has been made; however, it is desirable that the functions be chosen such that the time derivative reduces to tau when T(t) is reduced to linearity. Likewise, the strain function E(ε) should reduce to linearity as a special case. Thus the physical interpretation to a new nonlinear Maxwell model has been defined.

The analysis of this model follows in an analogous manner to the linear Maxwell Model. By assuming that the stress in the viscous and elastic elements are equal and the strains in each element are additive to obtain the total strain, the following differential equation can be derived.

$$\sigma\left[\tau\frac{dT}{dt}\right] + \tau\frac{d\sigma}{dt} = \tau E(\varepsilon)\frac{d\varepsilon}{dt} \qquad 2.8$$

This form shows mathematically the effect of the time and strain nonlinearities on the classical Maxwell model (compare Equations 2.2 and 2.8). However, this equation can be reduced algebraically and by the chain rule of differentials to a more simplified form.

$$\sigma + \frac{d\sigma}{dT} = E(\varepsilon)\frac{d\varepsilon}{dT} \qquad 2.9$$

Equation 2.9 thus represents a generalized Maxwell model in differential form.

To use this model, a functional relationship for T(t) and $E(\varepsilon)$ is required. Further, an experimental strategy for determining material constants based on the functions is needed. Consider the simple case of stress relaxation from an instantaneous step strain at zero time. The inhomogenous term in Equation 2.9 disappears and thus enables separation and integration. Using appropriate initial conditions, the resulting relation for stress is:

$$\sigma(T) = \sigma_o \exp(-T) \qquad 2.10$$

At this be point a suitable functional form of T(t) may be proposed in Equation 2.11.

$$T = (t/\tau)^n \qquad 2.11$$

This functionality is offered for physical as well as practical reasons. First, Equations 2.10 and 2.11 taken together define the Williams-Watts (2-36) equation which has met with considerable success in modelling diverse dissipation phenomena which occur in materials (2-37 through 2-42). Equations 2.10 and 2.12 taken together are the exact form of Matsuoka's nonlinear modulus relaxation element, where his beta has been replaced by n. This substitution was performed because the exponential factor in the work of Rendell, and Ngai is called n. Moreover, the constants tau and n have been given physical significance by some authors (2-37 through 2-42). Second,

Equation 2.11 defines a simple two constant nonlinear function which facilitates data fitting and material parameter determination. Lastly, as the exponent approaches unity, the generalized viscous element reduces to the linear case. Thus, a usable functional form of T(t) has been defined in Equation 2.11.

Likewise, a logical functional relationship for $E(\varepsilon)$ must be obtained. Consider the simple case of instantaneous deformation. Here the linear stress dependence of Equation 2.9 disappears such that subsequent integration yields Equation 2.7a. Here, a simple nonlinear function is proposed to fit the instantaneous elastic deformation in the following equation.

$$\sigma(\varepsilon) = E(\varepsilon)\varepsilon \qquad 2.12$$
$$E(\varepsilon) = E^{o}\cos^{2}(a\varepsilon)$$

Again, this function is proposed for practical reasons. Although it has no physical basis, this empiricism has qualitatively the correct strain dependence. Further, Equation 2.12 defines a simple two constant nonlinear model. At this point the author wishes to point out that it is probably more suitable to utilize one of the more classical plasticity theories to describe the instantaneous deformation of the material instead of Equation 2.12. While a plasticity analysis would be more elegant, a nonlinear elastic analysis remains attractive for reasons of simplicity. Furthermore, it is the primary purpose of this work to demonstrate the rate (time) effects of the proposed generalized Maxwell Model, for which

Equation 2.12 plays no part. Therefore, we now have a usable format for implementing a generalized Maxwell model for solid state deformation in terms of arbitrarily chosen nonlinear functions for strain and time.

It is now desirable to test the proposed model under dynamic kinematics. If more complex kinematics are under consideration, it is often desirable to integrate the Maxwell model (Equation 2.9). By variation of parameters and application of the Boltzman superposition principle, the resulting integral equation can be expressed as:

$$\sigma(T') = \int_{-\infty}^{T} E(\varepsilon)\dot{\varepsilon}(T')\exp(T'-T)dT' \qquad 2.13$$

Where T' is the variable of integration and T is constant. Note that Equation 2.13 can be differentiated by the Leibnitz rule (2-43) to obtain Equation 2.9. For some deformation kinematics, it may be more convenient to use strain instead of strain rate functions in the integral expression. Equation 2.13 can therefore be integrated by parts once to obtain the following integral expression in terms of strain.

$$\sigma(T') = -\int_{-\infty}^{T} E(\varepsilon)\varepsilon(T')\exp(T'-T)dT' \qquad 2.14$$

Notice that conversion of Equations 2.13 and 2.14 back to laboratory time is accomplished by substituting the appropriate function chosen in Equations 2.11 and 2.12. Equations 2.13 and 2.14 now define the

integral equations which represent a nonlinear generalized Maxwell model.

Evaluating the performance of the theoretical development discussed above requires measurement of material parameters defined in Equations 2.11 and 2.12 for simple kinematics. Then a theoretical prediction of stress in a specified strain (rate) deformation can be compared to experimental results. One experimentally convenient strain deformation is that produced in a constant elongation rate Instron tensile testing machine. The kinematics for such a deformation can be written as:

$$\dot{\varepsilon}(T') = \begin{cases} -\varepsilon_o & -\infty<T'<0 \\ -\varepsilon_o(1 - (L(T')/L(T))^n) & 0<T'<T \end{cases} \qquad 2.15$$

Therefore, the resulting theoretical relation for stress in a material undergoing constant elongation rate deformation is given by the following integral equation.

$$\sigma(T') = \int_{-\infty}^{T} \varepsilon_o E(\varepsilon)\left[1 - (L(T')/L(T))^n\right]\exp(T'-T)dT' \qquad 2.16$$

Equation 2.16 can be conveniently integrated by numerical techniques. However, one may assume for small deformations that constant elongation rate is approximately equal to constant strain rate. With such a substitution, the integral (2.13) may be evaluated in closed form resulting in the following formula for stress at any time (t).

$$\sigma(T') = \cos^2(a\varepsilon(T))\varepsilon(T)E^{\circ}\int_{-\infty}^{T}\left[1 - (T'/T)^n\right]\exp(T'-T)dT' \qquad 2.17$$

Now a method for experimental verification of theoretical performance exists.

In summary, a generalized Maxwell Model has been developed for modelling the stress-strain behavior of viscoelastic solid materials. The analysis of this model follows analogously with the linear Maxwell model. In fact, the nonlinear time contribution in the generalized Maxwell model translates into a weighting function which alters the limits of integration of the resulting integral model. The application of this model is limited to small strains and to materials which have only one stress relaxation mechanism. Further, the relaxation spectrum must be identical for all levels of stress and time for each material. Amorphous polymers in the glassy state seem likely candidates to follow such a generalized theory.

The fact that the chosen functional forms of nonlinear time and strain behavior are somewhat arbitrary adds flexibility to the generalized theory. However the important conceptual contribution resulting from this formulation is that fitted material parameters are independent of deformation kinematics.

2.3. Mechanical Deformation Experimental Procedure

The experimental campaign to evaluate the performance of the generalized Maxwell model developed above will be described in this section. Material constants for several different glassy polymers are determined by fitting Equation 2.11 to stress relaxation experiments. Subsequently, constant elongation rate tensile tests are used to compare to the theoretical predictions of Equation 2.16 using the same material parameters.

Several glassy polymers of various molecular weights were assembled for mechanical testing. The sample compositions are summarized in Table 2.1. Of special importance is the relative magnitude of the molecular weight of the polymer relative to its intrinsic entanglement molecular weight (2-44,2-45). Also, the relative glass transition temperatures of the glasses (2-46) are noted. Samples were fabricated into tensile bars (nominally 1.2 by 0.3 centimeters in cross section) by cutting from a molded sheet. The polymer sheets were molded in a flat press compression molding machine, and were cooled slowly in the mold to allow thermal stresses to be relieved. Tensile specimens were carefully polished along their cut edges to remove saw marks and surface flaws.

All tensile experiments were conducted at room temperature on a floor model TTD Instron tensile testing machine. Sample strain was measured using an Instron model G-51-11 extensiometer connected to the chart drive with servo control. Constant time intervals were recorded such that strain rates could be calculated. True stress was

Table 2.1. A summary of material parameters of glassy polymers which were used in deformation studies.

Sample	Weight Averaged Molecular Weight	Molecular Dispersity	Glass Transition Temperature	Entanglement Molecular Weight
		Polycarbonate *		
120G	23500	2.16	150 °C	2500
100G	28450	2.49	150	2500
130G	34000	2.44	150	2500
		Polystyrene		
S104	165000	1.05	100	35000
685D **	305000	1.95	100	35000
S107	390000	1.10	100	35000
		Polysulfone ***		
P1700	57000	6.48	190	2600
P3500	76000	4.78	190	2600
		Poly(methyl methacrylate) ****		
M2805	29300	2.49	105	6000

* Lexan is a trademark of The General Electric Company.
** Styron is a trademark of The Dow Chemical Company.
*** Udel is a trademark of The Union Carbide Corporation.
**** Makrolon is a trademark of The Bayer Company of Germany.

calculated by determining the sample cross sectional area reduction as a function of strain. A Poisson's ratio of 0.35 was used for these calculations. All data reduction was performed by computer using data digitized from chart paper. All materials were deformed in a rate spectrum between 0.0000508 to 0.00508 meters per minute.

Room temperature stress relaxation experiments were performed on each material at several different levels of initial stress for a duration of 100 minutes. The initial stress was generated by an "instantaneous" step in Instron cross-head separation. The limitations of such a procedure will be discussed in the next section.

Theoretical prediction of mechanical behavior based on measured material parameters was accomplished by numerical integration of Equation 2.17 using a Runge-Kutta-Fehlburg algorithm (2-52). This single step technique features a variable step size based on an error estimate. For this application the integration error is estimated as the difference between simultaneous determination of a second and third order approximation.

2.4. Mechanical Modelling Results

The experimental results from mechanical testing of glassy polymers will be presented in two categories. First, fitting of stress relaxation data to Equations 2.10 and 2.11 for the determination of material constants will be discussed. Next, evaluation of the performance of Equation 2.17 for stress-strain curves at several deformation rates will be performed.

2.4.1. Relaxation Behavior of Glassy Polymers

At this point it is useful to consider the nature of the Williams-Watts (2-36) relaxation equation (Equations 2.10 and 2.11). The combined term Tau^{-n} may be considered to be an effective rate constant for an exponential decay. This constant has fractional units depending on the value of n. The exponent n may be considered a shape factor which has a range between zero and one. Figure 2.1 shows the effect of n on the shape of the monotonic decay. It is evident that n tends to accelerate decay when time/Tau is less than unity, and decelerates decay when time/Tau is greater than unity.

The kinematics described in Equation 2.15 are experimentally impossible to achieve. Instantaneous step strains are, at best, approximated by finite deformation rates. Further, the limitations of a mechanical strip chart recorder produce overshoot when tracking rapid transients. This overshoot is caused by electrical and/or inertial effects. These transients are particularly large during onset or termination of high rates of deformation. Therefore, in stress relaxation experiments from a step strain, the initial stress is impossible to measure.

However, the two material parameters in the Williams-Watts (2-36) equation can still be solved for by considering three relaxation data points (instead of two) and determining an "apparent initial stress" as well as tau and n. Experimentally, at least five stress relaxation spectra of 100 minutes duration were performed on each material at various levels of initial stress up to approximately

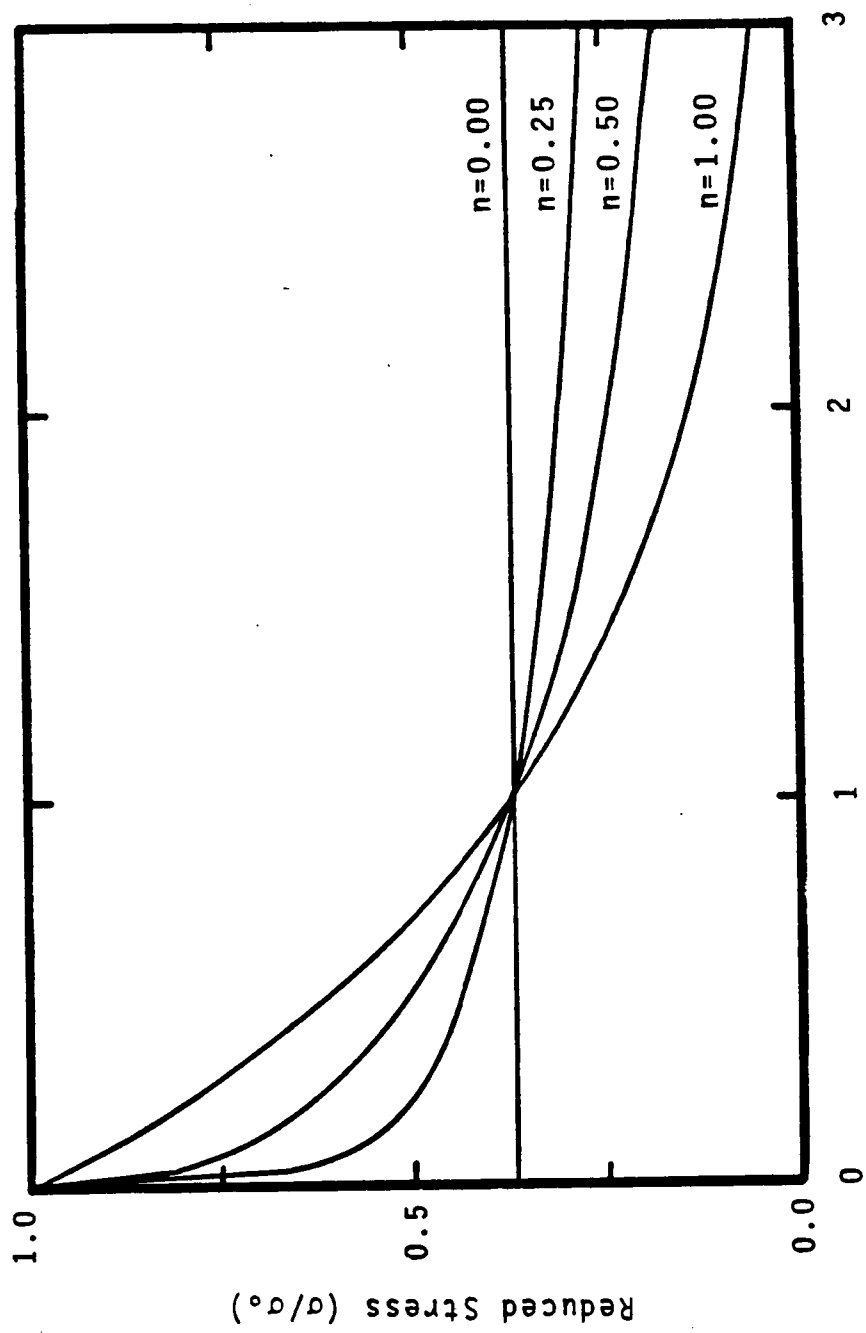

Figure 2.1. Effect of shape factor on the relaxation behavior in the Williams-Watts formulation.

90 percent of the fracture or yield stress. The relaxation behavior was normalized by the stress which occurred after 100 minutes such that comparisons can be made. It is determined that on a percentage basis the stress relaxes at the same rate over all levels of initial stress. Table 2.2 illustrates this observation for S104 polystyrene. Thus it is assumed that an average relaxation curve adequately describes the behavior of a glassy polymer during a single step stress relaxation experiment. This assumption is less applicable for materials which exhibit a macroscopic yielding behavior, especially at stresses near the yield stress. Polycarbonate showed such accelerated relaxation behavior. Since the high stress cases relaxed approximately ten percent faster than the average, no attempt was made to account for this behavior from a theoretical basis. However, the accelerated relaxation apparently results from the superposition of multiple relaxation mechanisms near the yield condition. Conceptually one may alter tau and n to be stress (or strain) dependent, but for simplicity only an averaged relaxation spectrum will be considered here.

On the other hand, no material tested exhibited zero stress relaxation at any level of applied initial stress or time. This observation implies that no finite rate deformation is linearly elastic. Independent studies (2-24 through 2-28) have modelled the initial material deformation as linearly elastic so as to fit a modified Bingham Plastic construction. The results obtained above are in sharp contrast to the work of Brinson (2-24 through 2-28) who

Table 2.2. Stress relaxation spectra for S104 polystyrene at various levels of initial stress. Data are normalized to the state of stress after 100 minutes.

	Reduced Stress ($\sigma(t)/\sigma(100)$)					
	Approximate Initial Stresses (MPa)					
Time (min)	40.8	31.8	27.0	20.7	15.9	Averaged Relaxation
0.01	1.1881	1.1851		1.1597	1.1808	1.1784
0.02	1.1799	1.1802		1.1519	1.1769	1.1721
0.05	1.1731	1.1666	1.1658	1.1472	1.1691	1.1639
0.10	1.1622	1.1565	1.1585	1.1394	1.1572	1.1542
0.20	1.1499	1.1413	1.1499	1.1333	1.1532	1.1451
0.50	1.1349	1.1229	1.1364	1.1163	1.1378	1.1291
1.00	1.1227	1.1111	1.1253	1.1070	1.1245	1.1177
2.00	1.1077	1.0993	1.1118	1.0968	1.1127	1.1052
5.00	1.0873	1.0823	1.0971	1.0806	1.0949	1.0879
10.00	1.0723	1.0656	1.0811	1.0651	1.0752	1.0715
20.00	1.0532	1.0420	1.0561	1.0279	1.0494	1.0453
50.00	1.0232	1.0235	1.0311	1.0217	1.0256	1.0250
100.00	1.0000	1.0000	1.0000	1.0000	1.0000	1.0000

modelled the initial deformation as linearly elastic. The average relaxation assumption used in the present work seems no less practical than the previously reported Bingham model assumption (2-27,2-28).

Average relaxation behavior at 20 degrees Centigrade for each material listed in Table 2.1 (page 23) was fit to the Williams-Watts (2-36) equation using data at times of 0.01, 1.00 and 100.00 minutes by a computer search algorithm. See Appendix B for details. The relaxation spectra are then renormalized to the computer generated apparent initial stress (time=0.00 min.). The results of these computer fittings are listed in Table 2.3. It is evident that the averaged relaxation spectrum is dependent on polymer type as well as molecular weight parameters. In order to attempt to construct a continuum among polymer types, Table 2.4 introduces a new variable called the reduced molecular weight (Rm). This independent variable is used for the correlation of measured rheological parameters among all the glasses studied. The reduced molecular weight is defimed as the weight averaged molecular weight divided by the entanglement moleculat weight and it describes the averaged number of physical polymer chain entanglements per molecule. Table 2.4 thus shows the fitted material parameters for each relaxation spectrum in Table 2.3. Generally speaking, the shape factor n decreases with molecular weight while tau and the effective rate constant both increase. The values reported in Table 2.4 for polycarbonate agree well with those reported by Matsuoka (2-33). The order of magnitude of tau seems greatly dependent on the polymer type.

Table 2.3. Result of Williams-Watts fit to stress relaxation spectra in glassy polymers. Data are normalized to the zero time initial stress by extrapolation of the linear fit.

	Normalized Stress ($\sigma(0)/\sigma(t)$)								
	Sample Identification								
Time	Polycarbonate			Polysulfone		Polystyrene			Poly(methyl methacrylate)
(min)	120G	100G	130G	P1700	P3500	S104	685D	S107	M2805
0.00	1.0000	1.0000	1.0000	1.0000	1.0000	1.0000	1.0000	1.0000	1.0000
0.01	0.9503	0.9092	0.8691	0.8576	0.6478	0.9531	0.9069	0.8495	0.9735
0.02	0.9462	0.9032	0.8611	0.8548	0.6425	0.9480	0.8995	0.8417	0.9721
0.05	0.9415	0.8974	0.8543	0.8493	0.6396	0.9413	0.8899	0.8303	0.9676
0.10	0.9367	0.8927	0.8517	0.8465	0.6377	0.9335	0.8810	0.8221	0.9627
0.20	0.9325	0.8866	0.8452	0.8437	0.6357	0.9261	0.8717	0.8132	0.9579
0.50	0.9248	0.8790	0.8386	0.8395	0.6315	0.9132	0.8587	0.8006	0.9502
1.00	0.9204	0.8734	0.8320	0.8381	0.6283	0.9040	0.8487	0.7906	0.9452
2.00	0.9143	0.8673	0.8286	0.8361	0.6267	0.8939	0.8374	0.7802	0.9394
5.00	0.9066	0.8599	0.8193	0.8337	0.6230	0.8799	0.8221	0.7657	0.9316
10.00	0.9005	0.8524	0.8127	0.8298	0.6199	0.8666	0.8104	0.7543	0.9267
20.00	0.8920	0.8465	0.8048	0.8275	0.6183	0.8454	0.7969	0.7424	0.9159
50.00	0.8817	0.8356	0.7948	0.8212	0.6140	0.8287	0.7772	0.7259	0.9023
100.00	0.8739	0.8249	0.7859	0.8164	0.6103	0.8088	0.7593	0.7129	0.8886

Table 2.4. A summary of material parameters obtained from fitting the stress relaxation data in Table 2.3 to the Williams-Watts equation.

Sample ID	Molecular Weight	Rm	n	Tau(min)	Tau^{-n}
			Polycarbonate		
120G	23500	9.59	0.1055	17.71E09	0.0829
100G	28500	11.63	0.0765	226.3	0.1353
130G	34000	13.88	0.0587	3048.	0.1848
			Polystyrene		
S104	165000	4.71	0.1613	1.49E06	0.1010
685D	305000	8.43	0.1125	9.50	0.1641
S107	390000	11.14	0.0792	87.28	0.2350
			Polysulfone		
P1700	57000	22.01	0.0215	1.48E27	0.2531
P3500	76000	29.34	0.0162	5.58E32	0.3012
			Poly(methyl methacrylate)		
M2805	29300	4.44	0.1607	5.92E7	0.0563

It is appropriate to examine the numerical stability of the material parameter search scheme. A study of the Williams-Watts (2-36) equation reveals that the value of tau represents the time at which the normalized stress is reduced to a value of (1.0/e) or 0.368... In this application tau represents an extreme extrapolation of the range of the data. As a result, only the order of magnitude of Tau is meaningful. The effective rate constant Tau^{-n}, however, simply corresponds to the value of a characteristic relaxation parameter ($-\ln(\sigma/\sigma_o)$) at a time of one minute. This value is within the range of the data. Thus the effective rate constant and the shape factor are numerically stable to calculate and therefore meaningful in terms of available significant figures.

The fitted relaxation curves of Table 2.3 (page 30) are plotted in Figure 2.2 for polycarbonate, Figure 2.3 for polystyrene, Figure 2.4 for polysulfone, and Figure 2.5 for poly(methyl-methacrylate). All data form straight lines on these plots of the logarithm of relaxation parameter versus the logarithm of time. The significance of such a plot is that a line of slope (shape factor) one indicates a linear dashpot element. The straightness of the fit speaks to the ability of a two constant model to fit the relaxation data. It is emphasized that Figures 2.2 through 2.5 imply that only two material parameters are sufficient to describe the stress relaxation behavior over four orders of magnitude in time.

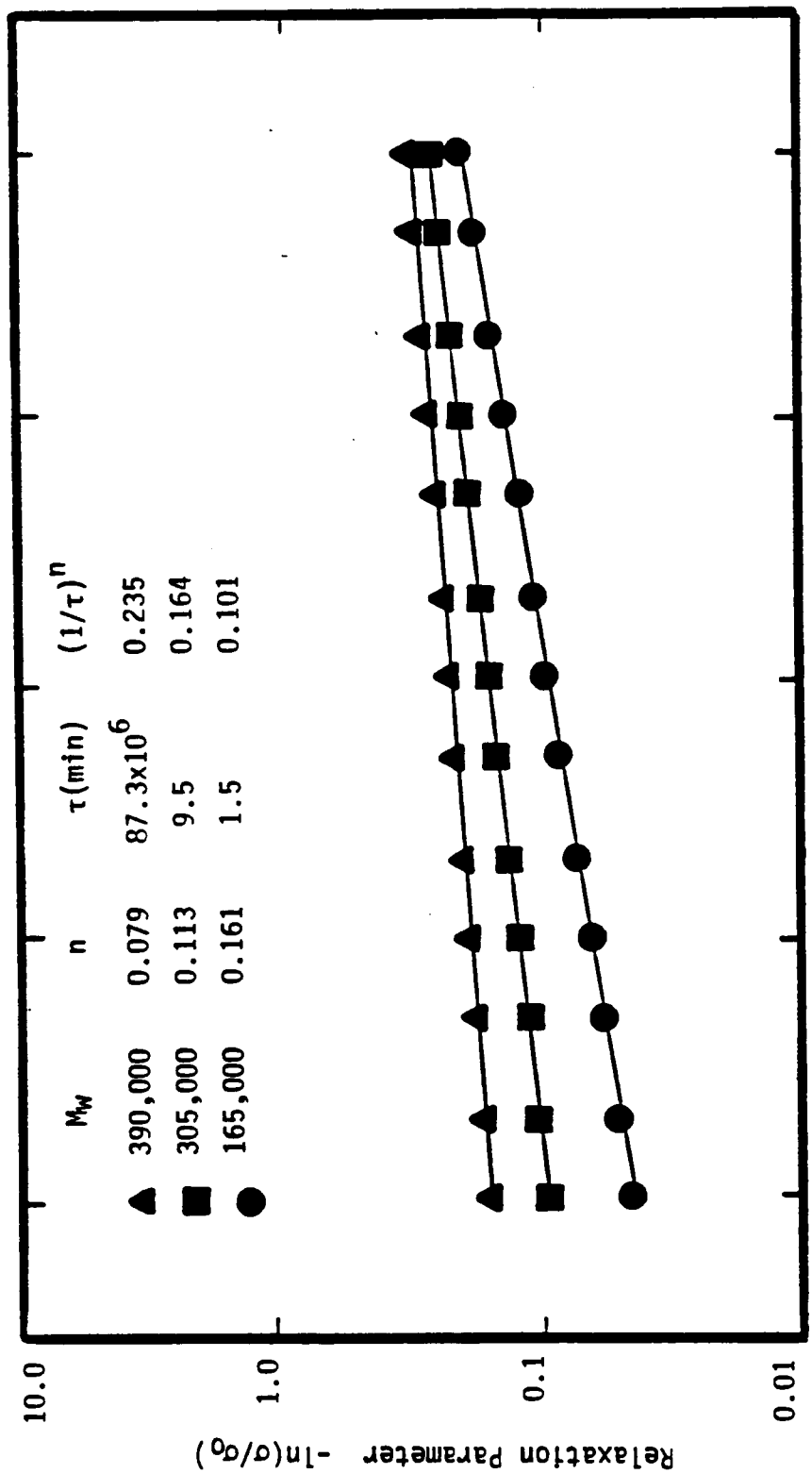

Figure 2.2. Polystyrene stress relaxation spectrum from step strain at zero time.

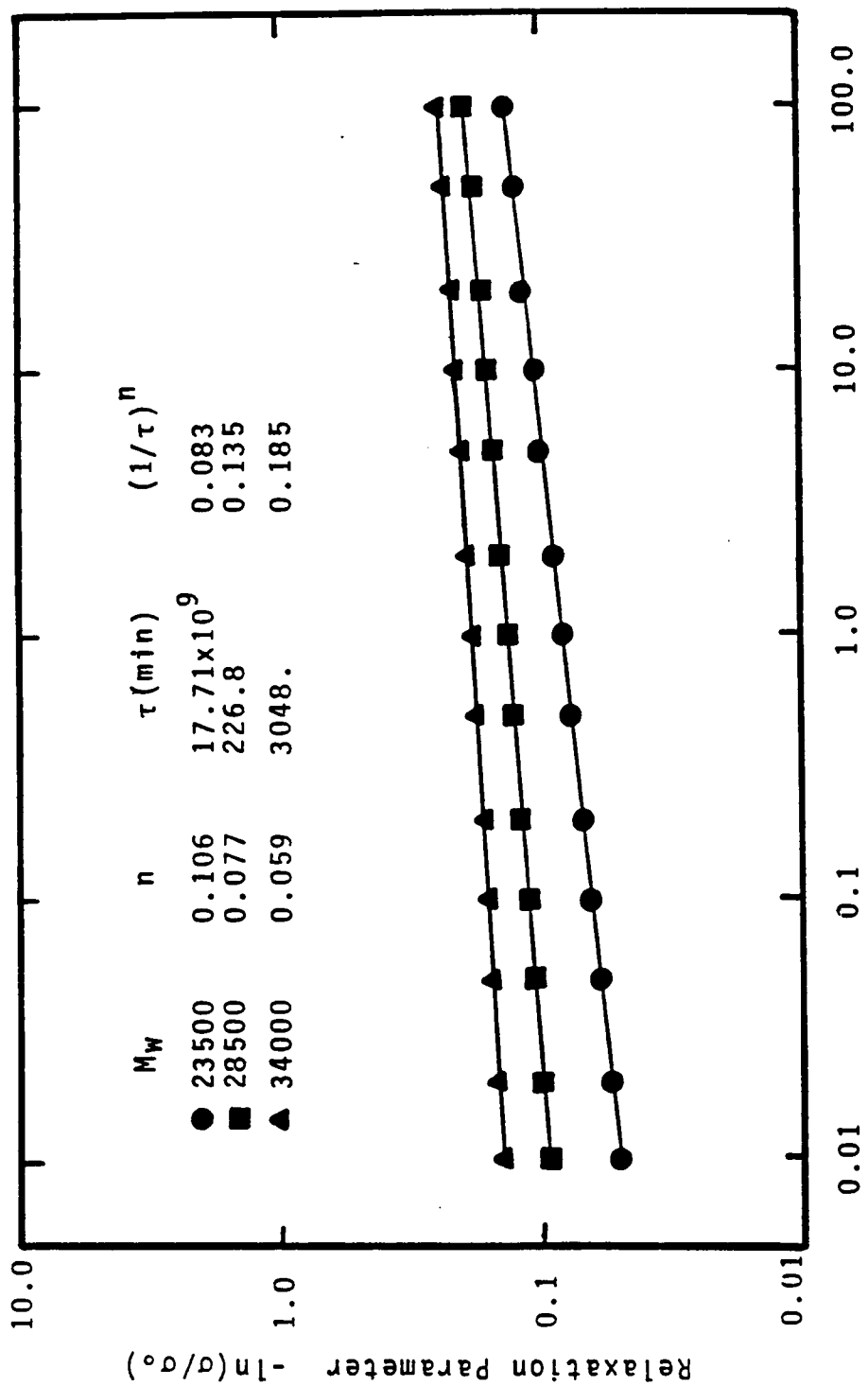

Figure 2.3. Polycarbonate stress relaxation spectrum from step strain at zero time.

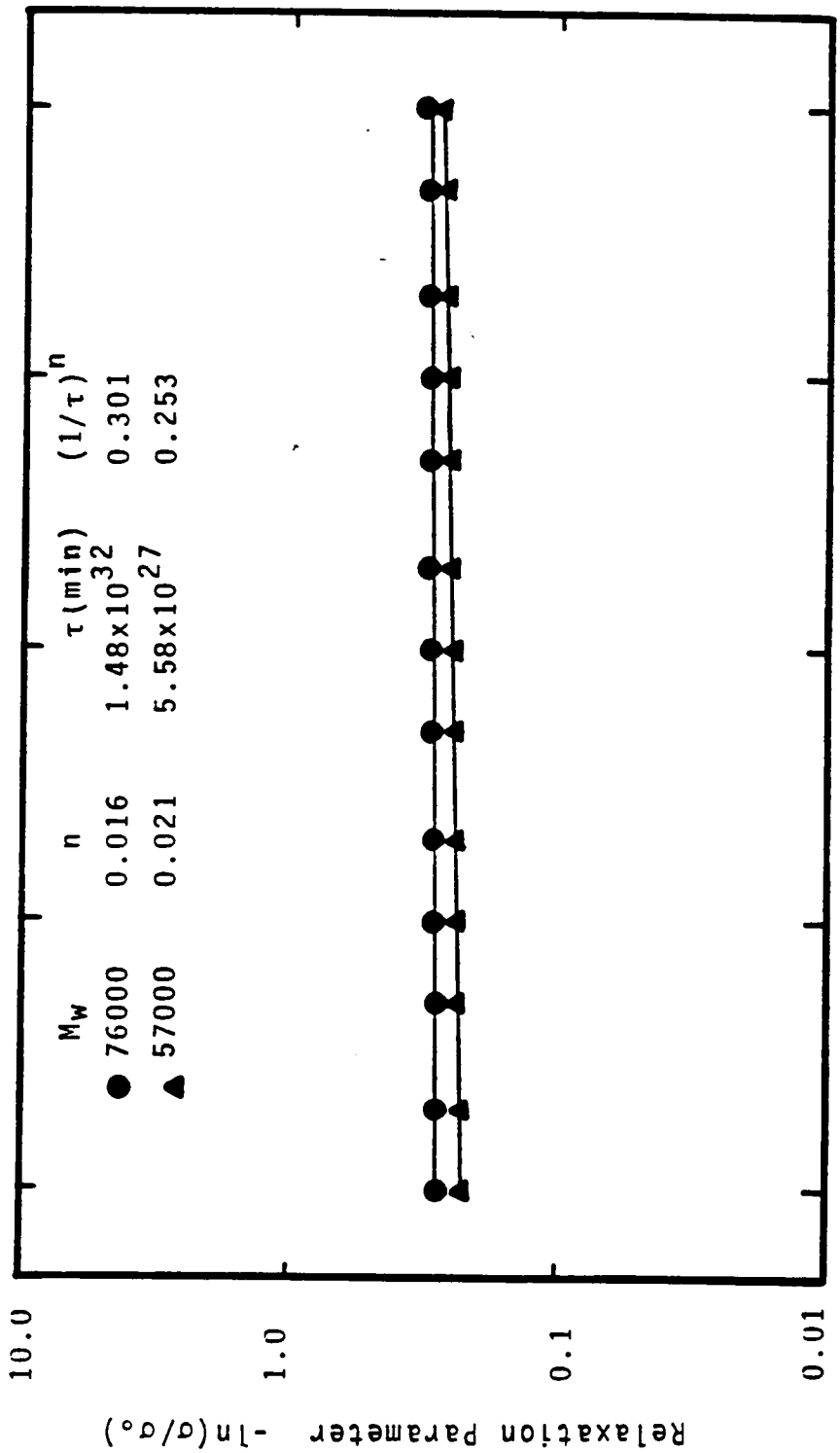

Figure 2.4. Polysulfone stress relaxation spectrum from step strain at zero time.

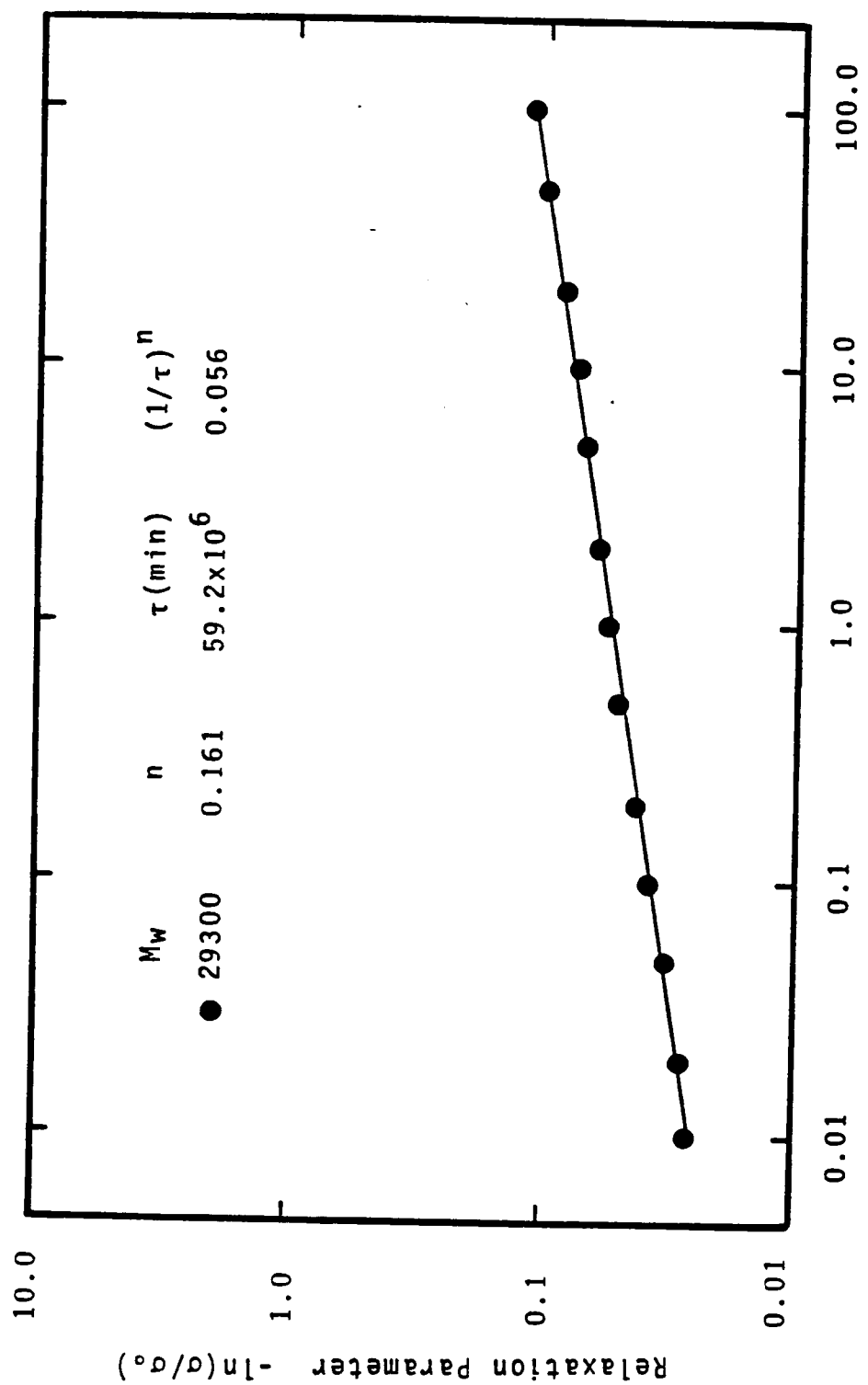

Figure 2.5. Poly(methyl methacrylate) stress relaxation spectrum from step strain at zero time.

The material parameters presented in Table 2.4 (page 31) seem to correlate best with the weight averaged molecular weight. The characteristic time constant for each material is plotted versus reduced molecular weight in Figure 2.6, while the shape factor is plotted versus molecular weight in Figure 2.7. Further, the effective rate constant is plotted versus reduced molecular weight in Figure 2.8. It is evident from these plots that correlations with molecular weight as well as temperature (relative to the glass transition) may be possible.

A study of the effect of temperature on the stress relaxation spectrum of polysulfone was performed. This material was chosen because of its high glass transition temperature and the relative ease of doing mechanical tests at elevated temperature as opposed to cryogenic tests. Figures 2.9 and 2.10 show the relaxation behavior at 20, 60, and 100 degrees Centigrade for low and high molecular weight polysulfones respectively. The dependence of the rheological parameters (tau, n, and $(1/tau)^n$) as a function of temperature are summarized in Table 2.5 and plotted in Figures 2.11, 2.12 and 2.13 respectively. It is evident that as the temperature is increased, the material parameters moderate, which results in less long term mechanical stability. That behavior is described by increased magnitude in shape factor and decreased effective rate constant as well as decreased time constant. These trends are similar to the ones reported by Matsuoka (2-33) for his studies on polycarbonate.

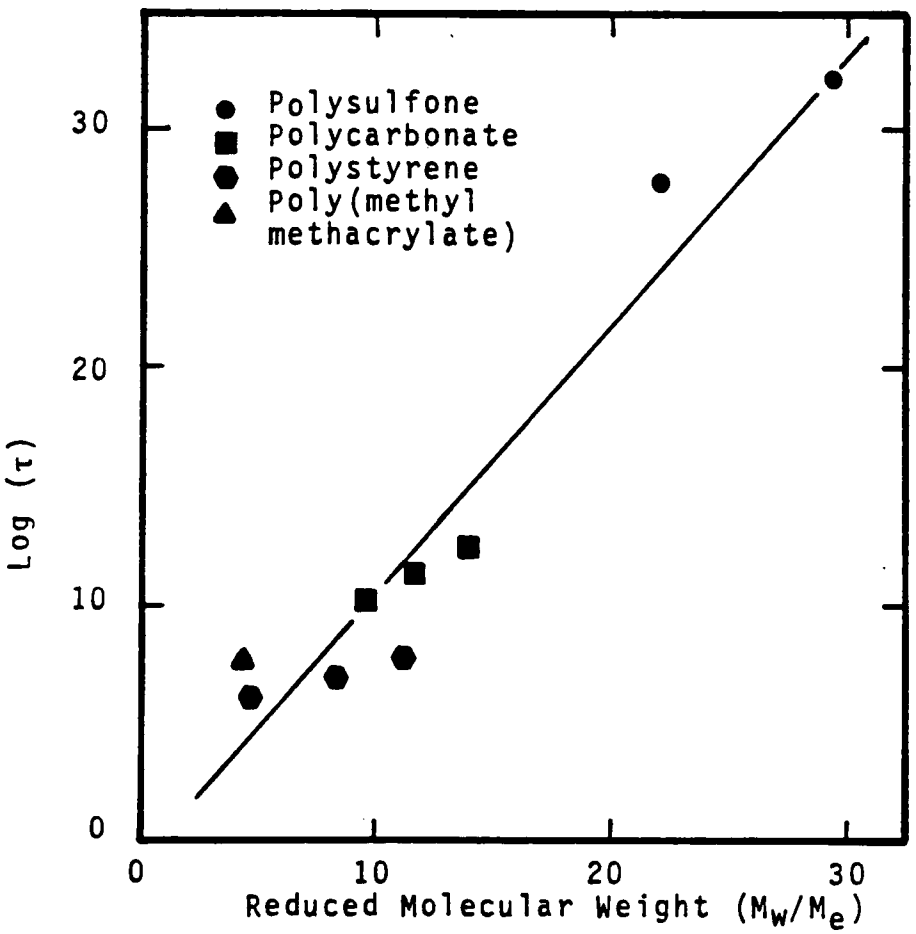

Figure 2.6. Molecular weight dependence on the material time constant.

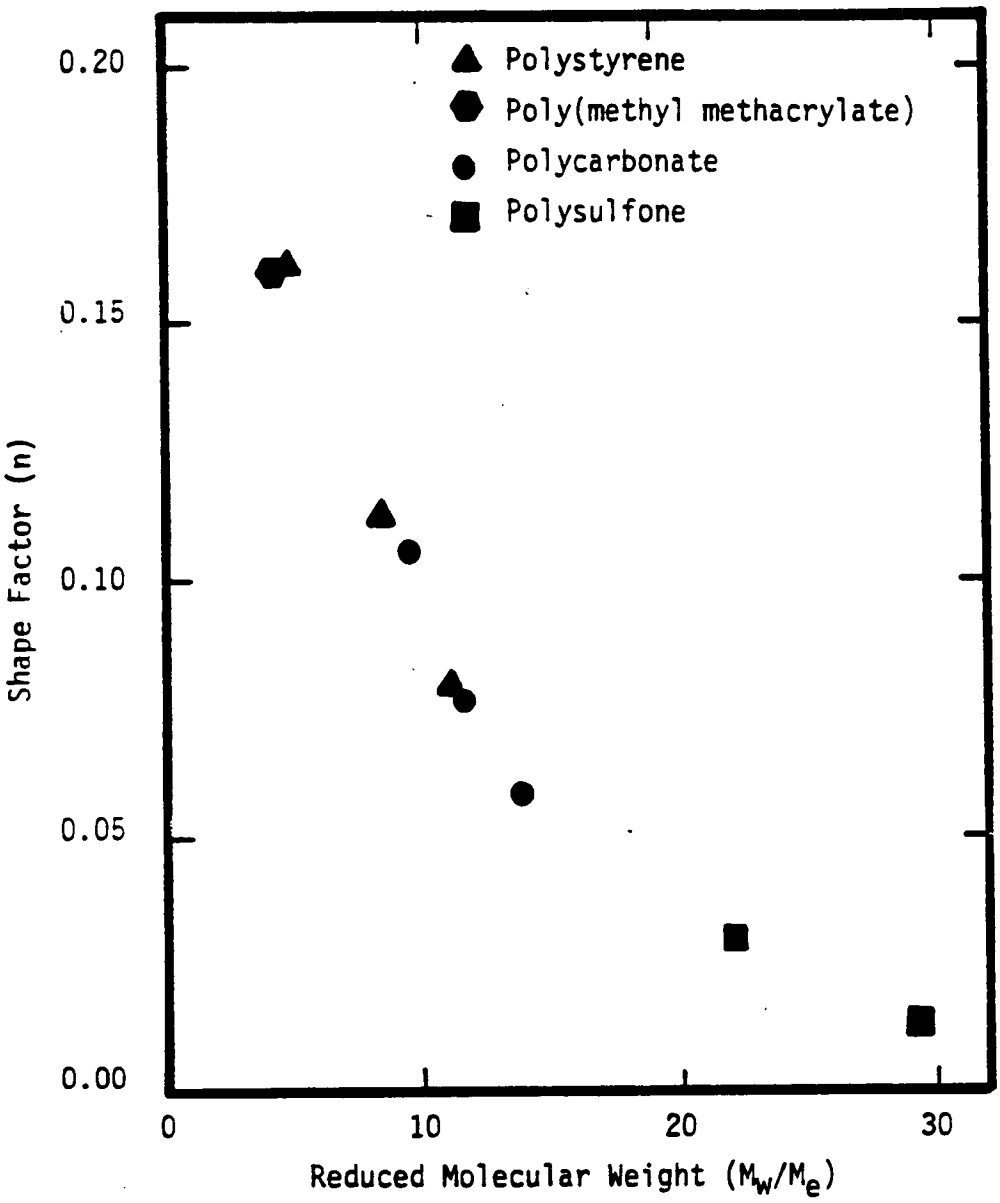

Figure 2.7. Molecular weight dependence on the exponent shape factor.

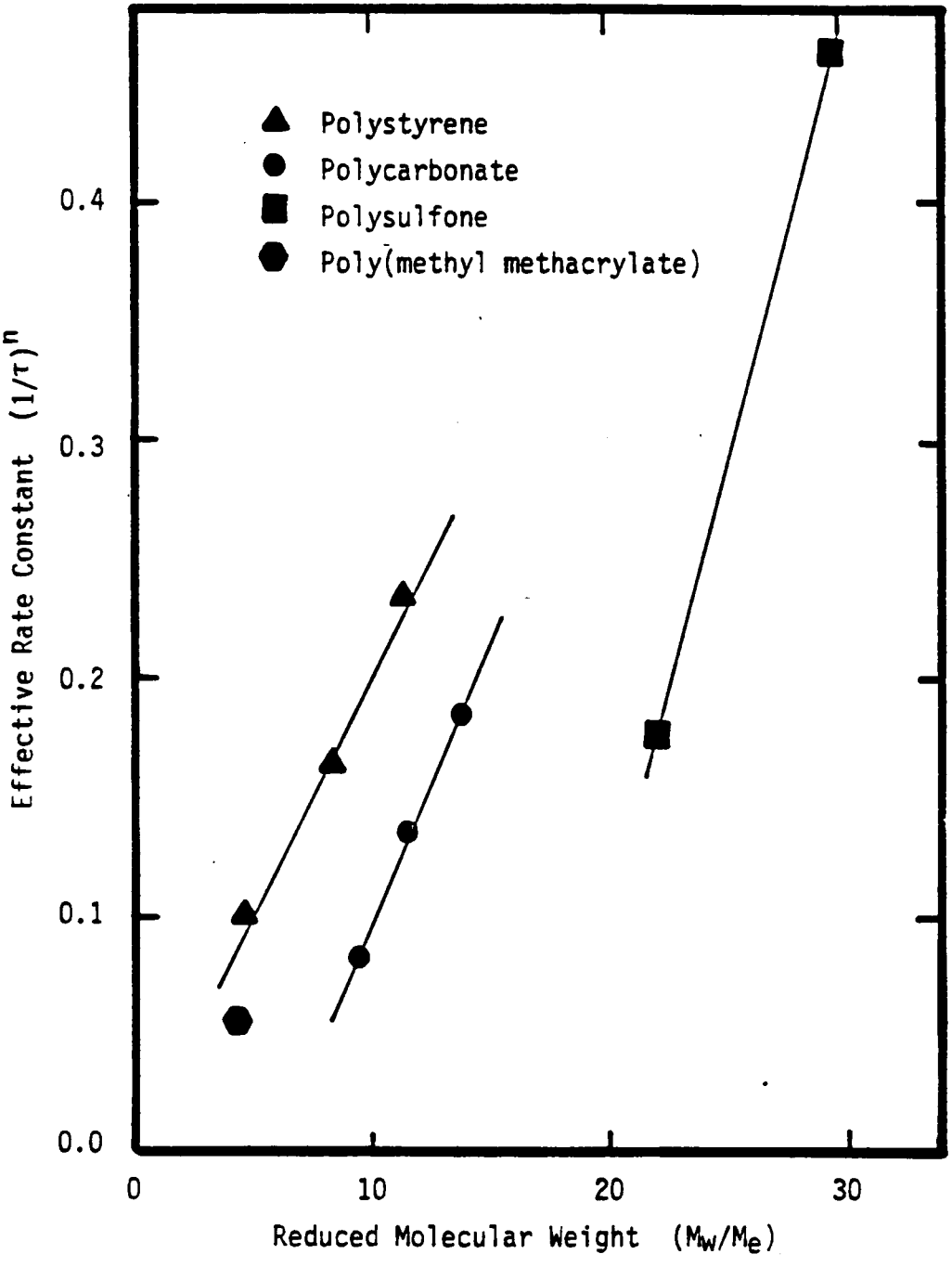

Figure 2.8. **Molecular weight dependence on the effective rate constant.**

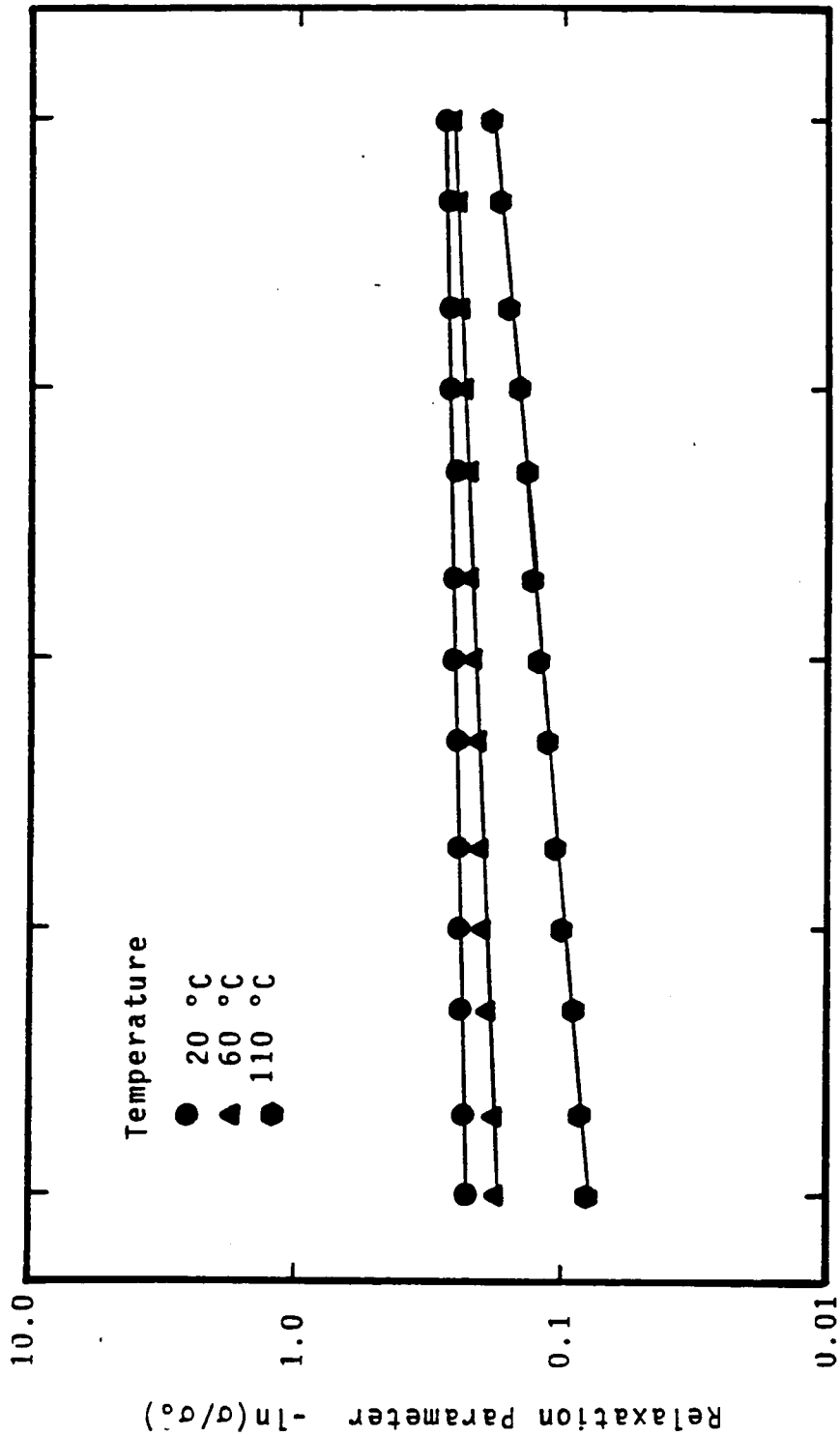

Figure 2.9. Polysulfone (P1700) stress relaxation spectrum at various temperatures.

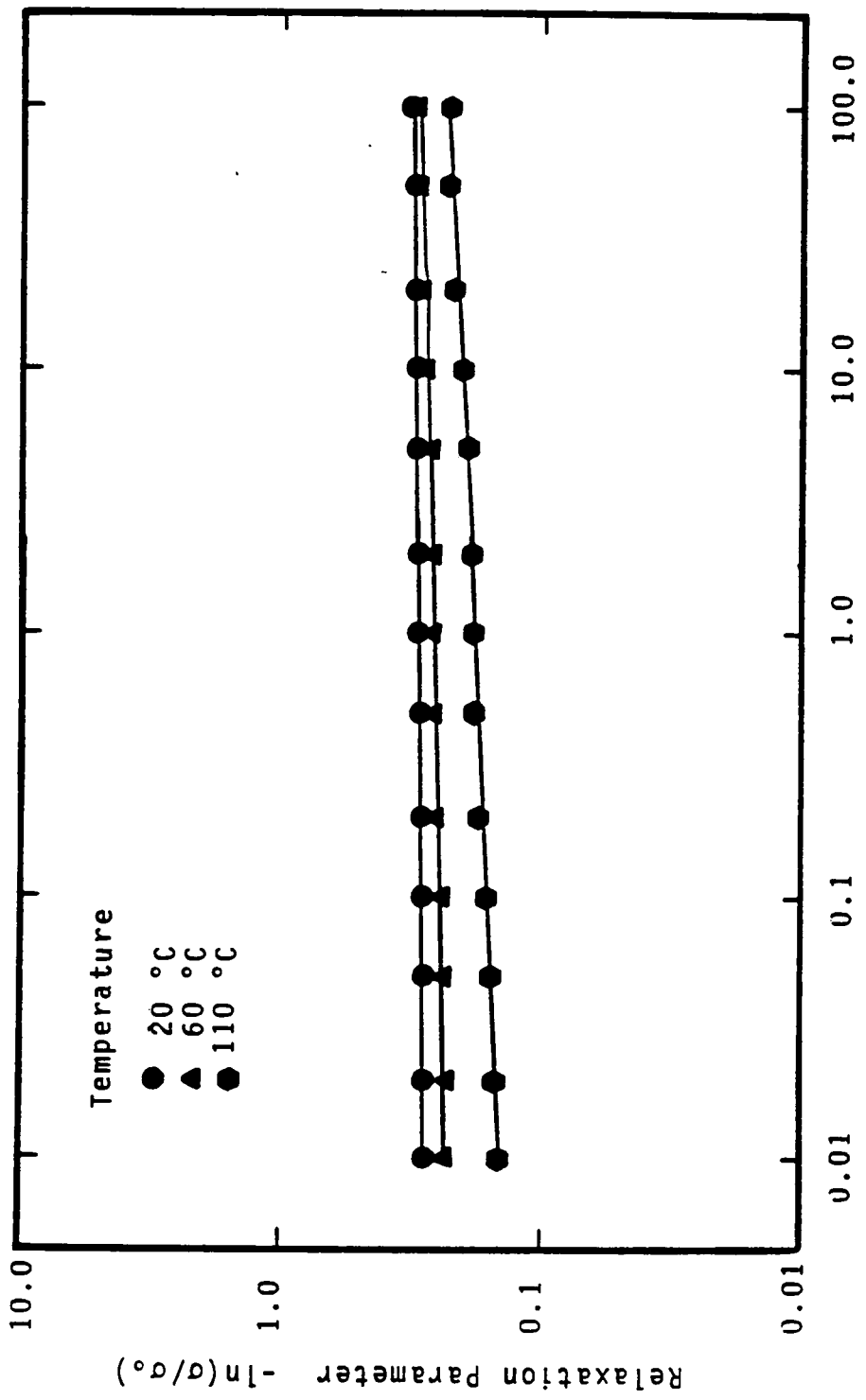

Figure 2.10. Polysulfone (P3500) stress relaxation spectrum at various temperatures.

Table 2.5. Rheological parameters of polysulfones as a function of temperature.

Material	Temperature	n	Tau	Tau^{-n}
P1700	20 °C	0.0216	5.57E27	0.2531
P3500	20	0.0162	1.48E32	0.3012
P1700	60	0.0432	2.89E15	0.2145
P3500	60	0.0315	1.35E18	0.2685
P1700	110	0.0932	6.17E09	0.1224
P3500	110	0.0500	4.30E14	0.1855

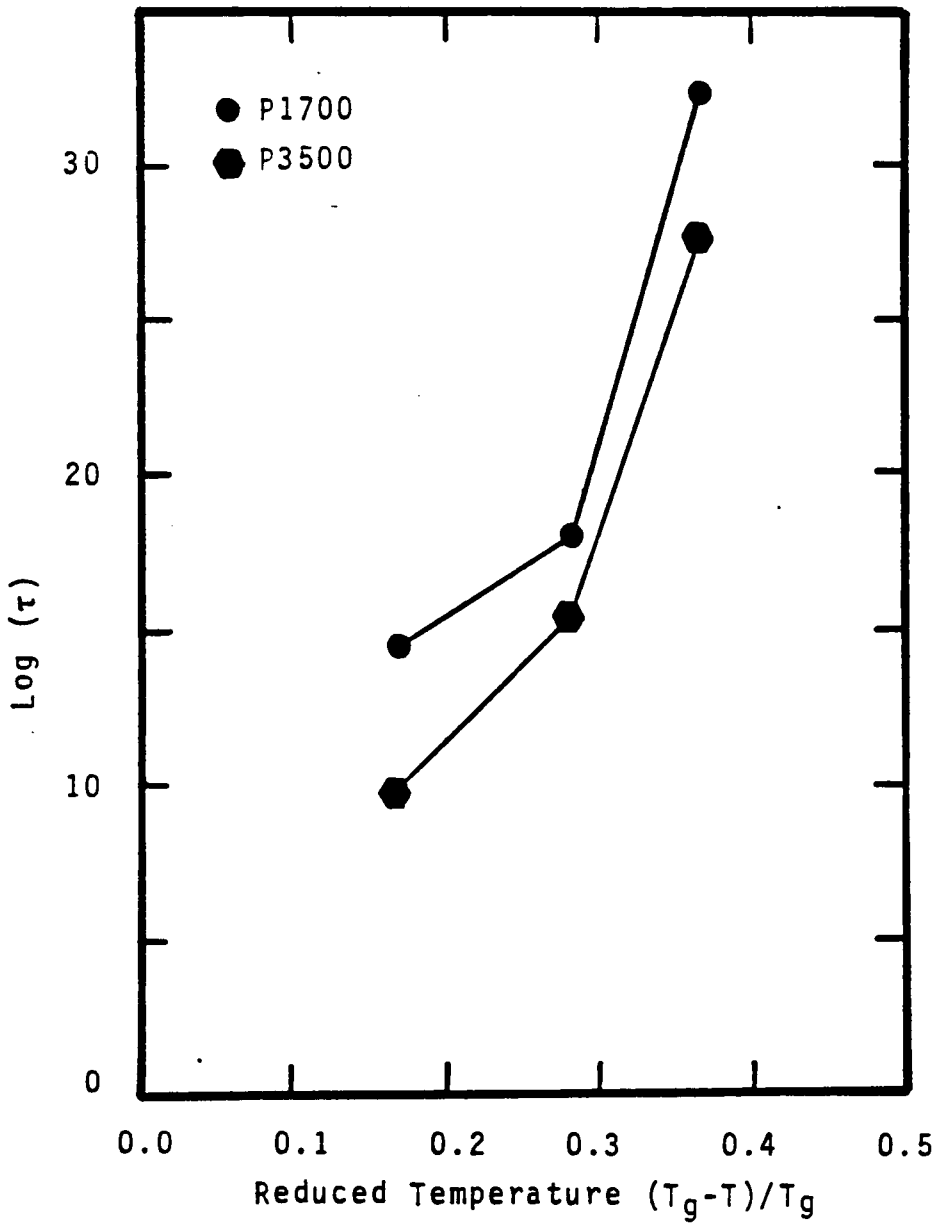

Figure 2.11. Influence of temperature on the material time constant in polysulfones.

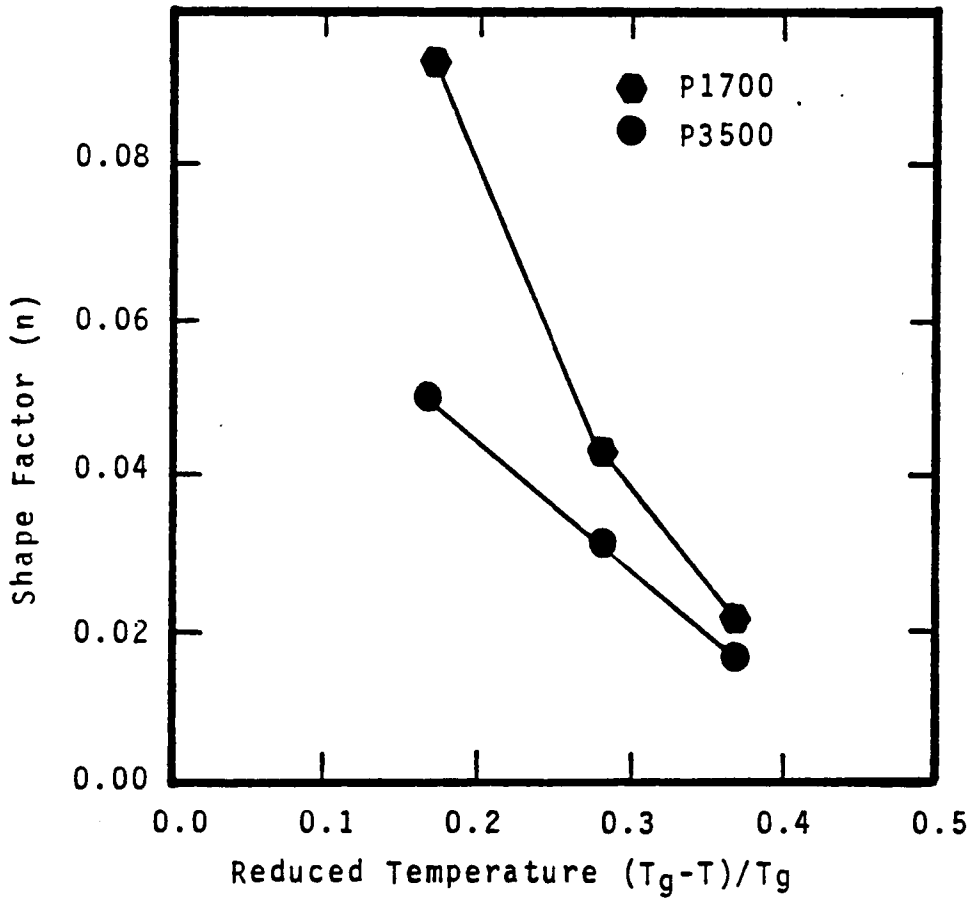

Figure 2.12. Influence of temperature on the exponent shape factor in polysulfones.

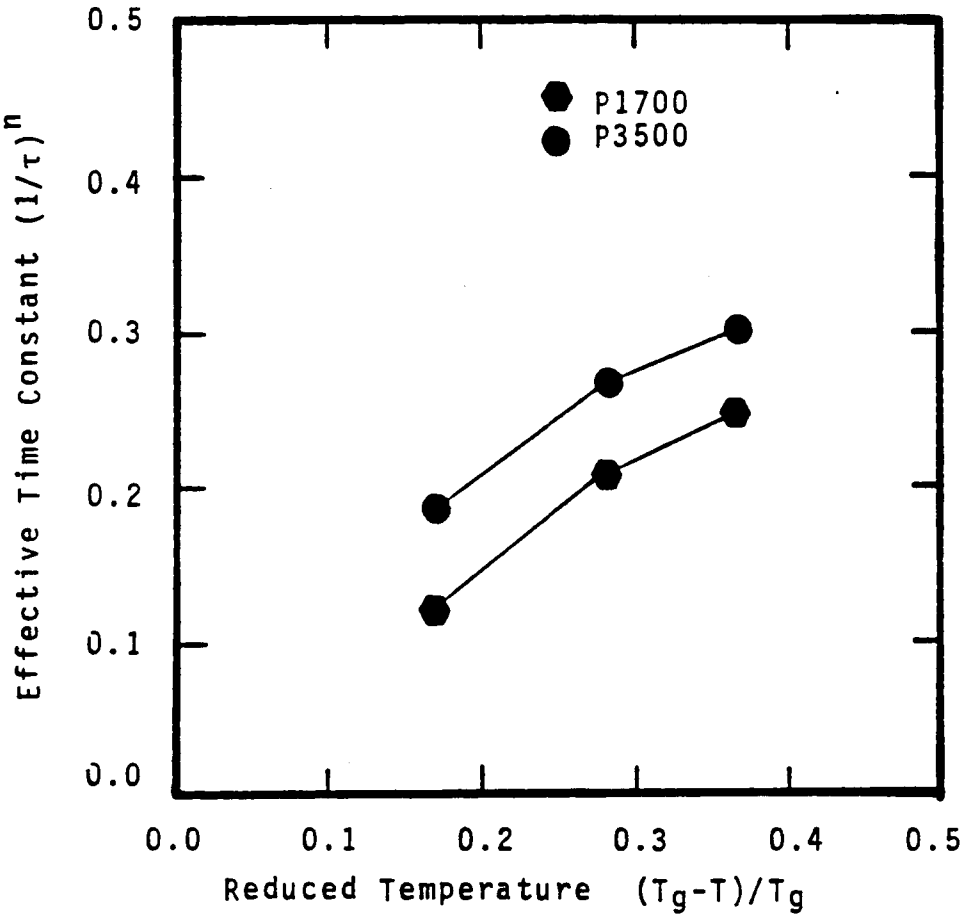

Figure 2.13. Influence of temperature on the effective rate constant in polysulfones.

2.4.2. Rate Dependence on Tensile Properties

It has been shown in the last section that two material parameters are sufficient to describe the relaxation behavior of glassy polymers using the Williams-Watts (2-36) dissipation formulation. This result implies that a dynamic state of tensile stress may be described by the generalized Maxwell model (Equation 2.13) regardless of the deformation kinematics. In this section the performance of the model will be tested by examining experimental results from a series of constant elongation rate tensile deformations and comparing them to the theoretical predictions.

For each material three stress-strain curves were produced at Instron crosshead rates of 0.0000508, 0.000508 and 0.00508 meters per minute. The 0.0000508 meters per minute speed was chosen as the slowest deformation available from the Instron machine. The slow speed tends to amplify the effect of stress relaxation during the tensile test. The 0.00508 meters per minute speed was chosen as the fastest rate available which did not induce error due to inertial effects (lag and overshoot) in the mechanical recording device. The 0.000508 meters per minute speed was chosen simply as a representative intermediate speed. Elapsed time was recorded with an event marker on the strip chart recorder such that strain versus time information may be obtained. These strain functions are plotted in Figure 2.14 and are used to determine the limits of integration for Equation 2.17. The slopes of these curves correspond to the strain rate of the deformation and are approximately 0.0004, 0.004, 0.04 reciprocal

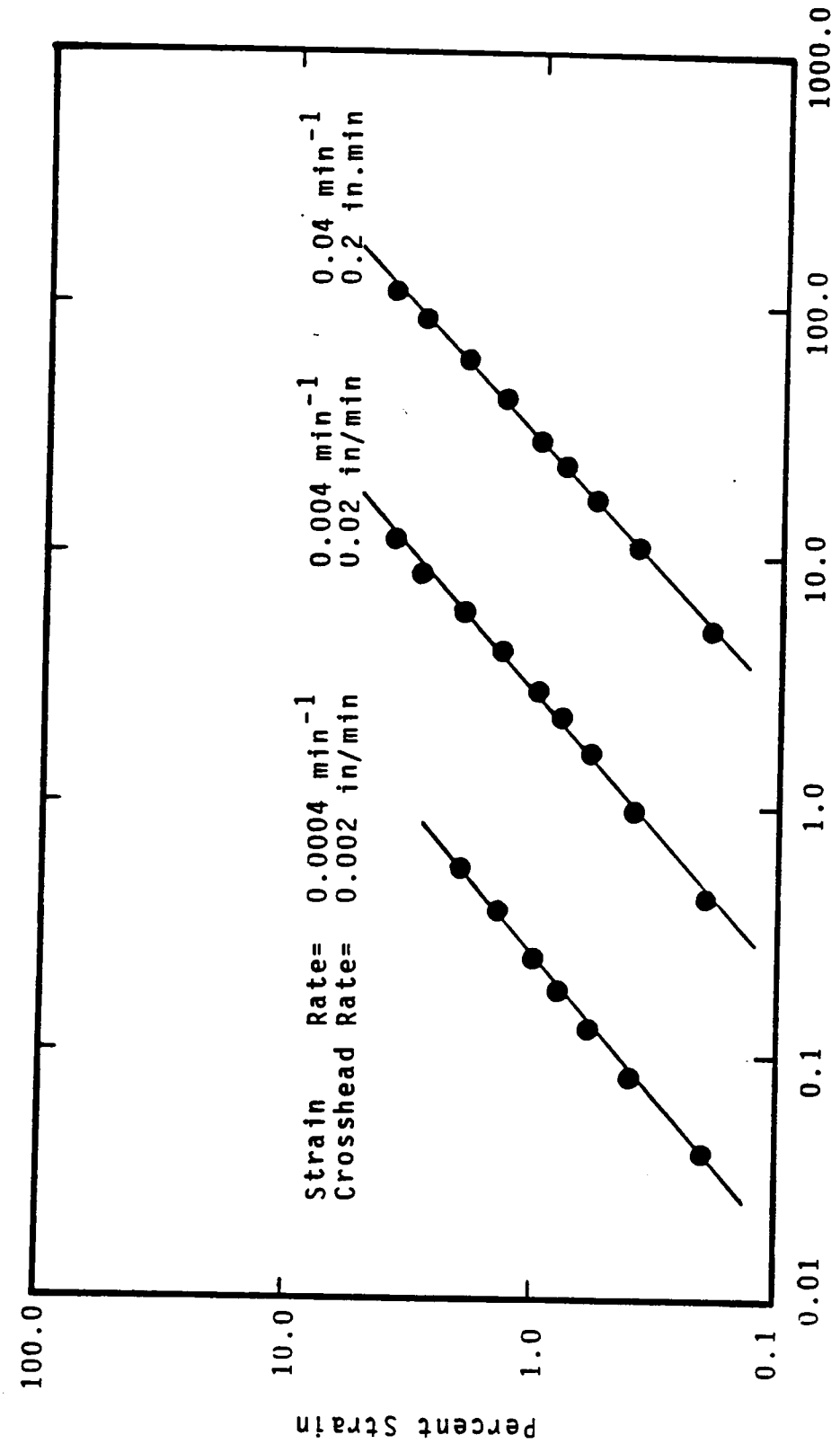

Figure 2.14. Strain functions for materials deformed at three rates.

minutes. These average strain rates are assumed constant with time and deformation and are used in the constitutive equation.

The stress versus strain versus time mechanical data for each material are treated in the following way. It is assumed that an instantaneous deformation stress-strain function exists. While this function is not experimentally possible to determine, it is deduceable on a theoretical basis. Mathematically it is that deformation which corresponds to spring element deformation in the Maxwell element. The non-Hookean deformation is described by Equation 2.12. This function can be obtained from a finite rate deformation stress-strain curve by dividing the observed stress by the relaxation factor calculated from the viscous element. The relaxation factor for these deformations is calculated as the integral in Equation 2.17. These factors are presented in Table 2.6 for the three deformations of poly(methyl-methacrylate). The hypothetical instantaneous deformation stress function for this material now appears as column two in Table 2.7, and is calculated by dividing the stress observed at the fastest deformation rate (column three) by the appropriate relaxation factor found in column two Table 2.6. Subsequent theoretical stress determination for the slower rates are then calculated using the instantaneous stresses as a reference and then multiplying by the appropriate relaxation factor. In other words, a theoretical prediction for stress in any finite rate deformation can be calculated from the multiplication of stress-strain results from another deformation rate experiment with an appropriate ratio of relaxation

Table 2.6. Relaxation factors calculated from integration of Equation 2.15 for Instron deformation of poly(methyl methacrylate).

Strain Rates $(min)^{-1}$						
	0.04		0.004		0.0004	
Strain	Time (min)	Relaxation	Time (min)	Relaxation	Time (min)	Relaxation
0.0000	0.000	1.0000	0.000	1.0000	0.000	1.0000
0.0050	0.115	0.9669	1.28	0.9512	13.8	0.9294
0.0100	0.250	0.9624	2.80	0.9451	28.5	0.9211
0.0150	0.400	0.9595	4.21	0.9415	41.5	0.9164
0.0200	0.510	0.9579	5.80	0.9383	58.0	0.9122
0.0250	0.730	0.9555	7.60	0.9358	74.0	0.9088
0.0300	0.890	0.9541	9.20	0.9339	90.0	0.9060
0.0350	1.060	0.9528	11.00	0.9319	105.0	0.9038

Table 2.7. Rate dependent stress strain functions calculated from relaxation parameters in Table 2.6 for poly(methyl methacrylate).

		Strain Rate $(min)^{-1}$		
		0.04	0.004	0.0004
Strain	Instantaneous Deformation Stress (MPa)	Observed Stress (MPa)	Calculated Stress (MPa)	Calculated Stress (MPa)
0.0000	0.0	0.0	0.0	0.0
0.0050	12.3	11.9	11.7	11.4
0.0100	23.4	22.5	22.1	21.5
0.0150	33.9	32.5	31.9	31.1
0.0200	43.3	41.4	40.7	39.5
0.0250	50.7	48.4	47.4	46.1
0.0300	57.2	54.6	53.4	51.9
0.0350	62.2	59.3	58.0	56.2
Average Observed Percent Error			0.5	1.5

integrals. These results appear as columns four and five in Table 2.7 (page 51). Comparison to actual observed results appears as an error index which represents the averaged absolute deviation from the seven finite stress levels reported. The data presented in Table 2.7 are plotted in Figure 2.15. Similar time dependent stress-strain plots for polycarbonate appear in Figures 2.16 through 2.18. Likewise, stress-strain plots for polystyrene appear in Figures 2.19 through 2.20. Stress-strain plots for polysulfone appear in Figures 2.21 through 2.22. In most cases the error observed between the experimental and theoretical behavior is less than the diameter of the data points. More detailed stress-strain-time mechanical data for experimental and theoretical results are found tabulated in Appendix A for each material studied.

Having determined a relationship for the instantaneous deformation of the nonlinear spring element, it is desirable to fit the data to some functional form such as the one suggested in Equation 2.12. This two constant trigonometric model can be fitted to the mechanical data using two selected nodes at finite stress levels. If one defines a secant modulus (2-47) as the instantaneous stress at any strain divided by the strain, then Figure 2.23 illustrates that the stiffness of the material decreases with increasing strain. This observation demonstrates the need for a non-Hookean spring element in the generalized model. The decreasing function shown in Figures 2.23 through 2.25 is suggestive of an even cosine function and it also motivated the empiricism of Equation 2.12. A fit of the

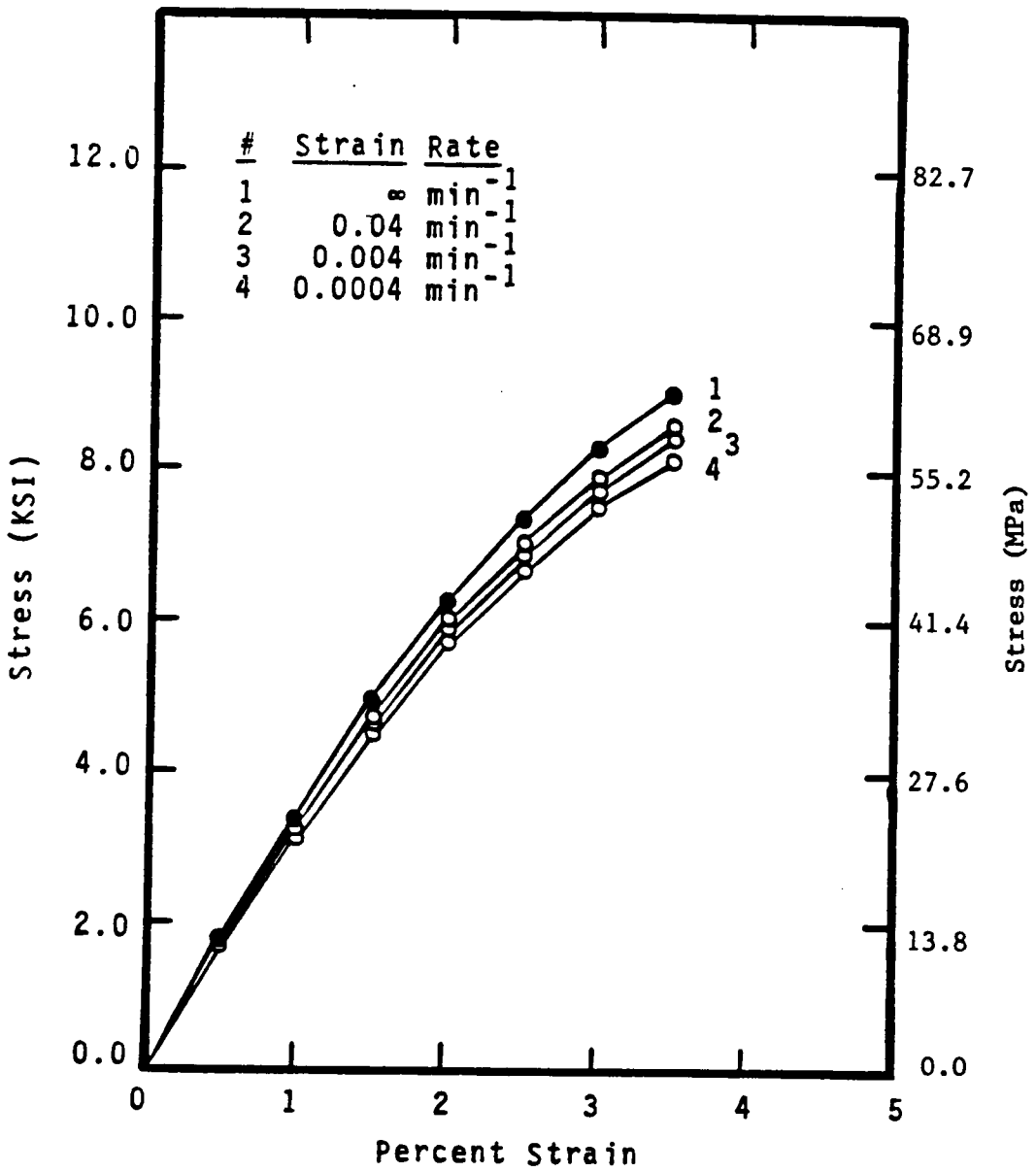

Figure 2.15. Rate dependent stress-strain behavior of poly(methyl-methacrylate).

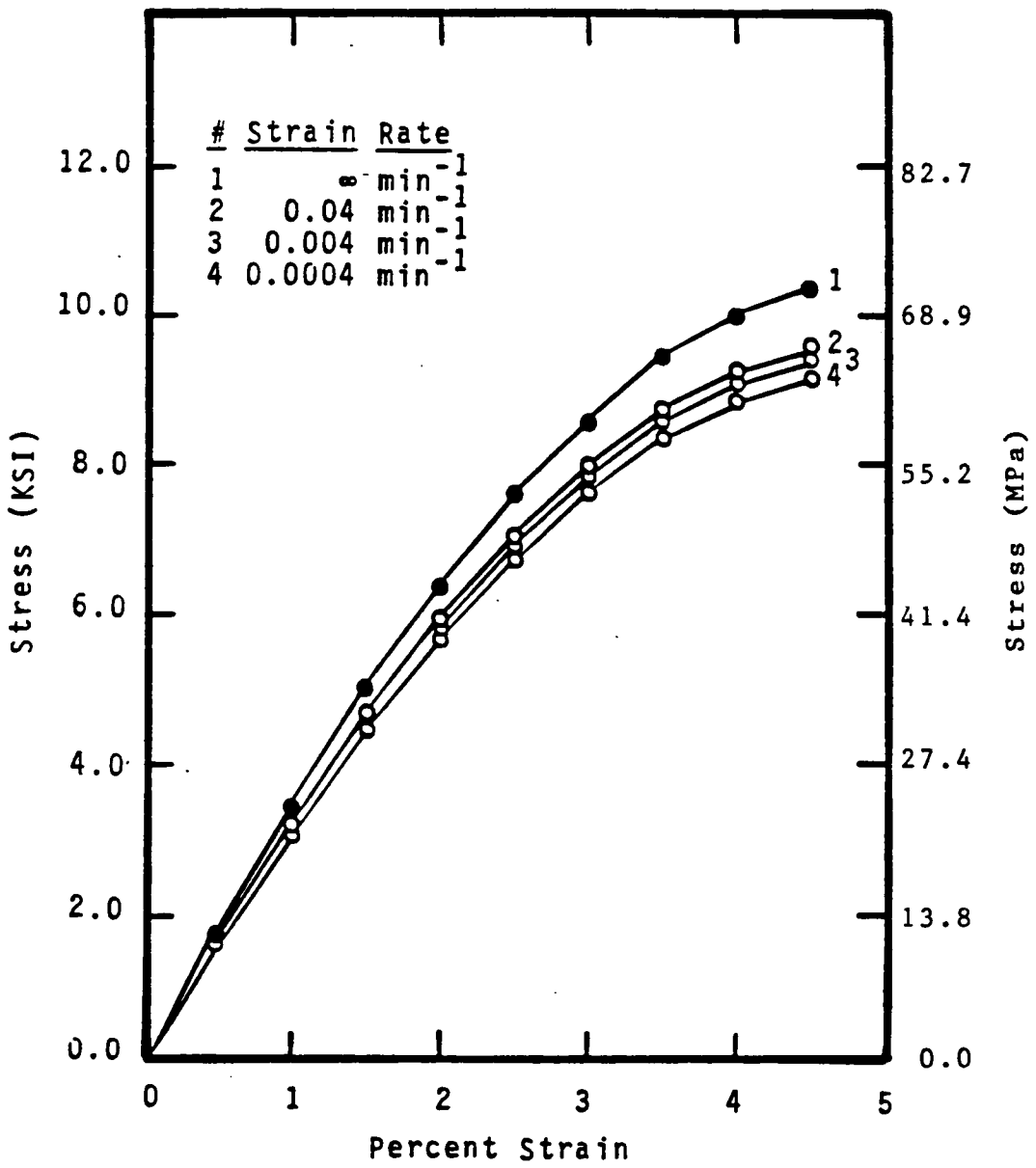

Figure 2.16. Rate dependent stress-strain behavior of polycarbonate (120G).

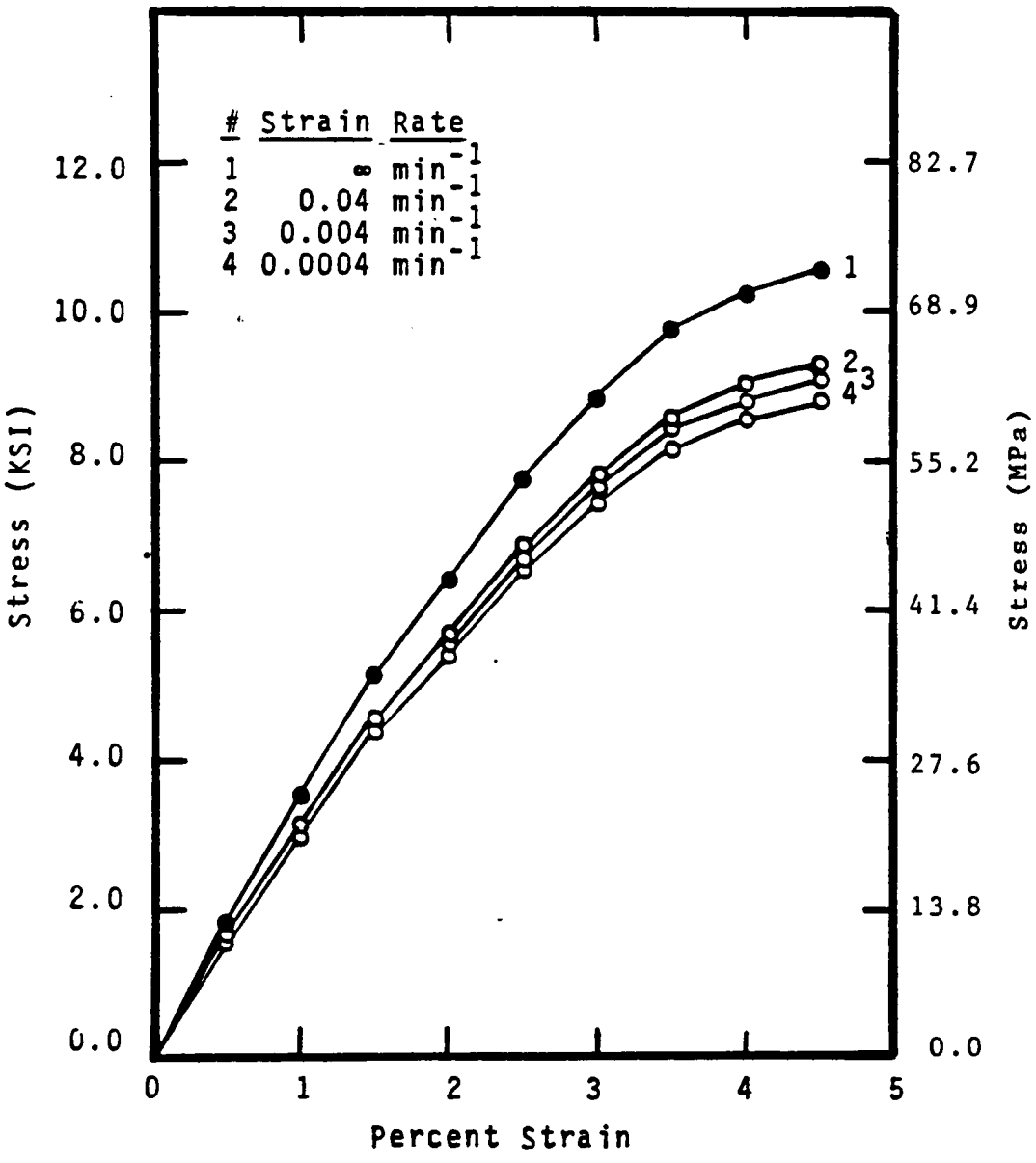

Figure 2.17. Rate dependent stress-strain behavior of polycarbonate (100G).

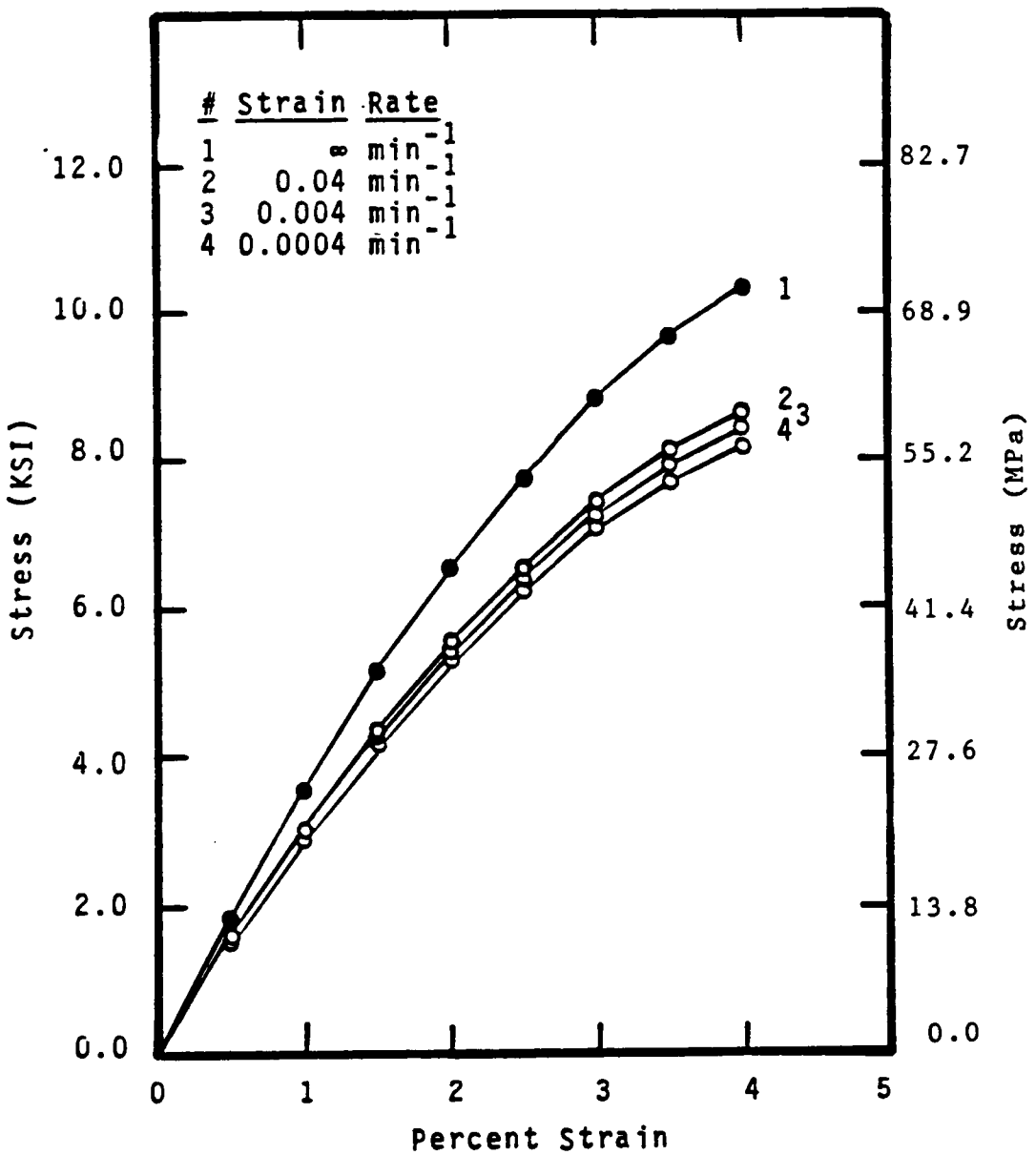

Figure 2.18. Rate dependent stress-strain behavior of polycarbonate (130G).

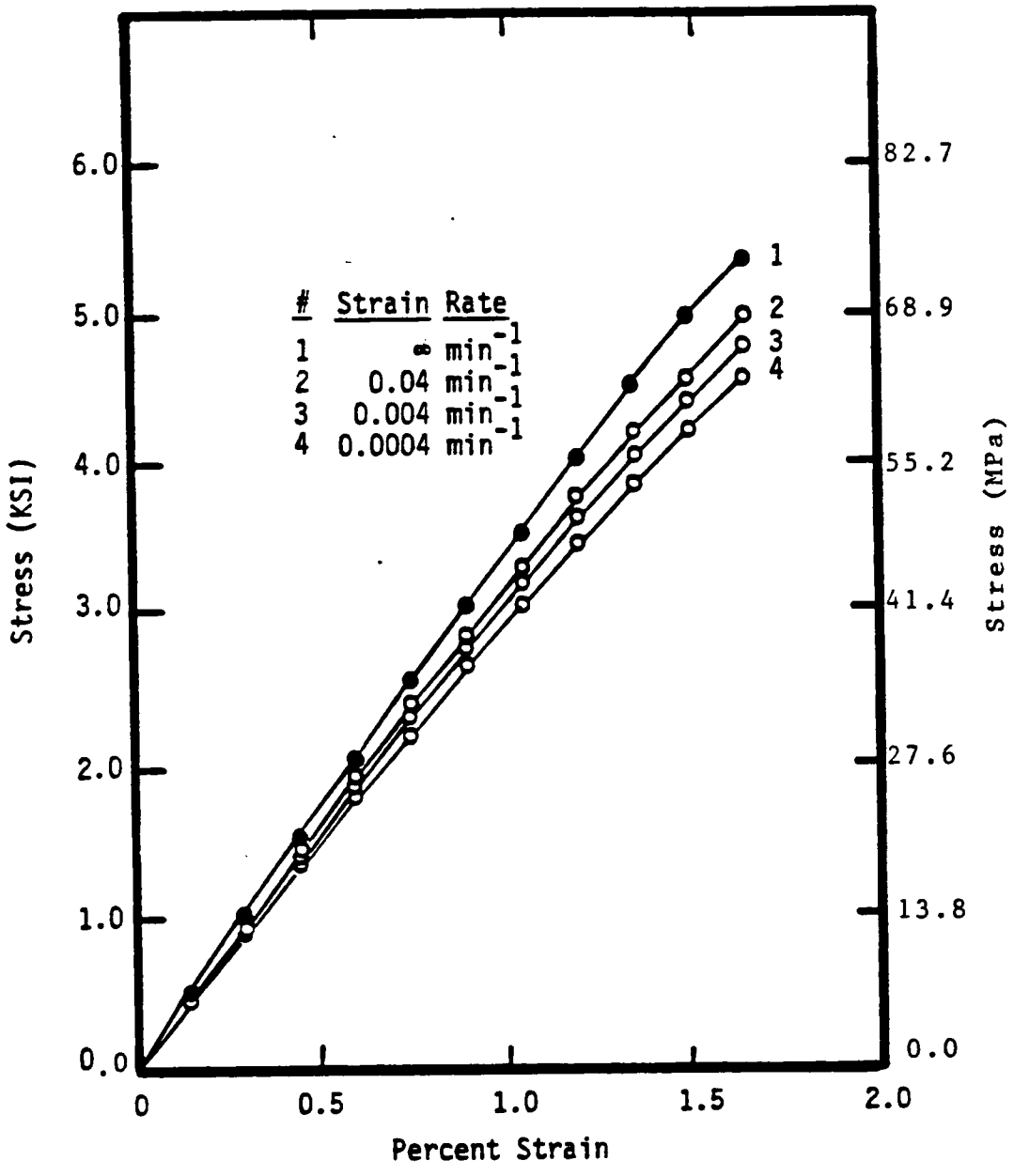

Figure 2.19. Rate dependent stress-strain behavior of polystyrene (S104).

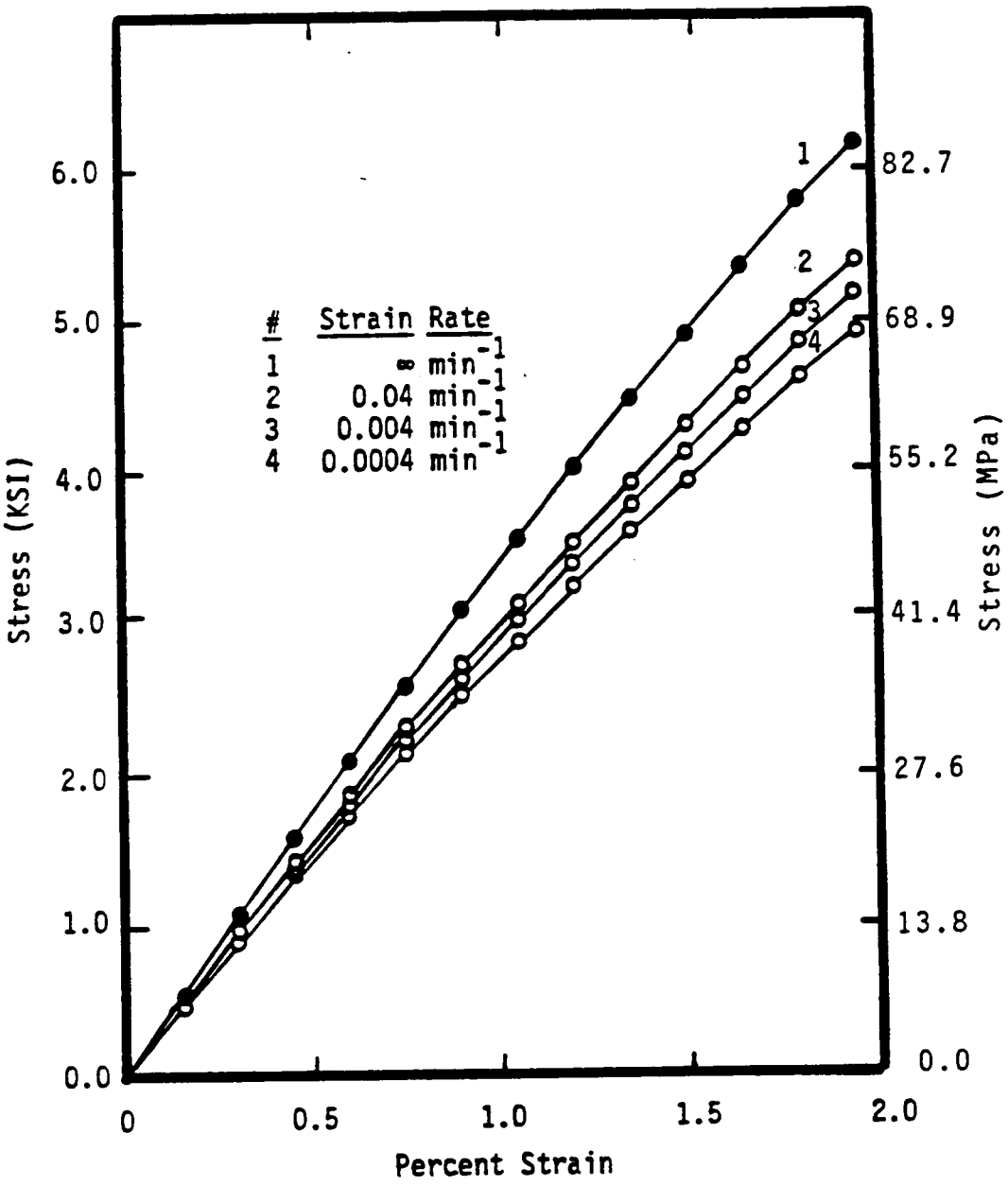

Figure 2.20. Rate dependent stress-strain behavior of polystyrene (685D).

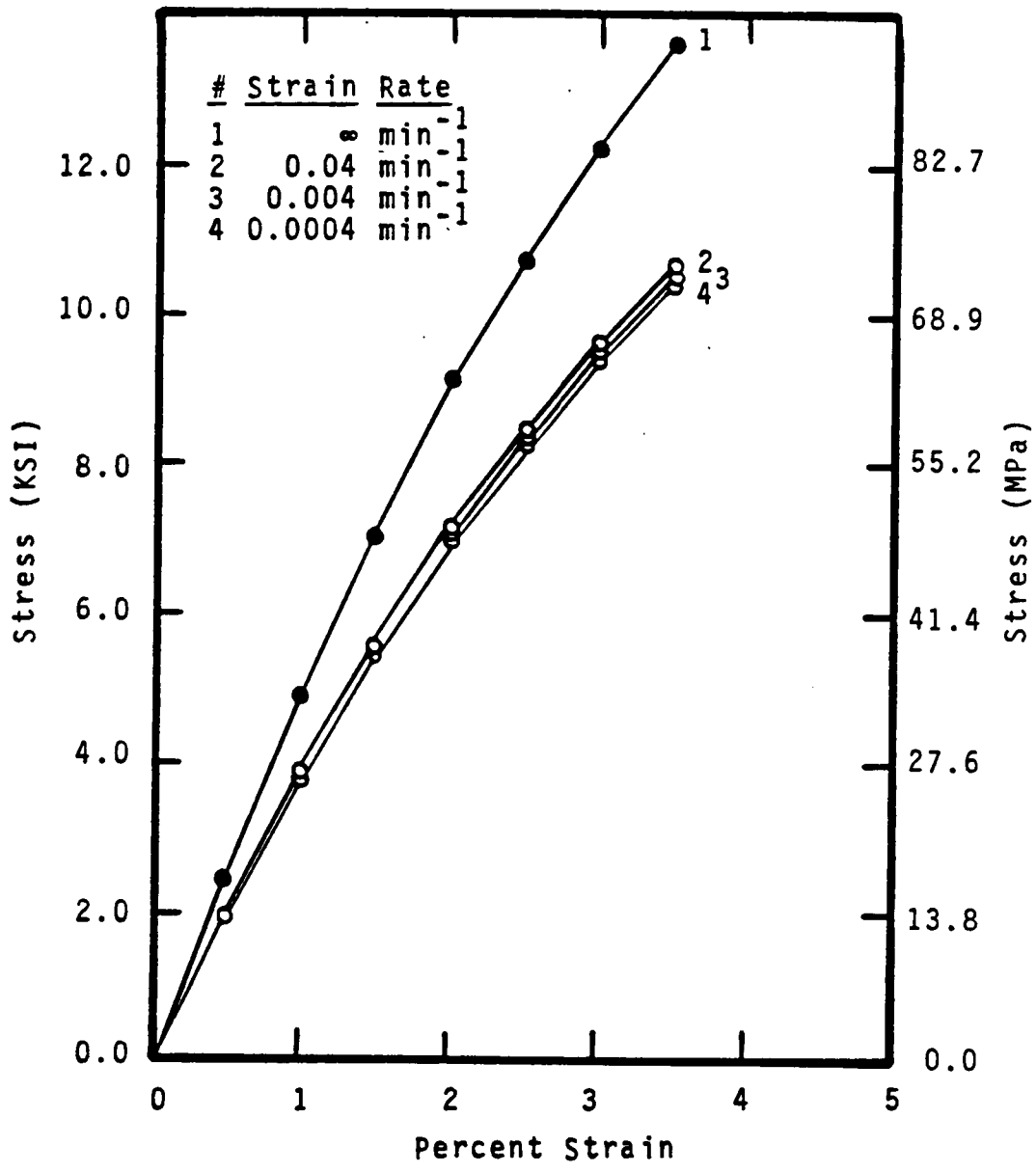

Figure 2.21. Rate dependent stress-strain behavior of polysulfone (P1700).

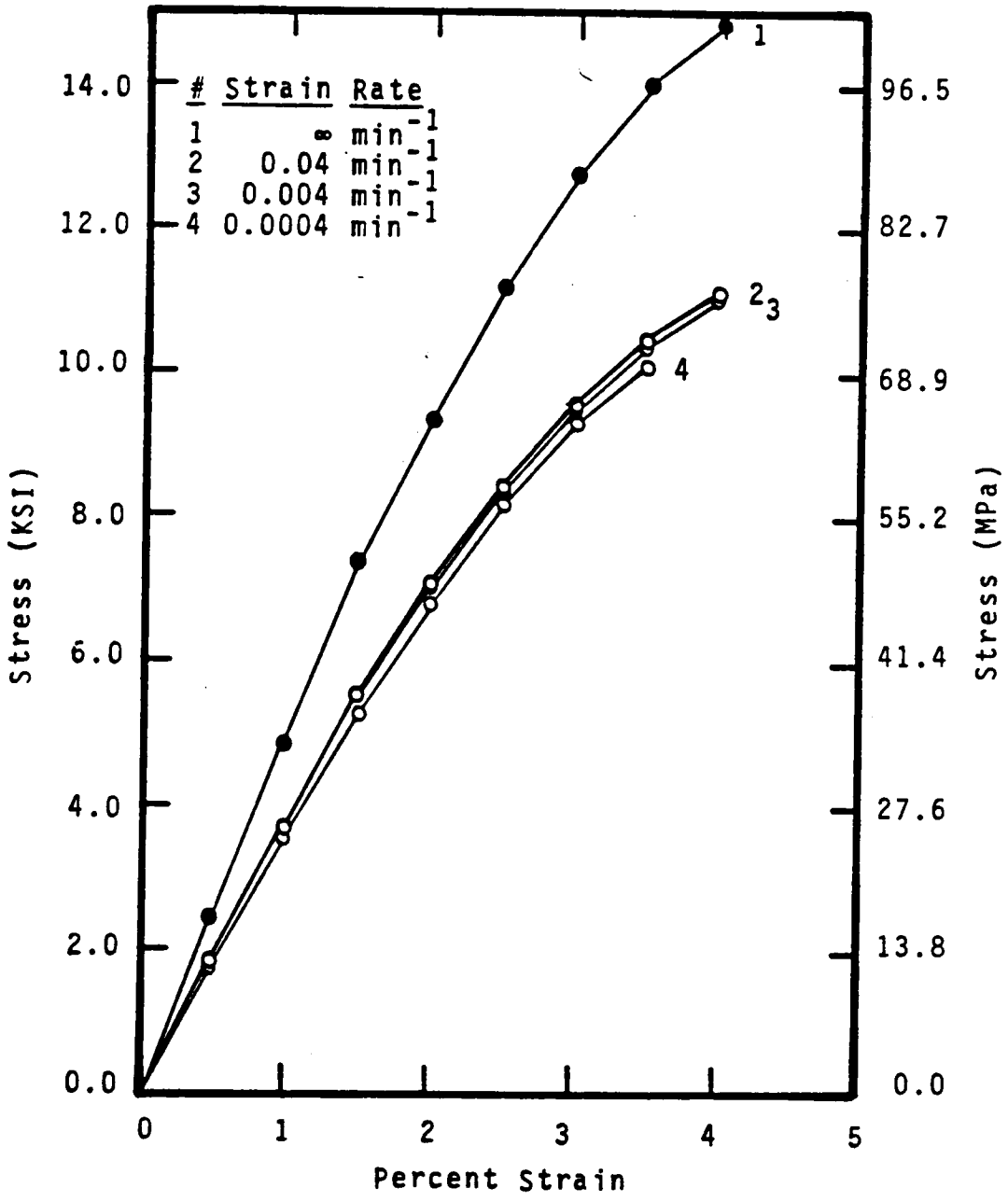

Figure 2.22. Rate dependent stress-strain behavior of polysulfone (P3500).

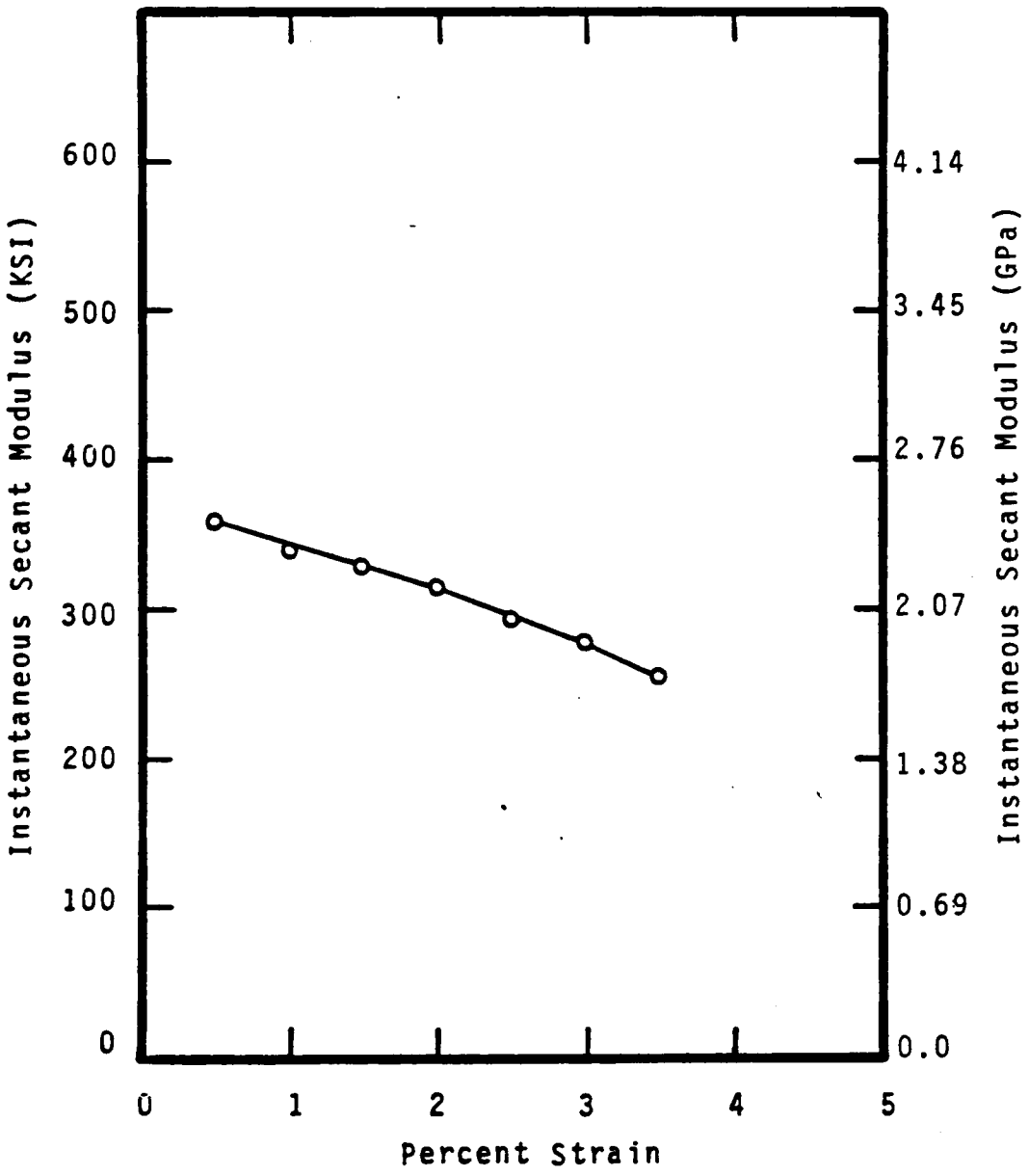

Figure 2.23. Instantaneous secant modulus as a function of strain for poly(methyl methacrylate).

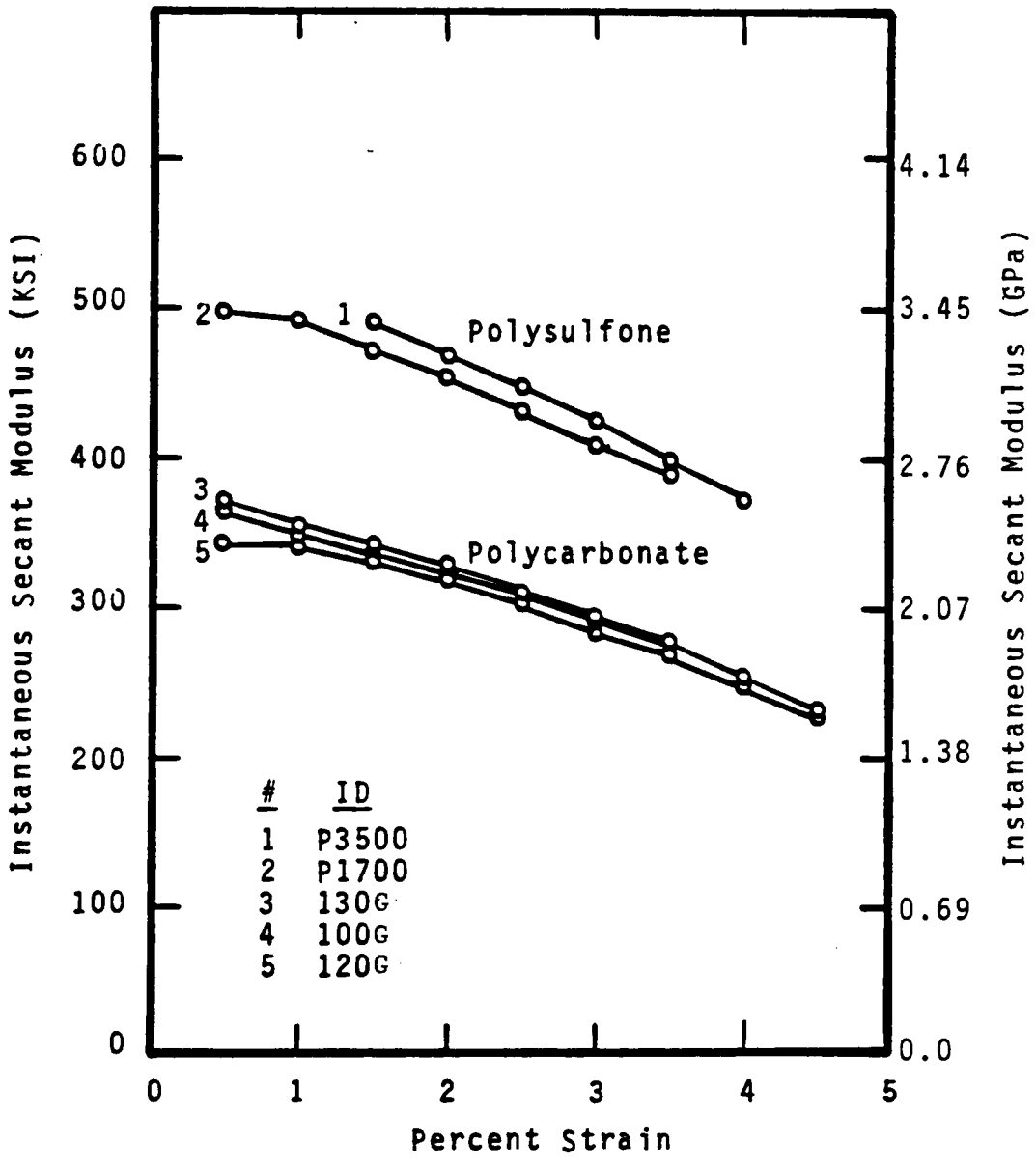

Figure 2.24. Instantaneous secant modulus as a function of strain for polycarbonates and polysulfones.

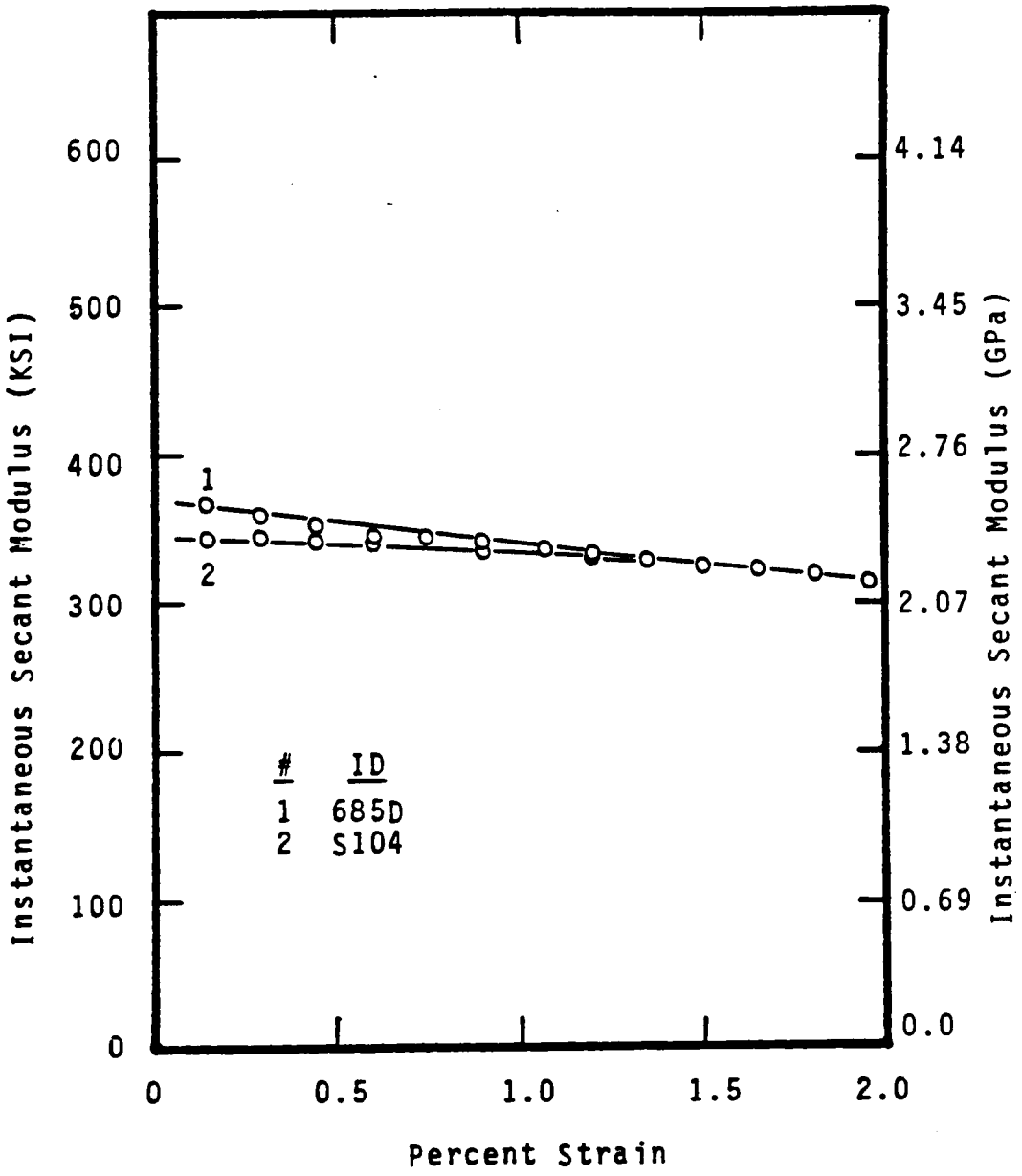

Figure 2.25. Instantaneous secant modulus as a function of strain for polystyrenes.

poly(methyl-methacrylate) stress-strain data to Equation 2.12 was generated by a recursive relation and the results are summarized in Table 2.8. One sees in general a good degree of fit using the constants a=15.50 and E=2.39 MPa. Another interesting result of the cosine squared fit is the inherent ability to predict a yield stress. Taking the derivative of Equation 2.12 with respect to strain, we obtain:

$$\frac{d\sigma}{d\varepsilon} = E^{o}\left[\cos^{2}(a\varepsilon) - 2a\varepsilon\cos(a\varepsilon)\sin(a\varepsilon)\right] \qquad 2.18$$

Setting the first derivative equal to zero results in the following implicit condition which defines the strain at yield:

$$\tan(a\varepsilon_{y}) = 1/2a\varepsilon_{y} \qquad 2.19$$

Using a value of a=15.50 obtained for the poly(methyl-methacrylate) fit, the model predicts a yield strain of 4.2 percent. Experimentally, the material was shown to fracture before the onset of yield, precipitating a brittle failure.

The instantaneous stiffnesses for polysulfone and polycarbonate are presented in Figure 2.24 (page 62) as a function of strain, while Figure 2.25 (page 63) shows a similar plot for polystyrene. A summary of the cosine square fit parameters for each material is found in Table 2.9 along with the predicted yield strains according to Equation 2.19. It is noted that in general, the fit predicts the

Table 2.8. A cosine squared two parameter fit of instantaneous deformation of poly(methyl methacrylate).

Strain	Instantaneous Deformation Stress (MPa)	Secant Modulus (GPa)	Cosine Squared Fit (MPa)	Percent Error
0.0000	0.0	------	0.0	0.00
0.0050	12.3	2.46	11.9	-3.60
0.0100	23.4	2.34	23.3	-0.16
0.0150	33.9	2.26	33.9	0.00
0.0200	43.3	2.16	43.4	0.13
0.0250	50.7	2.02	51.2	0.99
0.0300	57.2	1.91	57.2	0.00
0.0350	62.2	1.77	61.3	-1.49

Fit parameter "a" equals 15.50 inverse strain units.
Fit parameter "E" equals 2.39 MPa.

Table 2.9. A summary of cosine squared fit parameters for theoretical instantaneous loading of glassy polymers.

Sample ID	Reduced Molecular Weight	Effective Modulus (GPa)	a	Percent Yield Strain
		Polycarbonate		
120G	9.59	2.42	14.75	4.4
100G	11.63	2.48	14.54	4.5
130G	13.88	2.48	14.63	4.5
		Polystyrene		
S104	4.71	2.39	13.71	4.7
685D	8.43	2.46	21.80	3.0
S107	11.14	------	-----	---
		Polysulfone		
P1700	22.01	3.16	14.20	4.6
P3500	29.34	3.59	14.23	4.6
		Poly(methyl methacrylate)		
M2805	4.44	2.39	15.49	4.2

glassy polymers yield strain to be approximately 4.5 percent. Comparing to the actual observed yield strains presented in Table 2.10, it is seen that the cosine squared model tends to underpredict the observed yield strains. The observed instantaneous moduli shown in Table 2.9 (page 66) and the observed yield behavior shown in Table 2.10 may be compared to the previously reported mechanical properties for these materials as summarized in Table 2.11 (2-48).

2.5. Discussion of Mechanical Modelling Results

The generalized Maxwell Model as developed in Section 2.2 has been demonstrated to effectively model the stress relaxation processes associated with glassy polymer deformation. In this section the significance of both the static and dynamic modelling results presented in the previous section will be developed. Next the correlation between rheological parameters and material constants will be suggested. Lastly the potential impact of the present work on classical rheology will be discussed.

The generalized Maxwell Model presented here is thus a semi-empirical four constant fit which is composed of a nonlinear viscous relaxation superimposed on a nonlinear elastic deformation. These contributions are separable mathematically. The viscous relaxation is composed of a two constant time integral which is composed of a fading memory exponential. This formulation is semi-empirical in that it is based on a physical model (spring and dashpot in series) but there is no evidence that the model corresponds

Table 2.10. Observed glassy polymer yield behavior.

Sample ID	Stress (MPa)/Strain Strain Rate 0.04 min^{-1}	0.004 min^{-1}	0.0004 min^{-1}
		Polycarbonate	
120G	66.1 0.057	65.1 0.056	61.2 0.047
100G	67.0 0.056	65.6 0.054	62.6 0.050
130G	64.5 0.056	62.5 0.051	59.5 0.048
		Polysulfone	
P1700	78.6 0.042	74.5 0.039	73.1 0.038
P3500	80.0 0.046	80.0 0.044	79.7 0.045

Table 2.11. Accepted glassy polymer mechanical properties (2-48).

Material	Yield Stress(MPa)	Modulus (GPa)	Ultimate Stress(MPa)	Percent Strain
Polystyrene	-----	2.28	43.4	1.0-2.5
Polysulfone	70.3	2.48	----	50-100
Polycarbonate	62.1	2.38	65.5	110
Poly(methyl methacrylate)	-----	2.76	62.1	2-10

to any part of the structure of the glass. That is to say, it is a model which is based on a continuum response of the material and not a molecularly based theory. Elastic deformation is based on a two constant function which has no physical basis. This empiricism was motivated simply by the shape of the secant modulus functions. The four material parameter model as a whole performs well especially in the initial stages of the deformation.

The comparative inability of the generalized Maxwell Model to describe the time dependent deformation near the yield condition has two causes. First the existence of only one relaxation time constant assumes there exists only one mode of relaxation. As a material nears its yield point, there may exist a distribution of molecular conformations which may create a spectrum of relaxation time constants. Secondly the unsophisticated nature of the elastic element model makes it difficult to track rapidly changing behavior at or near the yield condition. Perhaps it is this behavior which would be better served by the application of a plasticity theory. With these limitations in mind, we will proceed to discuss the measurement of rheological parameters in static deformation and the influences of molecular weight on solid state deformation.

As evidenced by Figures 2.2 through 2.5 (page 33 through page 36), 2.9 (page 41) and 2.10 (page 42), the ability of the two constant Williams-Watts (2-36) dissapative equation to model mechanical stress relaxation is striking. The degree of fit indicates that the rheological parameters remain constant over four orders of magnitude

in time. The apparent universality of these parameters can be used to great advantage since correlations between rheological and material parameters can now be established.

For example the relaxation time constants and shape factors can be related to the molecular weight of the glass. For this analysis, the continuum between different polymer types is formed by making use of the concept of entanglement molecular weight. Every polymer glass has an intrinsic molecular weight between physical entanglements. Apparently, this molecular segment length is governed by the physics of the glassy state as defined by polymer chain rigidity, size of pendant groups, as well as other factors. If the apparent molecular weight of a polymer is normalized by its entanglement molecular weight, then a reduced molecular variable is formed. This variable describes the ability of the glass to support or transmit stress between adjacent molecules through physical entanglements. As can be seen in Figure 2.6 (page 38) there seems to be some direct relationship between the time constant and reduced molecular weight at those thermal conditions. Likewise, an inverse relationship between the shape factor and reduced molecular weight exists as seen in Figure 2.7 (page 39). Conceptually one can now build molecular weight effects into the constitutive equation by fitting the rheological parameters to the material composition.

The effect of the glass transition temperature relative to the test temperature on the rheological parameters of the glass is best seen in Figure 2.8 (page 40). The observation is that as the glass transition temperature is raised, the rheological response in terms of the effective rate constant seems to shift to the higher molecular weight materials. These results suggest a study of the influence of raising the test temperature relative to the glass transition on the rheological parameters of the glass.

The effect of thermal activity on the rheological behavior of glasses is somewhat inconclusive. It seems clear from Figure 2.11 through 2.13 (page 44 through page 46) that increasing the test temperature towards the glass transition tends to suppress short term relaxation behavior in favor of long term stress relaxation. Perhaps some reduced temperature variable (as suggested in these figures) which is referenced to the materials glass transition temperature would be of help in trying to understand the thermal behavior of different polymers. This work has shown that there exists some solid state rheological function with respect to thermal activity relative to the glass transition temperature, however, more study is needed to quantify this effect.

Since no strain measurement device capable of operating at elevated temperatures was available, it is regretted that no high temperature time dependent deformation studies were made. However, based upon the success of the room temperature experiments, there is no reason to expect poor performance of the relaxation model.

The correlations which can be developed between material parameters and rheological parameters are interesting; however, another interesting feature gained from obtaining constant rheological parameters is the ability to describe elapsed time in terms of a Deborah Number. The Deborah Number can be thought of as a measure of the relative magnitude of mechanical relaxation which has occurred over any time. For the application to the generalized Maxwell Model as outlined above, a reduced Deborah Number can be defined as the following.

$$N_{De}^{r} = (t/\tau)^{n} \qquad 2.20$$

Now it can be shown that the effective rate constant as described in Figure 2.8 (page 40) is equivalent to the above Deborah Number evaluated at a time of one minute. Thus it is seen that the short time relaxations increase with the reduced molecular weight parameter.

The Williams-Watts (2-36) equation is one specific solution to the generalized viscoelastic model; however, the relaxation processes which are manifest during static deformation should remain active in a dynamic system. Even though the instantaneous deformation stress function is not available experimentally, the model can still be evaluated using a finite rate deformation as a reference condition. Figures 2.15 through 2.22 (page 53 through page 60) show excellent agreement between observed behavior at slow deformation rates and predicted behavior based on the observed behavior at the fastest rate

multiplied by a ratio of relaxation integrals (see Appendix A). Thus it is shown that the stress relaxation process in deforming glasses can be modelled from the behavior observed in static deformation. The effect of various magnitudes of Deborah Numbers can be seen graphically by comparing Figures 2.15 (page 53) and 2.22 (page 60). For example, the polysulfone samples have considerably more short time relaxations than the poly(methyl methacrylate) samples. This interesting observation is due in part to the low exponential shape factor which seems characteristic of high molecular weight materials. Thus it seems that low shape factors are indicative of more stable long term behavior, while large shape factors are indicative of more stable short term behavior. It would be desirable to further investigate the behavior of polysulfone under conditions of ever increasing strain rate in order to verify the short term activity.

The experiment suggested above leads one to consider the impact behavior of these materials. Qualitatively speaking, polystyrene has very low impact strength and fracture energy. Conversely, polysulfone is extremely tough under conditions of shock loading. The ability of a material to absorb large ammounts of energy under impact is related to the short term stress dissipation properties. As indicated in Figure 2.1 (page 26), as the shape factor decreases toward zero the short time stress relaxation response becomes greater and approaches a singularity. On this basis a correlation between the rheological shape factor and impact resistance of a material is suggested. Table 2.12 (2-49) presents impact properties (2-48) of the four

Table 2.12. Impact strength for polymers used in this study (2-49).

Material	Tensile Impact Energy to Break	Shape Factor
Polystyrene	11-30 N-M	0.08-0.16
Poly(methyl methacrylate)	20-34	0.16
Polycarbonate	258-366	0.06-0.11
Polysulfone	271-339	0.02

glasses studied here and compares them to the measured shape factor. As expected, the shape factor is generally inversely proportional to the impact resistance.

We will now discuss the time independent behavior in the dynamic tensile tests. The instantaneous deformation stress-strain function, which is only a theoretical abstraction, appears as the solid data point lines in Figures 2.15 through 2.22 (page 53 through page 60). This nonlinear deformation corresponds to stretching of the spring element alone. The cosine squared fit is an empirical model chosen for its shape and simplicity. The modulus parameter "E" obviously corresponds to the stiffness of the material, while the trigonometric parameter "a" is related to the location of the yield stress. This simple model describes the nonlinear time independent deformation quite well. It is emphasized that the fitted modulus parameter does not necessarily correspond to the commonly reported moduli for these materials. This discrepancy is most pronounced in materials such as polysulfone where there is considerable short time relaxation. The fitted modulus for polysulfone is thirty percent higher than that which is reported because of the short term relaxation effect.

The resulting instantaneous secant modulus behavior with respect to strain is thus a decreasing function as a result of the cosine squared term. Experimental results show that the molecular weight effect on the modulus of the material is slight. Generally speaking the modulus is increased with molecular weight, but this

effect is decreased at high levels of strain. Figures 2.23 though 2.25 (page 61 through page 63) illustrate this phenomenon graphically. Apparently material deformation tends to destroy any structural advantages (in terms of stiffness) of higher molecular weight materials.

Attention will now be turned to other aspects of the model. Another interesting advantage which the generalized Maxwell Model has over the linear theory is the ability to predict non-Newtonian creep behavior. The linear Maxwell construction predicts Newtonian creep. One usually employes the Kelvin (Voight) or Jefferies construction. However, consider the differential equation described in Equation 2.9. For the kinematics of creep, the time rate of change of stress disappears allowing for easy integration to the following equation for strain in terms of time. This equation is completely analogous in form to the linear Maxwell Model.

$$\varepsilon(T) = \frac{\sigma^{o}T}{E} + \varepsilon_{o} \qquad 2.21$$

Allowing for "T" to be a nonlinear function of laboratory time, the form for T(t) given in Equation 2.11 is substituted into Equation 2.18, and the following relationship for strain as a function of time is obtained.

$$\varepsilon(t) = \frac{\sigma^{o}}{E} (t/\tau)^{n} + \varepsilon_{o} \qquad 2.22$$

Alternatively Equation 2.22 can be expressed in terms of the generalized Deborah Number.

$$\varepsilon(t) = \varepsilon_o(N_{De}^r + 1) \qquad 2.23$$

Equations 2.21 through 2.23 are nonlinear expressions for strain in terms of elapsed time. Specifically they are power law relationships. The resulting predicted creep behavior is plotted versus time in Figure 2.26 for the rheological parameters measured for the three polycarbonates. The ordinate axis may be interpreted as the amount of creep strain relative to the initial strain. As with stress relaxation, the higher molecular weight material shows greater short time response. Further, on a percentage basis, the creep response is the same for each material regardless of the initial strain. This is the analogue of the assumption used in the stress relaxation experiments. Figure 2.26 shows qualitatively the expected creep response of a material in tension; however, the power law relationship is fundamentally different from the exponential predictions obtained with the Kelvin and Jefferies models. It is noted, however, that empirical power relationships have previously been used to describe the creep behavior in materials (2-31,2-50). It would be desirable to investigate the creep behavior of the glassy polymers studied here to evaluate the power law prediction of the generalized Maxwell Model for creep kinematics.

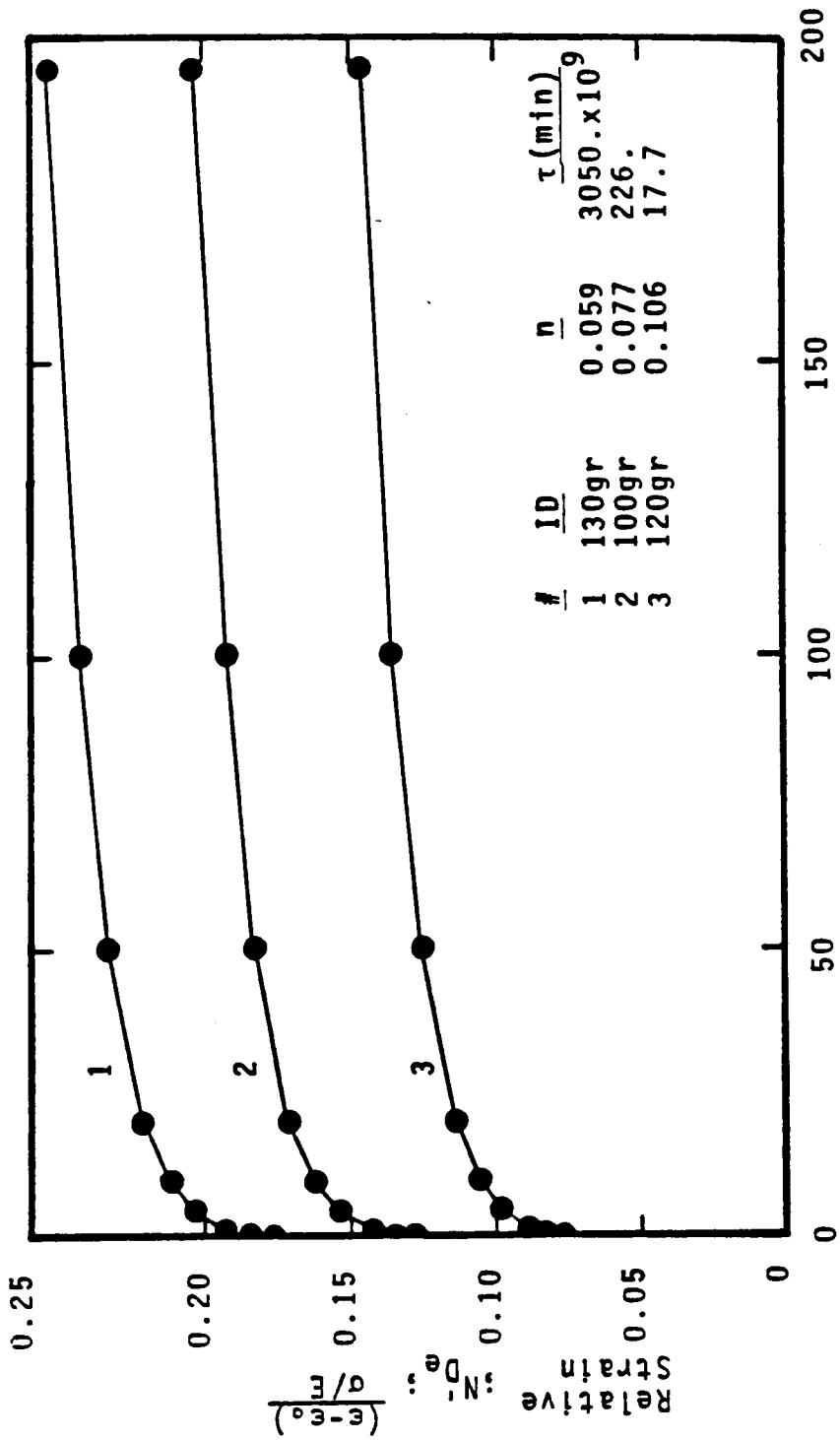

Figure 2.26. Non-Newtonian creep behavior predicted by the generalized Maxwell model for three polycarbonates.

The creep predictions of the model can however be tested in a general qualitative manner. It has been shown that in glasses such as poly(methyl methacrylate) the rheological shape factor is relatively high which is indicative of more transient long term deformations. Conversely the polysulfones exhibit considerably lower values for n which theoretically produce more stable long term behavior. Table 2.13 presents creep data (2-50) for three materials used in this study. It is observed that the acrylic polymer is considerably less resistant to creep than the polycarbonate or polysulfone. This observation is in accordance with the theoretical prediction based on experimental measurement.

The time dependent relaxation effects mentioned above should be discussed in terms of the apparent viscosity of the material. The ability of the generalized Maxwell model to predict relative creep or impact resistance is a manifestation of a time dependent viscosity. Consider Equation 2.7b, which is the expression for viscous stress dissipation in the Maxwell element. This equation can be simplified algebraically and by the chain rule of differentials to obtain an expression for viscous stress in terms of the elastic modulus multiplied by a dimensionless rate of strain.

$$\sigma = E(\varepsilon)\frac{d\varepsilon}{dT} \qquad 2.24$$

Substituting Equation 2.11 into the above relation and differentiating with respect to time, the expression for viscous stress in terms of a

Table 2.13. Creep behavior for polymers used in this study (2-50).

	Creep Modulus (GPa)						
Material	1 hr	10 hr	30 hr	100 hr	300 hr	1000 hr	Shape Factor
Poly(methyl methacrylate)		2.83	2.71	2.59	2.48	2.36	0.16
Polycarbonate	2.38	2.31	2.26	2.21	2.17	2.14	0.06-0.11
Polysulfone		2.37		2.34		2.24	0.02

linear rate of strain is obtained. The fluid viscosity is thus expressed as the term in brackets.

$$\sigma = \left[E(\varepsilon)\frac{\tau^n}{n} t^{1-n}\right] \frac{d\varepsilon}{dt} \qquad 2.25$$

$$\mu = \left[E(\varepsilon)\frac{\tau^n}{n} t^{1-n}\right] \qquad 2.26$$

Viscosity is therefore a function of time, and the character of this function is determined by the value of n. A "time thickening" material (viscosity increases with time) is described by a value of n between zero and one, with characteristically good impact dissipation for low n and faster creep dissipation for high n (see Figure 2.1 page 26). Furthermore, a value of n equal to one precipitates the classical constant viscosity for the linear case.

The viscosity of the glasses investigated in this work are easily calculated using Equation 2.26 and the respective material constants. At a time equal to one second, the viscosities of S104 polystyrene and P3500 polysulfone (two extreme cases) at room temperature are 3×10^{11} Pa·s and 5×10^{11} Pa·s respectively. These viscosities are increasing functions of time with the polysulfone increasing at a faster rate (lower n). Figure 2.27 illustrates the time dependent viscosity graphically.

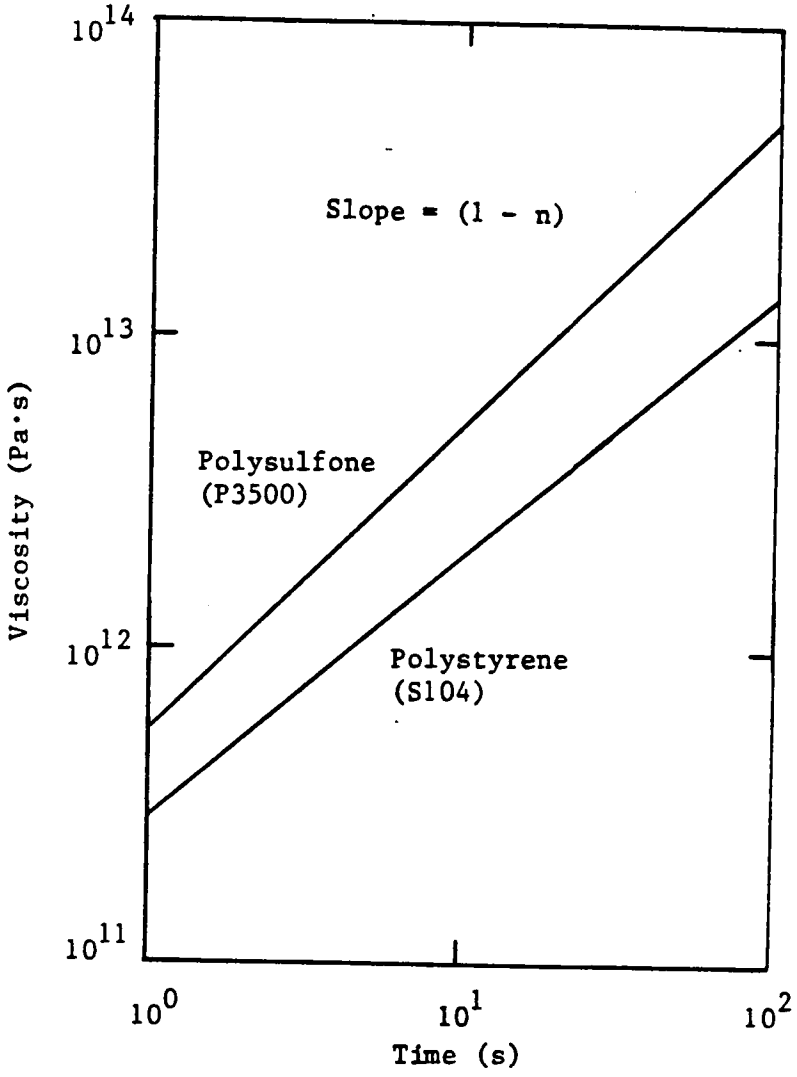

Figure 2.27. Time dependent viscosity function for two glasses.

This insight provides a deeper understanding of the mechanism by which the Williams-Watts relaxation element works in the case of viscoelasticity. The discrete multiple element relaxation terms, common in classical rheology, are replaced by a continuous spectrum of time dependent viscosity. The result is an experimentally more tractable constitutive equation due to the existance of only two material parameters.

In summary, a generalized Maxwell Model has been developed which has many advantages over the classical linear theory. First, the model has great versatility for the variety of usable nonlinear strain and time functions. Stress relaxation can be modelled quite well for static as well as dynamic kinematics by using a two constant Williams-Watts (2-36) exponential construction. Meanwhile the time independent elastic deformation can be modelled with a cosine squared fit. These two nonlinear generalizations have been incorporated into the classical Maxwell Model. The possibility of incorporating classical plasticity theory instead of an empirical nonlinear elasticity correlation exists, but has not yet been explored. Most importantly, the constant rheological parameters with respect to strain and time allow for the correlation of material parameters to the rheological parameters. Specifically, it has been observed that the magnitude of the shape factor n decrease, while the time constant tau increases with increasing molecular weight. Moreover, a modified Deborah Number can be defined which describes elapsed time in terms of the rheological parameters of the material. Lastly, the generalized

model will predict non-Newtonian behavior in creep as well, which the classical linear Maxwell element does not. The creep behavior as well as impact resistance are shown to agree qualitatively with the predictions of the theory based on the observed material parameters. These agreements are founded on the relative long and short term mechanical stability exhibited by the glasses. Therefore, the proposed generalized Maxwell Model has been shown to be a useful nonlinearization of the linear theory for the application to solid state deformation.

CHAPTER III

CHARACTERIZATION OF CRAZING IN GLASSY POLYMERS

3.1. Introduction to Crazing Behavior

In the previous chapter the tensile deformation of solid state viscoelastic materials was modelled using a constitutive equation which assumes a homogeneous deformation of the sample. For the case of polymers in the glassy state, this assumption is not always correct. Under certain conditions these materials exhibit an inhomogeneous deformation known as crazing. However the utility of the simple mechanical model, as demonstrated in the previous chapter for crazable materials, owes itself to the fact that crazed matter occupies less than one percent of the total specimen and that crazes constitute a microscopic yield phenomenon which does not seem to precipitate catastrophic material deformations such as necking, slipping or banding.

The material deformations associated with crazing do, however, play an important role in determining the mechanical properties of the polymer. For example, it is widely known (3-1) that addition of a few volume percent of rubber inclusions to a polystyrene matrix (high impact polystyrene) will transform an extremely brittle material into one which fails in a ductile manner. The mechanism for this material property transformation is that the rubber particles provide nucleation sites for the initiation of crazes. As a result the modified material is profusely crazed at high stresses while the pure

glass may only be lightly crazed. Therefore the crazing behavior acts to absorb deformation energy in the form of inhomogeneous, mechanically irreversible and highly oriented crazed matter.

Apparently initiated by Poisson's ratio dilational effects and significant lateral constraint, both which are associated with brittle glass deformation, crazed matter is characterized by relatively large localized strains and high void content. The surrounding bulk material remains at relatively low strain and low void content (possibly homogeneously distributed in the form of free volume), with the interface between the two media being sharp and well defined. It has also been observed (3-2) that cracks develop in the crazed matter and that ultimate catastrophic failure is associated with breakdown of the stress supporting microfibrils as the crack advances through the craze. Therefore a morphological study of crazed matter is important for a fundamental understanding of the mechanical properties of glassy polymers.

The existence of voids and cracks in well developed crazed polymer glasses provides an electron density distribution which motivates the scattering of electromagnetic radiation. Specifically small-angle x-ray scattering (SAXS) is an extremely useful tool for investigating the morphology of polymer crazes. The remainder of this chapter is thus a report of a SAXS study of the morphology of crazed polymer glasses whose mechanical properties were investigated in the previous chapter. The purpose of the study is to understand how the craze morphology affects the mechanical performance. We will continue

with a more in depth descriptive review of the known morphology of polymer crazes, followed by a theoretical review of the SAXS technique as applied to crazing of glassy polymers.

3.2. Review of Crazing Background and Literature

Two comprehensive reviews on the subject of crazing appeared in 1973 by Kambour (3-3) and Rabinowitz and Beardmore (3-4) . Kausch (3-5) has reviewed the literature from 1973 to 1978 in his book "Polymer Fracture." There have been developments on the subject of crazing since the writing of Kausch, and they will be discussed in this section. First, a phenomenological description of the well established aspects of crazing is given, followed by a review of the major experimental techniques, then the contributions to the craze literature since 1978 are reviewed, followed by a discussion of the goals of the present effort.

3.2.1. Phenomenonological Description of Crazes

Crazing, which occurs in amorphous and semi-crystalline polymers (3-5), appears to the eye as a series of tiny cracks (3-4,3-6). Crazes have many features in common with cracks: they grow perpendicular to the axis of principal stress (3-7,3-8), they reflect light in a manner similar to cracks (3-9,3-10), and they often precede fracture (11) . It was not until the work of Sauer et al. (3-12,3-13), that crazes were differentiated from true cracks. Using wide-angle x-ray diffraction techniques and stress analysis, they (3-12,3-13) deduced that crazes must contain a network of oriented

polymer connecting the bulk polymer interfaces. The oriented polymer, often called microfibrils, is able to support the stress.

Since that time, many electron microscopy studies of crazes have been performed (3-14 through 3-28). All of which support the conclusions of Sauer et al. (3-12,3-13). Generally, electron micrographs of crazed matter reveal a network of highly oriented fibrils and voids, whose dimensions are on the order of 10 to 20 nm.

Kambour (3-29) was the first to study the small-angle x-ray scattering behavior (SAXS) of crazes. His results revealed scattering centers of 7 to 10 nm, so he concluded that SAXS and electron microscopy experiments yielded comparable results. Since Kambour's initial SAXS experiment (3-29) many researchers have used SAXS techniques to characterize the morphology of crazes (3-30 through 3-32).

Despite the large number of experiments on crazing, no general agreement about specific craze morphology or craze initiation mechanisms has been reached. The confusion is probably a result of the wide range of experimental techniques and sample compositions that have been employed. However there are many characteristics of crazes which have been well established.

To the unaided eye crazes appear similar to cracks extending in a plane perpendicular to the axis of principal stress to cover almost the entire cross section. Like cracks, crazes tend to be wedge shaped with an angle between bulk polymer interfaces of less than five degrees (3-33). Crazing is considered a yield phenomenon (3-34); it

is the process by which an elemental volume of polymer strains approximately 100 percent under lateral constraint, while bulk polymer strain remains below two percent (3-7,3-35). The result is a sharply bound region of crazed matter consisting of oriented fibrils and voids which connect regions of undeformed polymer (3-15 through 3-18). This structure has been described as an open celled foam in which the void and fibril dimensions are approximately 20 nm in diameter and the void fraction is about 50 percent (3-31). The voided regions are interconnected such that liquids will diffuse throughout the crazed matter. The width of the craze (in the tensile direction) varies with distance away from the tip, and is usually less than one micrometer (3-15 through 3-18). Deformations associated with crazing are generally considered irreversible; however, some elastic recovery occurs upon unloading (3-35).

During fracture cracks propagate through various paths inside the craze (3-2) depending on the rate of strain. At low strain rates (3-2), cracks propagate through the central regions of the craze known as the midrib (3-2). The midrib is a section of the craze which contains a higher than average void fraction, and it extends the width of the craze perpendicular to the stress (3-2,3-15 through 3-18). High strain rates (3-2) produce cracks which alternate between bulk polymer interfaces and propagate in a random manner. In all cases crazes or highly voided craze like material provides the crack propagation medium (3-36,3-37,3-38).

A glassy polymer must meet several criteria before it will exhibit the crazing phenomenon. First, its number averaged molecular weight must be greater than twice the entanglement molecular weight (3-39). In the case of shock loading, the applied tensile stress must be greater than the characteristic crazing stress of the polymer, (3-7,3-8). However, if the crazing stress is not exceeded, a fatigue phenomenon may occur. That is, crazing may occur over time under lower than critical stresses (3-40).

3.2.2. Major Investigative Tools

For an instrument to be most useful in the study of the morphology of polymeric crazes it must be able to resolve features in the range of 10 nm to 1000 nm. Electron microscopy and small-angle x-ray scattering have been used to great extent in the morphology studies of crazes. These two topics will be dealt with separately in the following discussion.

At first, electron microscopy seems most desirable because of the ability to view crazed matter directly, but there are experimental difficulties. Scanning electron microscopy (SEM) studies of craze morphology are possible because cracks are known to propagate through crazes (3-36,3-37,3-38). Thus, by studying fracture surfaces, important information about crazes may be obtained. However, SEM studies of fracture surfaces are limited by the assumption that craze structure is unaffected during fracture.

Transmission electron microscopy studies (TEM) are possible only in thin films. Several types of studies are available: films microtomed from a crazed bulk sample (3-25), films microtomed from bulk uncrazed sample then strained to produce crazes (3-16), or solution cast films which are strained to produce crazes (3-11). Since there is doubt that the microstructure of crazes in films is the same as that formed in bulk samples, studies of crazes in thin films (1000 nm) have been controversial (3-15,3-41). Some researchers (3-25) have attempted to microtome films of crazes formed from the bulk. They reinforce the craze by diffusing a sulfur eutectic liquid into the voided regions, which solidifies before cutting and the solid later sublimes in the atmosphere of a microscope. However, this technique has been criticized as aging the craze structure (3-15,3-16,3-17). Thus microscopy techniques have severe experimental limitations for the application to crazing.

Recently, the largest contribution to the crazing literature using TEM has been given by Kramer et al. (3-2,3-11,3-36,3-37,3-38,3-42,3-43). They developed a method by which crazes in thin films may be observed under load in an electron microscope (3-11). Basically, the technique (3-11) involves bonding a thin film onto a copper mesh. By straining the grid, a permanent deformation may be applied to the film.

Lauterwasser and Kramer (3-2) studied microscopic mechanisms of craze growth and fracture. They found that crazes thicken predominantly by a surface drawing mechanism rather than fibril creep. It was also noted that void fraction of crazed matter is proportional to the surface stress of the craze interface during formation. The midrib has a higher void fraction than other regions because it was formed at the craze tip where stresses are higher. The other regions are formed by surface drawing after the craze has developed. The void fractions of these regions are lower because the surface stresses are lower. Since their micrographs revealed no voids adjacent to the advancing craze tip, these authors support the Taylor meniscus instability mechanism for craze formation (3-44) since no precraze voiding is required for this model. For fracture mechanisms it was noted that some fibril creep must occur or fracture will never happen. It was postulated that slow disentanglement of polymer chains occurs at the midrib, thus nucleating a crack. At this time further surface drawing occurs near the interface at high surface energies. Thus, the crack may propagate near the midrib or interface depending on which is energetically more favorable. Generally, at low strain rates cracks propagate at the midrib, while at high strain rates they propagate near the interface.

Farrar and Kramer (3-11) studied the microstructure of crazes in oriented polystyrene. They report that crazes formed parallel to the axis of orientation have a higher void fraction than crazes formed in isotropic media, which in turn have a higher void fraction than

crazes formed perpendicular to the axis of orientation. Similarly, craze thickness increases with increasing initial orientation parallel to the craze. Also, more crazes can be formed perpendicular to the orientation axis than parallel to it. These results are interpreted in terms of the tensile strength of the bulk polymer, and the ability to form fibrils.

Donald and Kramer (3-36) studied in more detail the mechanisms of craze tip advance than did Lauterwasser and Kramer (3-39). They employed stereo microscopy and tilting techniques to view the craze tip from a three dimensional perspective. Regions of lower density ahead of the advancing craze tip are observed and classified as fingers. These fingers are predicted by the meniscus instability theory (3-44). As the meniscus between bulk polymer and craze breaks down, fibrils are formed. A stress analysis is performed using this meniscus instability theory, and the wavelength of the instability is shown to correlate well with the distance between fibrils.

Donald and Kramer (3-37) also studied the effect of strain history on craze microstructure. By straining thin films in a stepwise manner, they attempted to prove an earlier theory. That is, the characteristic draw ratio of crazed matter is proportional to the surface stress of the craze as influenced by the bulk stress. However, it was found that the applied stress to the sample had no effect on the draw ratio of thickened crazes. They concluded that relaxation of craze surface stresses occurs quickly after each deformation and that surface stress is difficult to control.

Thirdly, Donald and Kramer (3-38) studied the effect of molecular entanglements on craze microstructure. They were able to study the effect of entanglement density using various polymers whose entanglement molecular weight varied from 43,000 (PTBS) to 2,500 (PC). A good correlation was observed between entanglement density and fibril draw ratio. Those polymers having a large entanglement molecular weight (Me) also have a large extension ratio. Therefore void fraction increases with entanglement molecular weight.

King and Kramer (3-43) studied craze intersections of biaxially stretched polystyrene. They showed that volumes intersected by crazes contain a higher void fraction than normal crazed volumes. The secondary craze exposes interconnections between the primary craze fibrils, which exhibit load bearing capability normal to the secondary craze, parallel to the primary craze. Even though craze intersections can bear stress in any direction, the volume has been considerably weakened by the biaxial deformation. Thus, craze intersections provide line nucleation sites for cracks, and fracture occurs at a lower stress than samples with no craze intersections.

Wellinghoff and Baer (3-45) classified polymeric glasses as to their deformation characteristics. Type one glasses craze at all temperatures below their glass transition temperature, and are characterized as vinyl polymers with bulky side groups. Type two glasses craze only at temperatures close to their glass transition temperature and exhibit other deformation processes such as shear banding. These polymers are characterized as polymers with flexible

main chains. It was found that all type one glasses can be transformed into type two glasses simply by forming blends of the two types. Type two polymers typically show less fibrillar strains than type one and the presence of shear bands stop the propagation of crazes.

Attention will now be focused on several important SAXS studies of polymeric crazes. SAXS experiments have one distinct advantage in that they are able to examine bulk samples while leaving them undamaged. Since the electron density difference between polymer and void is large, crazes provide intense scattering media. However, the craze may not be viewed directly, and data analysis is not straightforward (3-46,3-47). So far, no SAXS analysis procedure has met with wide approval, therefore the results are controversial and sometimes contradictory.

This contradiction may be due to varying experimental methods, sample compositions and sample preparation. The SAXS data have basically been treated in two ways, namely the Guinier (3-47) and the modified Porod analysis (3-48,3-49). Most methods attempt to characterize the size distribution function of scattering centers in the craze, but disagreement as to the nature of the scattering center exists.

Most of the SAXS studies of crazes have been done on the Kratky camera in the long slit geometry (3-10,3-31,3-32,3-48). Since scattering functions of crazes are known to be anisotropic, this method suffers from the difficulty of deconvoluting anisotropic

functions (3-50). Other SAXS experiments have been done in the pinhole geometry (3-31). Most of these results suffered from the use of photographic detectors and/or limited low angle resolution.

Brown and Kramer (3-48) performed SAXS experiments of crazes in bulk samples of polystyrene using the Kratky camera in the long slit geometry. Based on what one might expect from the scattering from fibrils, they termed the scattering in the tensile axis as anomalous, and the scattering in the nontensile direction as normal. Crazes are modelled as consisting of oriented fibrils spanning the width of the craze with no interconnections. The existence of the anomalous streak was said to originate from a slit scattering effect. The slit being defined by the craze interface with the polymer. This model, including fibril diameters calculated from SAXS results, is shown to be consistent with the Taylor meniscus instability theory (3-44) using stress analysis. They also cite results of TEM studies to support this model.

The work of Westbrook et al. (3-47) disagrees with the work of Brown and Kramer (3-48). Westbrook et al. reported on SAXS studies of polystyrene crazes done with pinhole geometry and a two dimensional position sensitive detector. They made issue of the anomalous streak (3-47). Noting a more intense anomalous streak than did Brown and Kramer (3-48), Westbrook et al. claimed the oriented rod model contains no mechanism by which x-rays could be diffracted in the tensile direction. Westbrook et al. assumes the anomalous streak as diffraction from voids and interprets it as a result of distances

between interconnections of fibrils. Therefore the open celled foam model of Kambour (3-25) was reinforced. Brown later (3-51) suggested the anomalous streak comes from reflections off the craze bulk polymer interfaces. Unfortunately, the reflection phenomenon was not considered in the papers of Brown and Kramer (3-48) or Westbrook et al. (3-47).

However, the suggestions of Brown (3-48,3-51) inspired further investigation of the anomalous streak by Westbrook et al. (3-40,3-52). Using a tilting technique, they showed that the anomalous scattering is predominantly a specular reflection phenomenon of x-rays off regularly occurring surfaces in the crazed matter. However, the question of the existence of slit scattering was apparently left unresolved.

3.2.3. SAXS Mechanisms from Crazes: A Resolution

Figure 3.1 shows two representative SAXS patterns from different molecular weight polystyrenes. The tensile axis direction shows a rather intense streak of scattered radiation while the diffuse scattering background is relatively isotropic. As indicated above there still exists spirited discussion as to the origin of the SAXS pattern from crazed matter. To date three mechanisms have been proposed: volume scattering from voids and/or fibrils contained in the crazed matter, slit scattering caused by dispersion through the lower density craze and diffuse reflection caused by surfaces created in the crazed material. These possibilities will now be discussed.

Until recently (1981) all SAXS studies of polymer crazes have interpreted results in terms of volume scattering. Researchers have analyzed and interpreted their data in various ways. For example, scattering models have included scattering from fibril features or microvoid features (or both), scattering by reflection and scattering from a slit. All experimentalists agree that the scattering represented by the rather isotropic intensity contours of Figure 3.1 (nontensile axis scattering) is resulting from a volume scattering effect. Citing TEM studies of intersected crazes in biaxially stretched polystyrene (3-43), this author (3-47) has chosen to adopt an open celled foam model of craze morphology where voided regions are defined by the polymer fibrils and the interconnections between fibrils. Thus, voids are considered to be the discontinuous phase and are isolated and defined well enough to respond independently to radiation. This type of void scattering model is supported by the diffuse isotropic scattering which is observed in polystyrene. Further evidence of this void volume scattering hypothesis was given in this author's Masters thesis (3-40). It was observed that the power of the isotropic scattering function decreased with increasing molecular weight (constant stress history). Independent TEM results (3-38) show that the void fraction of crazed matter also decreased with increasing molecular weight. These observations are self consistent given the above hypothesis. Thus for the present work, the nonanomalous scattering from crazes will be interpreted as volume scattering from voids contained in the crazes.

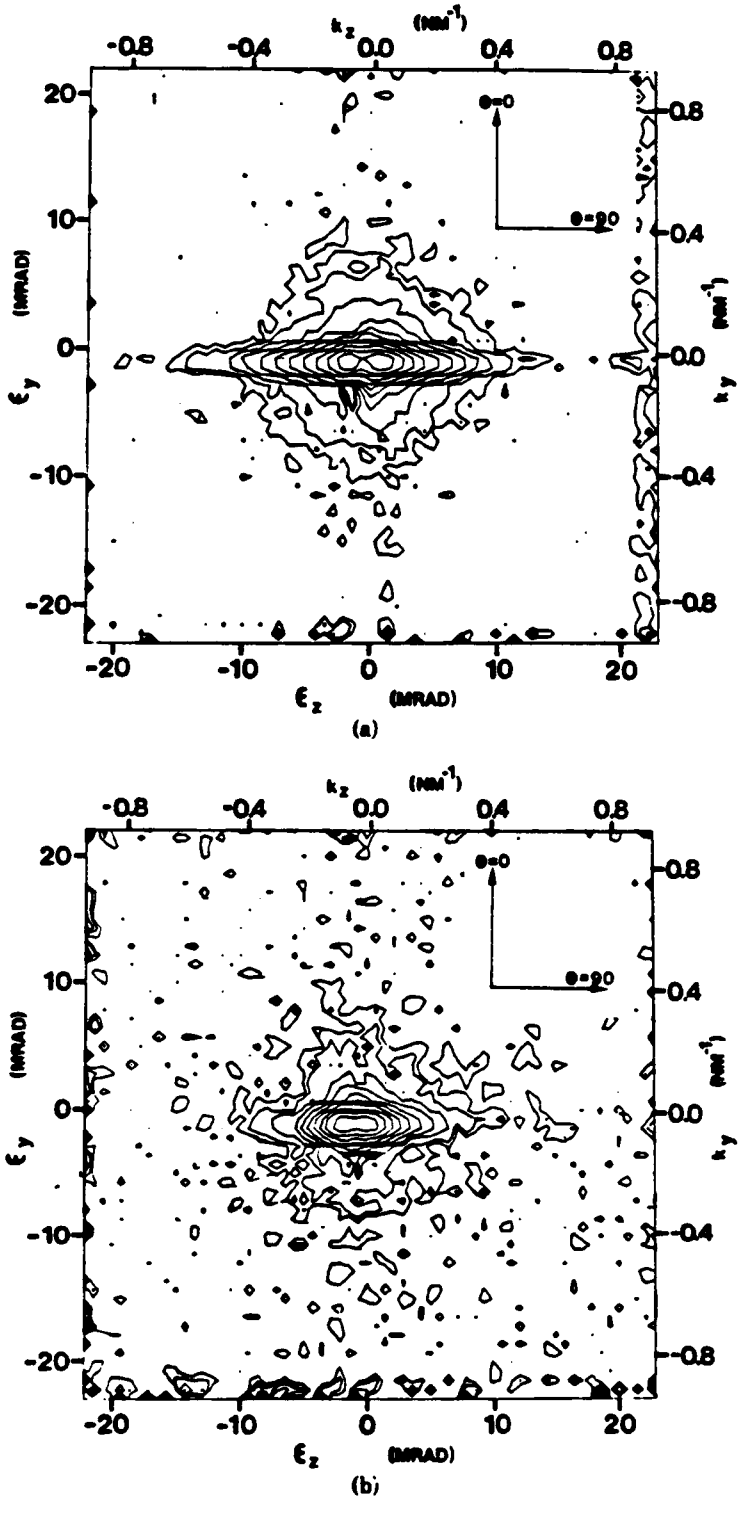

Figure 3.1. SAXS contour patterns from two different molecular weight polystyrenes.

The slit scattering effect has been proposed by Brown and Kramer (3-48). They use an oriented rod model to simulate the structure of crazed matter and developed two theoretical equations for scattered intensity. First for scattering in the nontensile axis for an assemblage of randomly spaced perfectly oriented rods, they write:

$$i = N_c A l_c (\Delta\rho)^2 V_f \pi D_f \frac{J_1^2(\pi D S_r)}{(\pi D S_r)^2} (2\Delta\theta)\lambda \qquad 3.1$$

where N_c=the number of crazes, A=the area of a craze, l_c=the width of a craze, $(\Delta\rho)$ =the electron density difference between polymer and void, V_f=the volume fraction of fibrils, D_f=the diameter of the fibril, J_1=the Bessel function of order one, S=scattering vector, λ=x-ray wavelength, and θ=the solid angle of the detector. They also give an equation for slit scattering as the following.

$$i_a = N_c A (\Delta\rho)^2 (1 - V_f)^2 \lambda^2 \frac{\sin^2(\pi l_c S_z)}{\phi_0 (\pi D S_z)^2} (2\Delta\theta)\lambda \qquad 3.2$$

where ϕ_0= the angle over which slit scattering will occur and l_c is the width of the craze.

Equations 3.1 and 3.2 were obtained by integration over the solid angle of the detector element (Kratky geometry). Realizing that exact values for N_c and A are indeterminate, these authors generated a meaningful equation by dividing Equation 3.2 by 3.1 to obtain the relative scattering power of slit scattering.

$$i_a/i = \frac{(1 - V_f)^2 \left(\frac{S_r}{S_z}\right)^2 \lambda^2 \sin^2(\pi l_c \bar{S}_z)}{V_f \phi_0 l_c J_1^2(\pi D \bar{S}_r)} \qquad 3.3$$

Finally using values of $\bar{S}_r=\bar{S}_z=0.026$ nm^{-1}, $\langle \sin \P 1\tilde{S} \rangle=0.5$, $\phi_o=0.02$ rad, D=6.0 nm, l_c=250 nm, and $V_f=0.2$, they estimate i_a/i to be 0.28.

Brown and Kramer (3-48) acknowledge that observed "...experimental (i_a/i) ratios are greater than 1000. It thus seems likely that while slit-like diffraction from crazes can account qualitatively for the anomalous intensity spike, other contributions such as that of reflection from craze surfaces must be more important." Kramer has further stated, however, that the effect of slit scattering should nonetheless be observable in the tensile direction, and must be accounted for in any theoretical treatment of the data.

Withholding comment for the moment on the validity of the model adopted by Brown and Kramer (3-48), their analytical development deserves further study. If one plots the function given in Equation 3.3 for the strength of the slit scattering relative to the volume scattering versus scattering angle using the material constants given by them, one obtains Figure 3.2a. The intensity ratio decreases by a slope of two (as they stated) but goes through an intense peak at approximatly 30 mrad. Data to be presented in this present study will show that volume scattering in this region of reciprocal space is finite and measurable for polystyrene and that large intensity maxima do not occur in the anomalous scattering in this region. It should further be noted that they (3-48) used material constants which are not widely accepted for their calculations. If one substitutes more commonly reported values for $V_f=0.5$, D=12.0 nm, and l=1000 nm

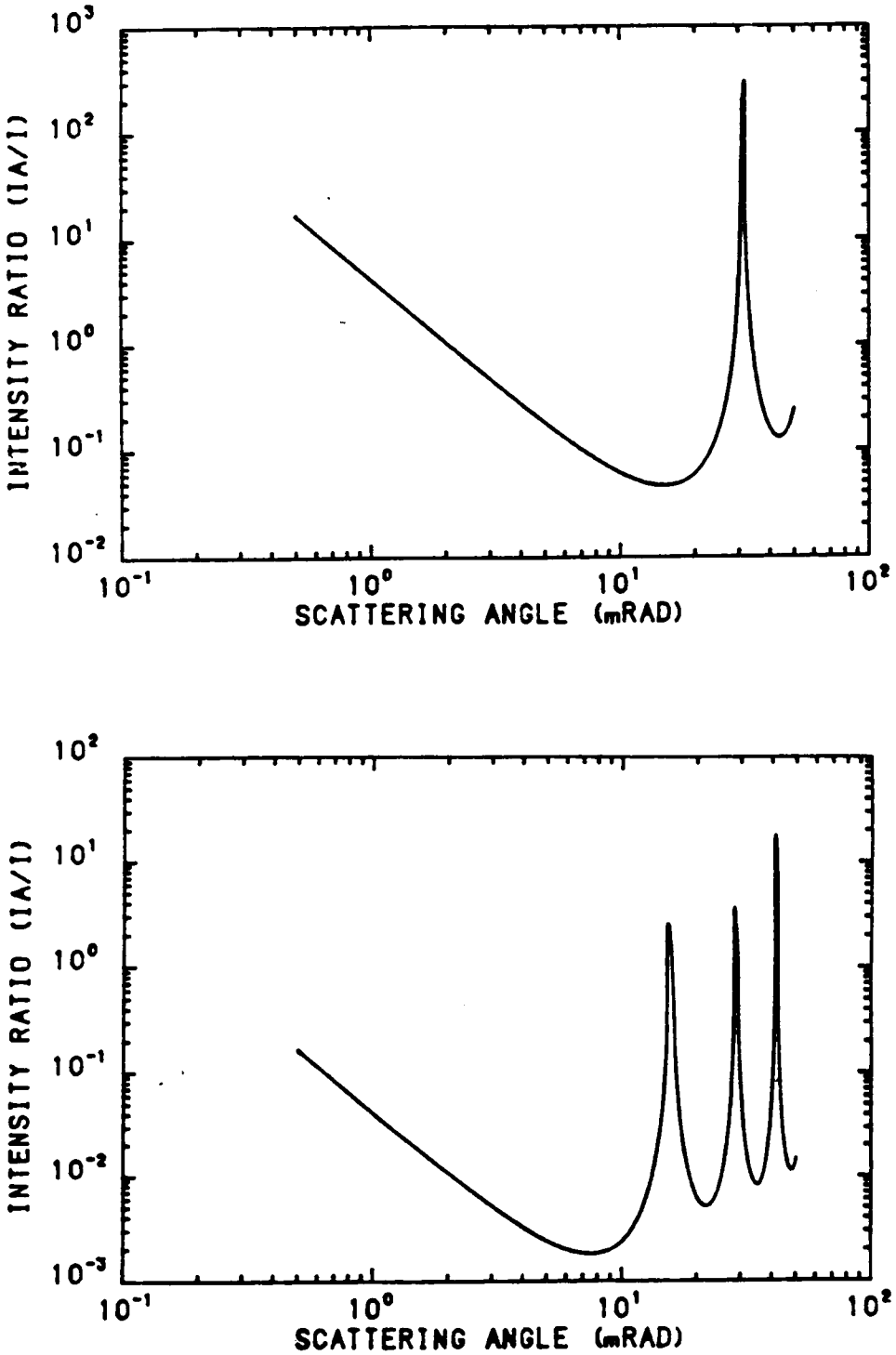

Figure 3.2. Relative strength of theoretical slit scattering as compared to volume scattering as predicted by Equation 3.3. A) For material parameters of <l>=250nm, Vf=0.2 and D=6.0nm. B) For material parameters of <l>=1000nm, Vf=0.5 and D=12.0nm.

(3-3,3-4), one obtains the plot in Figure 3.2b (page 103). The result is similar to 3.2a (page 103) except the slit effect is two orders of magnitude less intense.

It is noted that the large intensity peaks presented in Figure 3.2 a and b are due in part to the Bessel function for the volume scattering intensity approaching zero. Therefore the actual behavior of the slit scattering function is not clear. To help illustrate the slit scattering function for the crazed system it may be useful to examine the character of slit scattering from a single slit whose boundary is opaque. The equation for the intensity dispersion is given by the following equation whose derivation may be found in any treatment of elementary physics (3-53).

$$i/i_o = \frac{\sin^2(\pi l_c S)}{(\pi l_c S)} \qquad 3.4$$

$$S = \frac{2\sin\theta}{\lambda}$$

Using x-ray wavelength of 0.154 nm and two slit widths corresponding to the range of commonly reported craze thicknesses, the slit scattering intensity as a function of scattering angle is plotted in Figure 3.3. It is observed that the intensity reduces to negligible values for both cases at less than one milliradian which is out of the range of the present SAXS experiment. Further if the condition of infinite optical density difference in the slit boundary is relaxed, one would expect even less significance for the slit scattering intensity. Therefore the opinion of this author is that slit

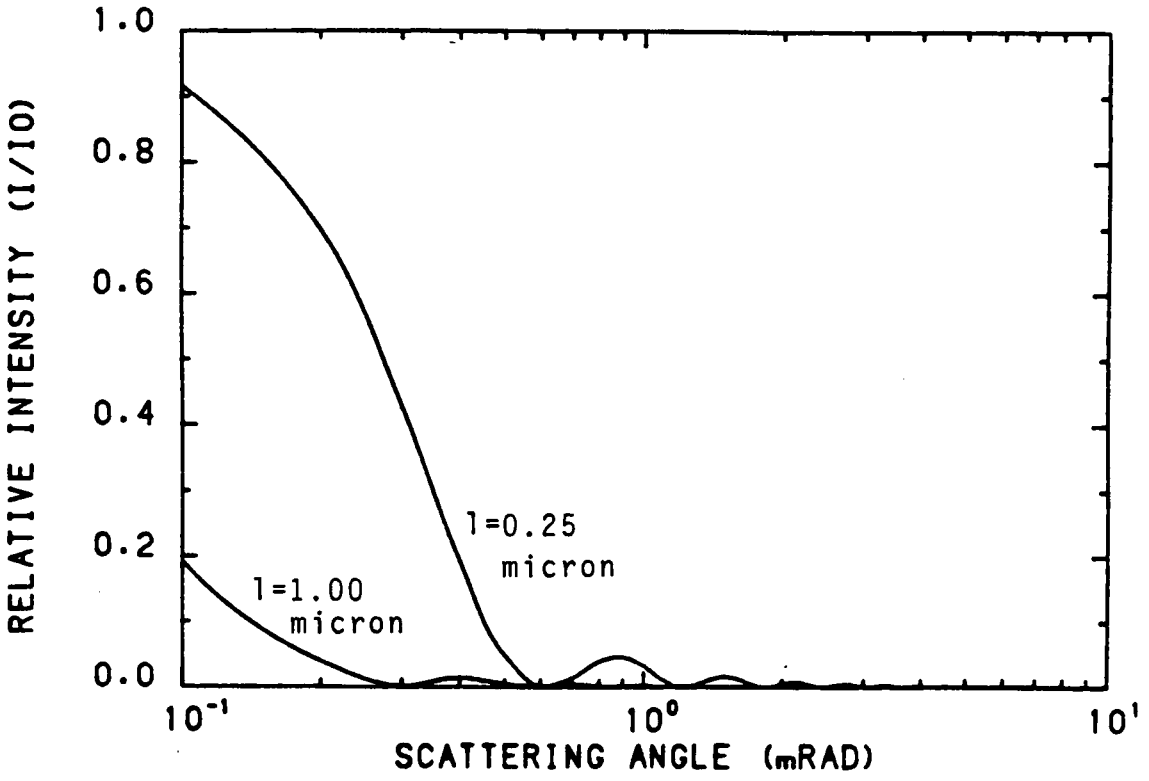

Figure 3.3. Slit scattering as predicted by Equation 3.4 for two values of slit width.

scattering can account for the anomalous scattering from polymer crazes neither quantitatively nor qualitatively and thus will not be considered further in this work.

The hypothesis for specular reflection mechanisms being the primary contributor to the anomalous streak for polystyrene crazes was first proposed by Brown (3-48,3-51); however, experimental evidence supporting this hypothesis was first presented by Westbrook et al. (3-52). Later Tang et al. (3-54,3-55) provided the first complete theoretical treatment of the reflection phenomenon for the application to crazing. She applied existing surface scattering theory (3-56 through 3-61) for the case of reflection from internal surfaces in crazed matter. Surface roughness in this case is defined as the average distance between fluctuations in microcrack formation in the craze. The elements of the surface scattering theory as described by Tang (3-54,3-55) will be briefly reviewed.

First it is noted that there exists great similarity between the mathematics of surface and volume scattering vector theory. The dimensionality of the former being one less than the latter. Figure 3.4 should be carefully consulted in order to define some relevant angles. The intensity scattered from surfaces is equal to the differential fraction dP of incident energy per unit solid angle $d\Omega=\sin\phi d\phi d\chi$ scattered into the the direction specified by the polar angle ϕ and the azimuthal angle χ. This intensity is given by the product of an optical scattering factor and a surface scattering factor (3-54,3-55).

$$I(s) = \frac{dP}{d\Omega} = (\text{Surface Factor})(\text{Optical Factor}) \qquad 3.5$$

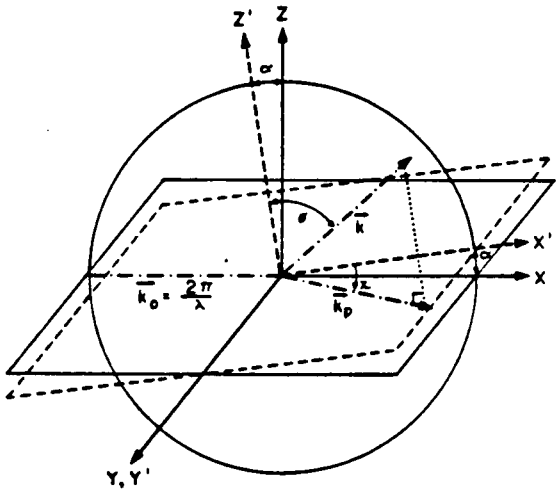

Figure 3.4. Geometry of SAXS experiment showing important angles for surface scattering vector theory.

The surface scattering factor is completely analagous to the volume scattering factor and it depends only on the statistical properties of the surface. This surface factor $g(S_p)$ is the product of the surface scattering invariant and the two dimensional Fourier transform of the surface correlation function.

$$\begin{aligned} g(\bar{S}_p) &= K_s \mathfrak{F}_2(G(\bar{r}_p)) \\ &= K_s \int_0^{\infty} G(\bar{r}_p) \exp(-i\vec{S}_p \cdot \vec{r}_p) d^2 r_p \end{aligned} \qquad 3.6$$

The optical scattering factor is needed in surface scattering treatments because surface scattering is a phenomenon which also depends upon the incident angle of the radiation relative to the surfaces as well as optical properties, polarizability and angular radiation characteristics of photons in the presence of an interface.

$$\text{Optical Factor} = \left(\frac{4\pi}{\lambda} \cos\phi\right)^2 (1 - \eta_{12}^2)^2 \left[\frac{\psi_\phi}{(\nu - iq\eta_{12}^2)^2} + \frac{\psi_\chi}{(\nu - iq)^2}\right] \qquad 3.7$$

where:

$$\psi_\phi = \frac{\nu\nu_o \cos\chi + \vec{K}_p \vec{K}_o \eta_{12}^2}{\nu_o - iq\eta_{12}^2} - \frac{i(1/\lambda)\nu \sin\chi}{\nu_o - iq_o} \qquad 3.8$$

$$\psi_\chi = (1/\lambda)\left[\frac{\nu_o \sin\chi}{\nu_o - iq_o\eta_{12}^2} + \frac{i(1/\lambda)\cos\chi}{\nu_o - iq_o}\right]$$

The polar angles ϕ_o and ϕ are measured from the normal of the average surface plane, the azimuthal angle χ is measured relative to the plane

of incidence, and q and q_o are the components of the wave vectors perpendicular to the average surface.

$$q_o = |\vec{K}_o|\cos\phi_o \qquad q = |\vec{K}|\cos\phi \qquad 3.9$$

$$\nu_o = \frac{2\pi}{\lambda}(\sin\phi_o - \eta_{12}^2) \qquad \nu = \frac{2\pi}{\lambda}(\sin\phi - \eta_{12}^2)$$

One can now assume that there exists a Gaussian distribution of correlation lengths, tau, which describe the relative smoothness or roughness of the surface. A tau of zero implies there will be no correlation between two different points on the surface; tau approaching zero implies a surface with densely packed irregularities. Hence a large tau implies large distances between irregularities. Thus the isotropic Gaussian correlation function $G(r_p)$ can be written as:

$$G(\bar{r}_p) = \exp(-\bar{r}_p^2/\tau^2) \qquad 3.10$$

Upon substituting this equation into the surface scattering factor (Equation 3.6) and integrating we obtain the following.

$$g(\bar{S}_p) = \frac{K_s 2\pi\tau^2}{(1 + (\bar{S}_p\tau)^2)^{3/2}} \qquad 3.11$$

Thus if the scattering intensity function is measured it is possible to determine tau.

Likewise a similar analysis for the nontensile axis volume scattering intensity function is possible. Here, a random distribution for the radius of scattering centers is assumed. Thus the correlation function for scattering center sizes can be calculated if given the intensity as a function of scattering angle. The corresponding equations governing these relationships can be expressed as follows:

$$I(\bar{S}) = K_v \mathfrak{F}_3(\gamma(\bar{r})) = K_v \int_0^\infty \gamma(\bar{r}_p) \exp(-i\vec{S}_p \cdot \vec{r}_p)\, d^3\vec{r}_p \qquad 3.12$$

where:

$$\gamma(\bar{r}_p) = \exp(-\vec{r}/l) \qquad 3.13$$

The scattering invariants, Kv and Ks, which are proportional to the total volume of scattering centers and the total surface area respectively, are calculated by the following formulae.

$$K_v = (1/2\pi^3) \int_0^\infty I(\vec{S})\, dV_s \qquad 3.14$$

$$K_s = (1/2\pi^3) \int_0^\infty g(\vec{S}_p)\, d^2S_p$$

For the application to polymer craze morphology, the average surface scattering correlation distance will be interpreted (3-54,3-55) as the average distance between microcrack discontinuities. Further, the average volume scattering correlation distance will be interpreted as the average radius of microvoids contained in the crazed matter.

The algorithms for computing the correlation functions for both the surface and volume scattering intensity functions were developed by Tang and published in her dissertation (3-54). These routines will be used in the present work for analyzing the scattering patterns obtained from crazed samples of polycarbonate, poly(methyl methacrylate) and polysulfone for comparison to the results of Tang (3-54,3-55) for polystyrene.

3.2.4. The Fractal Theory of SAXS

In the classical treatment of small-angle x-ray scattering, if the scattering centers have smooth, well defined surfaces, the high angle region of the scattering function obeys the Porod (3-62) approximation. In this case, the scattered intensity decreases to the inverse fourth power of the scattering vector, and the slope of the Porod plot is proportional to the surface area of the scattering centers in the sample. If, however, the scattering intensity does not obey the Porod law, and the surfaces are known to be rough and not well defined, then another interpretation for the morphology of scattering centers is needed.

Recently, the subject of fractal theory (3-63) (or fractional geometry) has been applied to identify geometric features of scattering centers via SAXS. These studies (3-64 through 3-67) have included systems of silica aggregates and gold colloids. A fractal object is characterized by the dependence of the total mass on the characteristic length scale for which the object is investigated.

$$\text{Mass} \sim \text{Length}^{D} \qquad 3.15$$

where D is the fractal or Hausdorff dimension and may not be an integer value.

Two characteristically different types of fractal systems which can be identified using SAXS are the porous and the aggregate systems. It has been shown (3-68) that, for scattering from porous materials, the limiting form for I(s) for large values of s can be written as:

$$I(S) \sim \pi N_o \Gamma(5-D)\sin(\pi(D-1)/2)\cdot S^{-(6-D)} \qquad 3.16$$

Thus I(s) is proportional to the power of 6-D, and for a smooth boundry surface, D=2. For aggregate fractal systems the scattering intensity is shown to have the following proportionality:

$$I(\vec{S}) = \mathfrak{F}_3(\rho_{el}(\vec{r})) = \int_0^{\infty} r^{D-d}\exp(-i\vec{r}\cdot\vec{S})\, dV_s \qquad 3.17$$

where I(s) is proportional to the power of -D. The porous model is used when the slope of the scattering curve is between -3 and -4, while the aggregate model is used when the slope of the scattering curve is between zero and -3.

Since the scattering centers in polymeric crazes are thought of as being rough and not well defined, this fractal scattering theory will be applied to the volume scattering functions observed from tilted crazed samples.

3.2.5. Other Studies

Recently, Brown (3-41,3-69) resumed his crazing studies with small-angle electron scattering (SAES) in an electron microscope. In a preliminary paper (3-69) he outlined a general method for studying SAES patterns for polymeric crazes and cracks using a tilting technique. Later, he (3-41) used this technique to compare the scattering patterns from thin films using SAES to scattering patterns from bulk samples using SAXS data obtained in a previous study (3-48). Brown showed from a theoretical standpoint that the scattering patterns from crazes using SAXS and SAES should be similar if the morphologies are identical. However, the comparison of the data revealed that crazes in thin films had features about three times larger than crazes in bulk samples. He attributed this result to residual toluene (solvent from solution cast films) acting as a plasticizer and the lack of lateral constraint in the thin films.

A theoretical treatment for predicting craze features was developed by Fellers and Huang (3-70). They predicted the average size of a volume element which guarantees that a fluctuation associated with crazing will occur in it. This volume element depends on the applied stress, modulus of compressibility and glass transition temperature. The calculated volume element for polystyrene is shown to be on the order of void sizes observed in crazes. An expression for the entanglement density versus molecular weight is also developed.

Wool and O'Connor (3-71) studied craze healing in polystyrene using optical microscopy. Molecular mechanisms of craze healing were treated analogously to crack healing. A healing envelope in temperature and time is developed. It is shown that even though a craze may appear healed the region still exhibits poor mechanical properties because the molecules have not had sufficient time for complete interpenetration by reptation. Thus, craze reformation occurs faster than the original formation.

3.2.6. Important Considerations for this Study

The variables of interest in this SAXS study of polymer crazes are the chemical composition and the molecular weight of the glass. These parameters seem to affect the character of the amorphous structure. This structure will be defined in the following discussion.

Amorphous polymers are so named because their molecules do not arrange themselves in an orderly way in the equilibrium solid state. Typically, these polymers are transparent because no periodic structure on the order of the wavelegnth of light is present to cause scattering. Glassy polymers will not crystallize because they generally have large side groups or rigid main chains which prohibit orderly packing. Amorphous polymers in equilibrium adopt a random coil conformation in which the location of the main chain is governed by a modified statistical excluded volume theory (3-72).

Even though amorphous polymers have no periodic structure, they do have heterogeneities (3-73,3-74). Some heterogeneities are known as entanglements and chain ends (3-70). Naturally, entanglements tend to strengthen the polymer matrix due to the fact that stress may be supported across an entanglement in directions other than the main chain direction. Unfortunately, there is no precise definition of an entanglement; however, the entanglement molecular weight can be determined from discontinuities in the rheological behavior of the melt. The entanglement number density as a function of molecular weight has been calculated for polystyrene using statistical analysis. Conversely, chain ends tend to weaken the polymer matrix since stress may not be supported in any direction across a defect. Chain ends are easily defined as the termination point of the main chain and their number density may be directly calculated for unbranched polymers using molecular weight data.

The amorphous structure of a polymer seems to be the most important variable in determining the crazing behavior (3-47). Statistical fluctuations in the number density of chain ends and entanglements may ultimately lead to voiding and fibrillation. For example, volume elements consisting of a high number density of matrix strengthening components (entanglements, etc.) and a low number density of matrix weakening components (chain ends, etc.) may fibrillate at low stress levels and vice versa.

The easiest method of changing the number density of structural elements of the polymeric glass is to change the chemical composition. There are several ways to study craze structure as a function of chemical composition. Two easily characterized variables are monomer unit and weight averaged molecular weight.

SAXS studies have shown that craze structures in polymers consisting of different monomer units are dramatically different (3-47). A comparison of polystyrene and polycarbonate craze scattering patterns reveal very few qualitatively similar features. The most obvious difference is the presence of a large intensity maximum in the transverse directions of the polycarbonate scattering pattern where the polystyrene pattern has none. Therefore the two systems must have dramatically different craze morphologies.

Crazing studies in different molecular weight polystyrenes have been reported by Tang (3-54,3-55) using the data analysis procedure outlined in the last section. Her results indicated that both the surface correlation distance, tau, and the volume chord length, l,

generally decreased with increasing molecular weight. Furthermore the volume scattering invariant, Kv, decreases with molecular weight while the surface scattering invariant, Ks, increases. These trends were reported in samples with identical stress histories. The above results of Tang (3-54,3-55) indicate that both the void fraction and the void size in the glass are decreasing with molecular weight. Further, the crack length decreases with increasing molecular weight as shown by tau. These results are consistent with known mechanical property trends in polymer glasses. That is, ultimate properties are enhanced by high molecular weights. In summary, Tang observed that higher molecular weight glasses can support a higher number density of crazes with lower void fraction, void dimensions and crack lengths.

It is the purpose of the present work to extend the crazing studies of Tang (3-54,3-55) to other materials such as polycarbonate, polysulfone, and poly(methyl methacrylate). The molecular weight effects of these materials on their crazing behavior will be studied and compared to the crazing behavior of polystyrene. Commercially available resins will be used for this study. From the results of these morphology studies, we may be able to understand why the polycarbonate materials have greatly enhanced ultimate properties compared to those of polystyrene.

3.3. SAXS Experimental Procedure

In this section, a discussion of the sample preparation and x-ray data analysis techniques will be given. Sample compositions and fabrication techniques will be discussed. Also, a brief discussion of the NCSASR SAXS equipment will be given.

3.3.1. Sample Preparation

Suitable samples for dynamic SAXS analysis of crazing must meet several specifications dictated by the limits of the systems. For a glassy polymer to craze, its number averaged molecular weight must be at least twice the theoretical entanglement molecular weight of the polymer. Also, the optimum path length of the x-ray in the sample is governed by the reciprocal of the linear absorption coefficient of the polymer. Lastly, varying states of molecular orientation will effect the sample performance. Since orientation is not a variable of interest in this study, care must be taken to minimize internal stresses by annealing. With these limitations in mind, samples were prepared in the following way.

The parameters of interest in varying sample compositions are weight averaged molecular weight and monomer unit. Because of their availability, commercial samples of polysulfone, polycarbonate, polystyrene and poly(methyl methacrylate) were used. Their compositions are summarized in the previous chapter in Table 2.1 (page 23).

The tensile bars are made by cutting from sheets of molded polymer whose thickness corresponds to the thickness of the tensile bar. The polymer sheets are compression molded in a picture frame mold. Pelletized polymer is placed inside the mold and processed in the following way:

1. Platens are heated to 80 degrees Centigrade above the glass transition temperature of the glass.
2. Preheat polymer inside mold at this temperature for ten minutes, such that a molten state is achieved.
3. Increase force on mold to 80,000 Newtons over a period of ten minutes, such that bubbles may escape.
4. Relieve pressure on mold and anneal for ten minutes at temperature, such that internal stresses are relieved.
5. Turn off hot press and cool to room temperature slowly. This process takes about five hours.

Steps four and five are done so that an isotropic sheet is made. The birefringence of the material is checked to assure the isotropic character. Samples are punched from sheet using an ASTM tensile bar punch. Lastly the cut edges are polished by stroking in the tensile direction with 600 grit sandpaper.

3.3.2. NCSASR SAXS Apparatus

The NCSASR SAXS apparatus at Oak Ridge National Laboratory has been described in detail in the literature (3-75,3-76) and in the dissertation of Tang (3-54). However, a summary of important characteristics is given here for clarity. The discussion will

briefly cover how the hardware and software are used in the experimental methodology as applied to crazing studies.

Now the major components of the x-ray device are listed and defined. Most of the features described here are represented in Figure 3.5 which is a schematic representation of the SAXS device.

A) X-ray Generator:- The x-ray generator is a 12.0 kilowatt Rigaku-Denki rotating anode device. When operating at 40kv and 40ma with a source to sample distance of 1.6 meters, the copper $K\alpha$ intensity can be as high as 2.5 x10**6 photons per square millimeter per second with a polished anode and good alignment.

B) Monochromation and Collimation: The characteristic K x-rays emitted by the copper anode are further separated into its alpha and beta components by reflection off a pyrolytic graphite single crystal. The monochromation is further achieved with a sophisticated electronic detection system. The angle of the generator with respect to the collimation apparatus is set so that copper K_α (0.154 nm) radiation is used. The beam collimation is accomplished through a pair of one square millimeter pinholes which are separated by 1.6 meters. The pinhole technique is used so that smearing of scattered intensity can be avoided, and thus the deconvolution of the data is not necessary.

C) Detector: The detector, which monitors scattered intensity, is a compound detector known as a two dimensional position sensitive detector. It consists of two selected resistance wires which are meshed and arranged to form a cartesian grid. The grid is virtually divided into 64 x 64 elements, according to the detector resolution

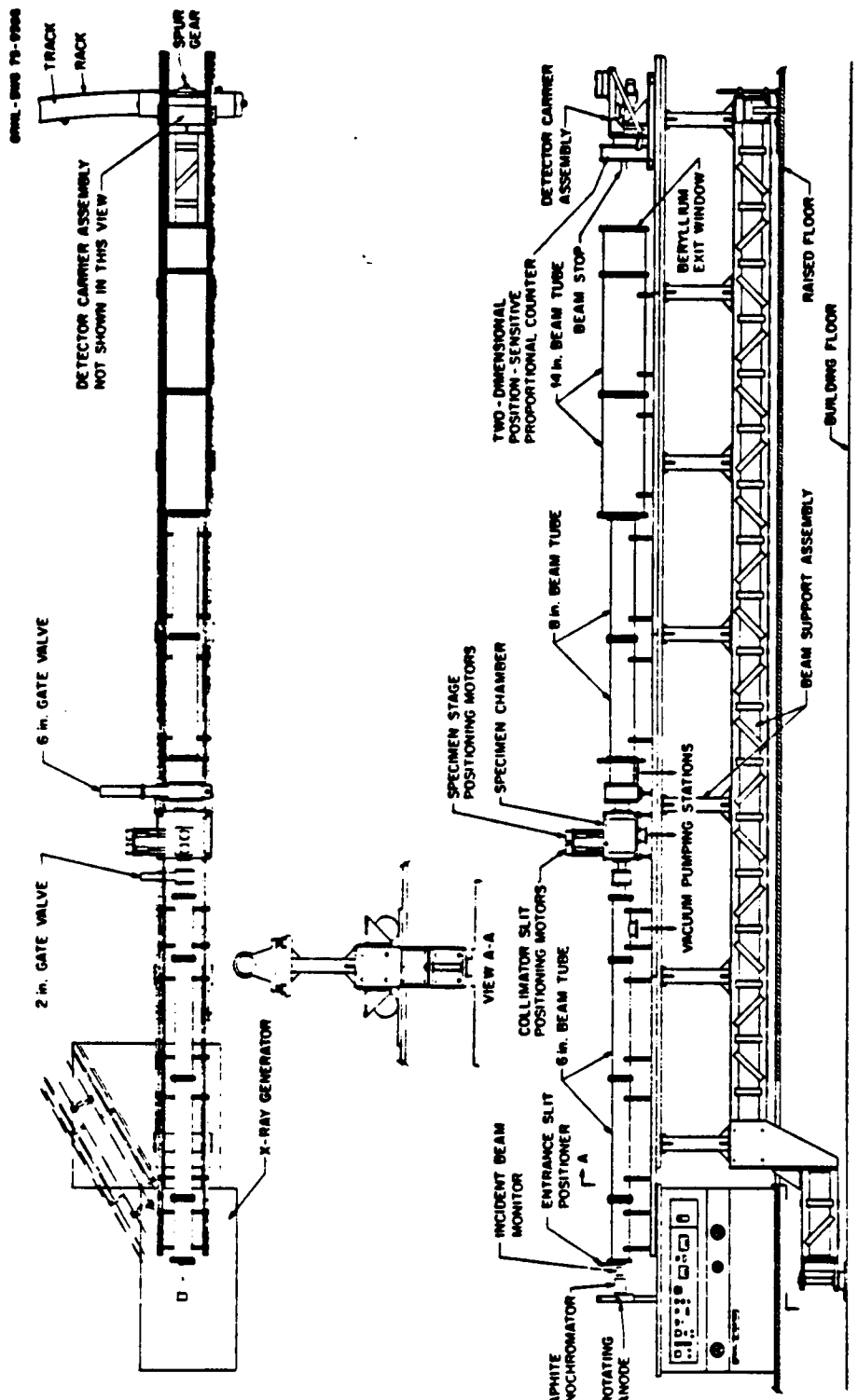

Figure 3.5. Schematic representation of NCSASR SAXS apparatus.

and the limitation of the mini-computer memory capacity. The size of each detector element is 0.324 x 0.324 centimeters making the size of the 2DPSD 20.7 x 20.7 cm. The intensity measured by each detector element is position encoded and directed by the microprocesser to store in a unique address in the computer memory. Therefore a 64 x 64 matrix of scattered intensity in two dimensions exists for each experiment. The distance between sample holder and 2DPSD is variable in increments of one meter from about one meter to about five meters depending on the angular range of interest. Since the scattering centers in crazes are anticipated to be in the range of five to 100 nm, the maximum small-angle resolution of the instrument is desired and the sample to detector distance is set at 5.126 meters.

D) Computer: The two major functions of the Modcomp computer system are to record and reduce data. The software which performs these functions is described qualitatively in the next section.

The first function of the computer is to record the scattered intensity as a function of detecter location. It accomplishes this by allocating specific locations in memory for each detector element. For each experiment a header record accompanies the data. The header record contains such information as: experiment number, equipment geometry, absolute intensity, sample constants, etc. The computer uses the header information when executing data correction and reduction routines. These routines comprise the second function of the computer. The intensity data are corrected by subtracting background radiation and normalizing for detector sensitivity,

transmission coefficient of the sample, etc. The computer will also reduce the contour plots to linearly averaged scattering intensity versus scattering angle plots by radial or slice averaging routines in the data analysis software.

As indicated above, the computer software enables the gathering, correction and reduction of data. The computer is operated by simultaneous foreground and background programs. The major software is qualitatively described here.

A) Foreground Programs: The major purpose of the foreground program 'SAXS' is to automate the hardware. The program operates stepping motors for the glassy carbon, 2DPSD position, sample stage, etc. It also prepares the header record and takes data.

B) Background Programs: The purpose of the background programs is to correct and reduce the two dimensional intensity data. A summary of some important background programs for data reduction is given:

FILE: To fetch and store two dimensional data from disc storage to working memory.

BKG,BKC: Two routines for subtracting background intensity while normalizing for detector sensitivity, transmission coefficient, absolute intensity, etc. BKC is used for samples with low signal to noise ratios. The acquisition of these background correction data sets will be discussed in the next section. The background correction programs compute the intensity for each detector element.

CONTOUR: Displays the corrected two dimensional data in contour plot form with a Tektronix cathode ray tube (CRT). Subroutine CEN lets one establish the center of the contour plot with a cursor in the CRT, and stores that position in the header record. Subroutines RAD and AVE reduce the two dimensional data to one dimensional form by performing circular or linear averages respectively.

MANAGER: manipulates data sets in the memory which are stored on a disc; one can read from or write to the disc, delete data, alter header records, etc.

3.3.3. Calibration of SAXS Apparatus

Calibration of the SAXS apparatus is a multistep process. The following experiments need to be done before useful scattering data can be taken: absolute intensity, 2DPSD sensitivity, background intensity, dark current intensity, and transmission coefficient measurements.

The absolute intensity of a small-angle x-ray scattering experiment is the ratio of its intensity to that of the primary beam. The intensity of the primary beam is defined as the rate of photon bombardment per cross sectional area of the sample. This measurement is required for calculations involving the absolute determination of scattering center size distribution and volume fractions. Several methods are available for determination of absolute intensity (3-77,3-78,3-79); however, the nickel foil method (3-78,3-79) is used because of its availability and ease of application.

The nickel foil method involves attenuating the x-ray beam with layers of nickel foil of uniform thickness, then plotting the transmitted intensity versus nickel thickness in a semi-logarithmic scale and extrapolating to zero thickness. Various layers of nickel foil, each having the same thickness (about 0.025 mm), are placed in the x-ray beam in the location of the sample with the beamstop removed. The 2DPSD is used here as a transmitted photon counter. Therefore the intensity value extrapolated at zero nickel thickness is the absolute intensity of the primary beam at the sample. This extrapolation is validated by the following equation:

$$I_{trans} = I_o \exp(-\mu t) \qquad 3.18$$

where:

Itrans= transmitted intensity

Io = absolute intensity

u = linear absorption coefficient of nickel

t = thickness of nickel

The true transmitted intensity, Itrue, is calculated by:

$$I_{true} = \left(\frac{I_{obs} - I_{dc}}{(1 - t(I_{obs} - I_{dc})} \right) \qquad 3.19$$

Where t=7 microseconds (dead time) for the current detection system, and Iobs is the observed or measured intensity expressed in counts/sec.

Dark current primarily originates from cosmic radiation and electronic noise in the detection circuits. A plot of transmitted intensity versus nickel thickness for the two x-ray powers used in this study is found in Figure 3.6. A linear extrapolation to zero thickness gives absolute intensities of 1,610,000 and 2,350,000 counts per second per square millimeter for 40 mA, 40 KV and 40 mA, 60 KV respectively.

A detector sensitivity correction is necessary because some portion of the detector resistance wire in the compound 2DPSD may have a different sensitivity to radiation than others. Possible causes of this effect include: portions of the detector area may be partially blocked by the beamstop or beryllium window support frame, variations in detector physics due to unequal aging rates, or nonuniform material processing properties. To calibrate the 2DPSD for this effect, a totally uniform radiation source is placed in the sample holder position such that the whole area of the detector has an equal opportunity to record radiation. Iron 55 is used as the source and it is run until several million counts are recorded. These data will allow the computer software to normalize detector sensitivity by scaling up the measured intensity to an appropriate amount. Figures 3.7 A and B show a typical detector sensitivity function and an empty beam scattering pattern.

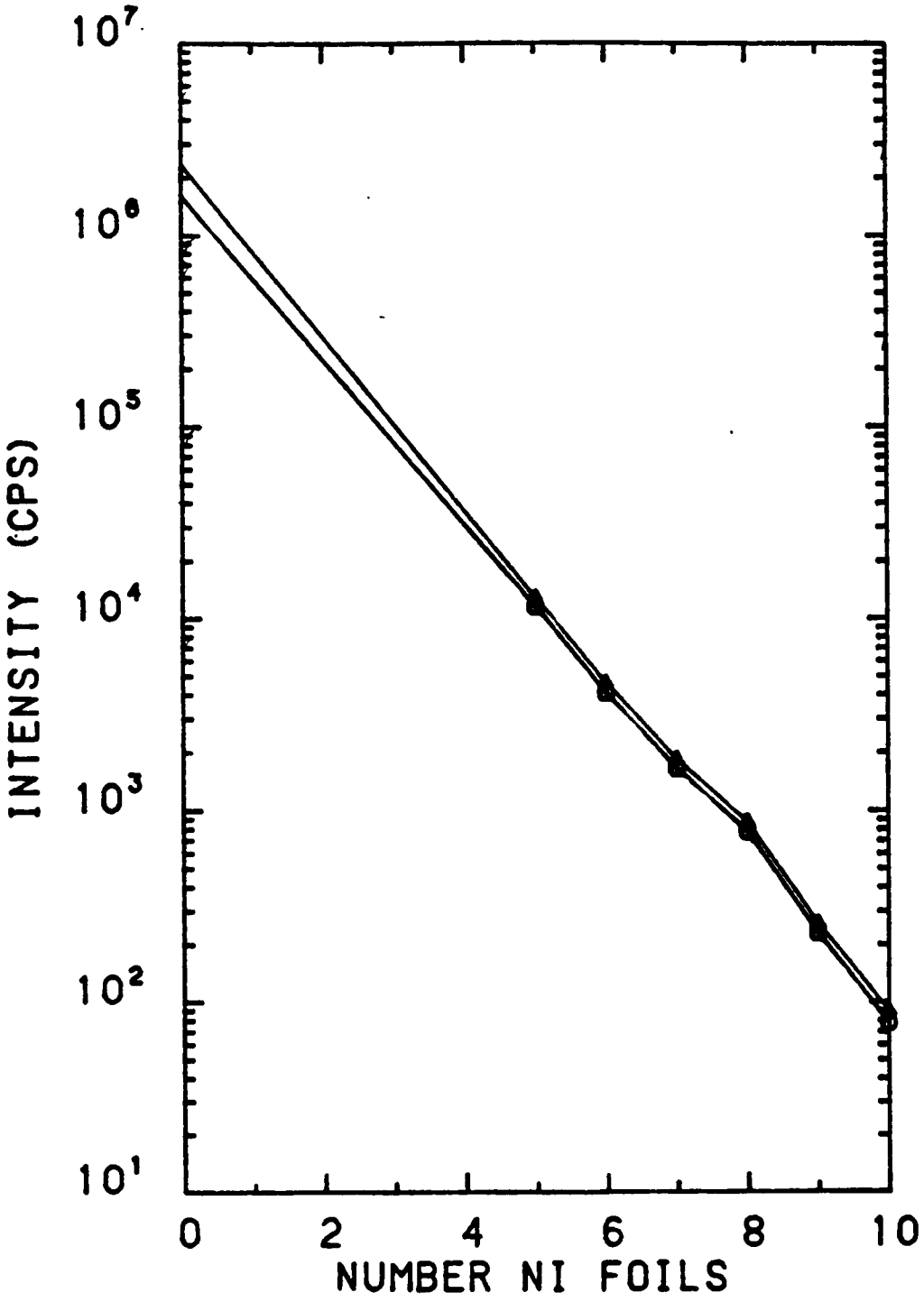

Figure 3.6. Absolute intensity of x-ray beam as determined by the nickel foil method.

A

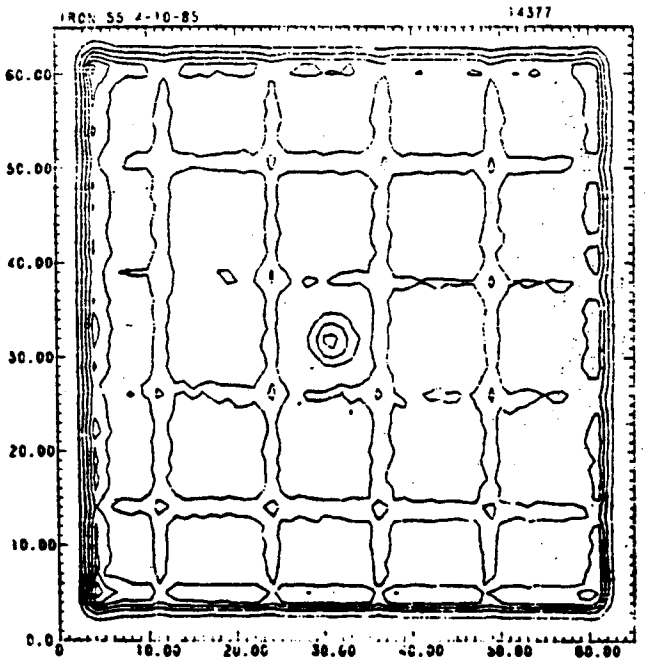

B

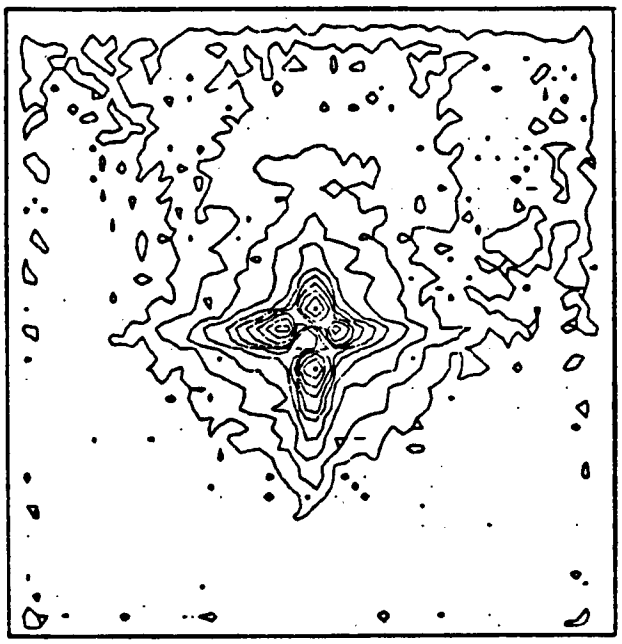

Figure 3.7. SAXS background correction scattering patterns. A) Detector sensitivity. B) Empty beam.

Dark current refers to the counts as registered by the detector when no x-rays are admitted to the detector. The dark current consists of the radition events that originate by cosmic radiation and electronic noise. This count rate is low (typically about 22 counts per second over the 64x64 array in a well shielded system) and must be subtracted from all scattering patterns. A dark current experiment is done by closing the sample chamber gate valves and recording stray intensity for an extensive period of time, normally not less than 1000 seconds. The experiment is done at full power so that the computer can record the beam monitor intensity for normalization purposes.

A significant background intensity exists due to the reflection off the second pinhole collimator (the major portion of the parasitic scattering). Since the pinhole has a square cross sectional area, the background pattern appears as a cross. The background intensity must also be subtracted from each scattering pattern (via subroutine BKC or BKG).

In some cases, the background intensity may be taken with a control sample in the beam. For the crazing studies, the scattering function of the polystyrene tensile bars with no stress history will be used as the background correction. In this way, the amorphous component of the scattering may be removed from the scattering from crazes.

Lastly, the transmission coefficient of the sample must be measured. The transmission coefficient is a function of the sample thickness, intrinsic absorption coefficient and mass density; the optimum thickness is the reciprocal of the linear absorption coefficient as suggested by Beer's law. The transmission coefficient may be calculated for any sample by the following equation:

$$T_m = \frac{I_{carsam} - 0.7(I_{sam})}{I_{carbon} - 0.7(I_{empty})} \qquad 3.20$$

where:

Tm=transmission coefficient of the sample

Igc=scattered intensity by the glassy carbon

Igcs=scattered intensity by the glassy carbon and sample

Is=scattered intensity of the sample alone

And the factor 0.7 is the transmission coefficient of the glassy carbon itself. The purpose of the glassy carbon is to profusely scatter radiation away from the beamstop, and increase statistical confidence.

3.3.4. Collection and Reduction of SAXS Data

This section will describe the method by which the samples are analyzed in the SAXS instrument, and the data reduction techniques.

Two dimensional contour plots are generated by the computer after data has been corrected for background scattering and normalized the detector sensitivity etc. These contour plots are useful for qualitative comparison of the data with respect to the variables of interest. To help quantify the data, averaged intensity slices of

specified azimuthal angles may be calculated. Figure 3.8 is a schematic representation of this process (using subroutines CEN and AVE in the program CONTOUR). For isotropic scattering patterns, a radial average around the beamstop may be done (subroutine RAD in the program RADIAL). The scattering patterns of crazes may be highly anisotropic, so slices at psi=90 and 0 degrees are taken to characterize the data. It is also assumed that the scattering pattern is symmetrical around the center of the scattering pattern. This allows the averaging of intensity data of the same scattering angles on both sides of the beamstop. The result is a plot of intensity versus scattering angle for a specific angle in the scattering plane.

The absolute scattered intensity as a function of scattering angle is used to calculate the invariant of the scattering function. The following equation is used to calculate the absolute intensity in electron units from the scattered data in counts per second.

$$I_{abs} = (P_{rad}/P_o)(Bmon/1000)(1/time \cdot (a/L)^2 \cdot i_e \cdot th \cdot T_m) \qquad 3.21$$

Where Po is the primary x-ray intensity, th=thickness of the sample, ie= the Thompson scattering factor, t=time, a/L=solid angle of one detector element subtended from the sample position, Bmon=x-ray beam monitor scaler, Prad=scattered intensity in counts per second, and Tm is the transmission coefficient of the sample.

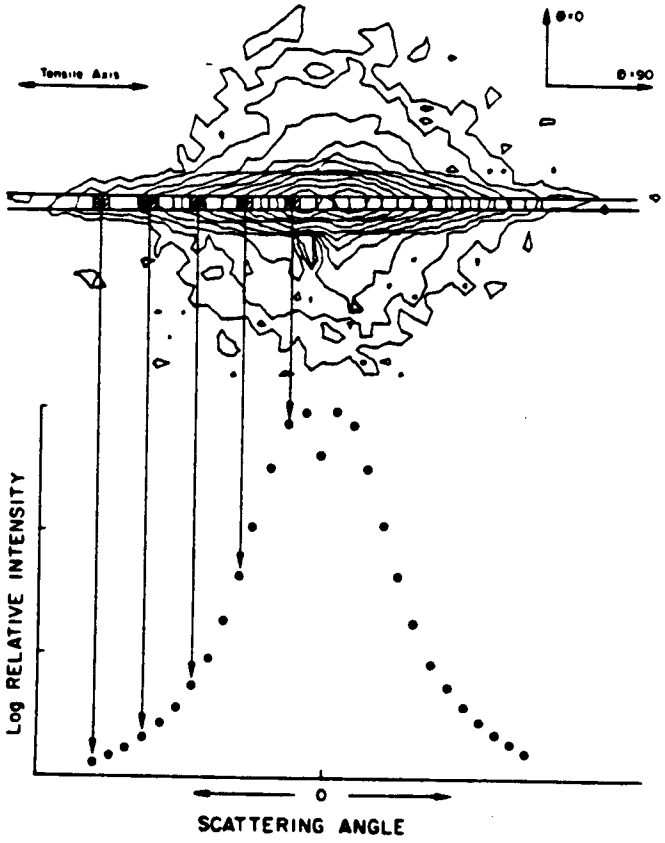

Figure 3.8. Schematic representation of SAXS data reduction technique for linear slices.

3.4. Results and Discussion

A report of the small-angle x-ray scattering behavior of crazed glassy polymers will be given in this section. The original objective of this research was to extend the polystyrene studies of Tang et al. (3-54) and this author (3-40) for other glassy materials using the on-line dynamic deformation sample holder at the NCSASR SAXS facility (3-76). However the unavailability of this sample chamber device forced an alternative investigative procedure for the current work. A secondary research scheme was devised. This plan included deformation of the samples at the University of Tennessee Instron facilities and then performing SAXS studies of the relaxed specimens at NCSASR. To achieve this goal, glassy samples were deformed at various rates spanning the range of the Instron tensile device to the point of yield. This procedure produced samples of various craze density. Subsequent SAXS experiments revealed, however, extremely weak scattering behavior even for the samples with the highest apparent craze density. This result is in part due to the effect of diminishing scattering power due to relaxation of the crazed matter (3-40). This observation was disappointing in that the author was unable to get significant scattering patterns with samples from which he had controlled the stress history. However, these preliminary negative results do indicate in a primitive sense that there must be vast differences in the crazing behavior of the more ductile polycarbonates compared to polystyrene.

Thus a third more qualitative approach was employed. Samples of each glassy polymer were deformed by three point bending until the material transformed from a transparent to a transluscent sample with no coherent transmission of light. The resulting material contained an extremely high craze density. Fortunately these materials also provided a satisfactory scattering power.

Obviously the quality of the investigation is somewhat compromised by the inability to completely specify the mechanical history of the materials. However, a large effect on the craze morphology has been shown to be produced by molecular weight variables and different polymer types (3-40,3-47). Therefore, the ensuing experimental results will be interpreted as a preliminary qualitative investigation of craze morphology in a variety of polymer glasses. The goal will be to better understand the large differences in ultimate properties exhibited by these materials from a study of their craze morphology.

3.4.1. Presentation of Results

Two SAXS patterns were obtained for each sample. One pattern was taken with the sample parallel to the detector plane (normal geometry) and the other pattern was taken with the sample tilted five degrees out of the plane of the detector (tilted geometry). The former scattering pattern contains components from both volume and surface scattering while the latter is composed of only volume scattering. A third pattern can be generated from the above two data sets by subtracting the tilted pattern from the normal pattern. This

is accomplished by using the tilted pattern as the background correction. The residual scattering (tilt corrected) is assumed to be the contribution of reflection to the normal scattering pattern. The scattering in the tilted pattern is assumed to be the contribution of volume scattering to the normal scattering pattern. The normal, tilted and tilt corrected two dimensional scattering patterns can be found in Figure 3.9 for polystyrene, Figure 3.10 for poly(methyl methacrylate), Figures 3.11 through 3.13 for polycarbonate, and Figures 3.14 and 3.15 for the polysulfones. In all patterns the normal to the craze plane is vertical.

It is observed that the polystyrene scattering pattern has the familiar reflection dominated function, while all the other scattering patterns show considerable less reflective component. In fact the reflective contribution is so weak in some samples that the streak is barely visible in the normal geometry SAXS patterns. It is interesting that the tilted SAXS patterns of polycarbonate crazes seem to be uniquely anisotropic. This anisotropy indicates the existence of nonspherical scattering entities with slight orientation in the tensile direction. Regardless of the presence of scattering anisotropy, all tilted scattering patterns were radially averaged to obtain the volume scattering intensity as a function of scattering angle.

Figure 3.9. Contour scattering patterns for polystyrene (685D). A) Normal geometry. B) Tilted geometry. C) Tilt corrected normal geometry.

A

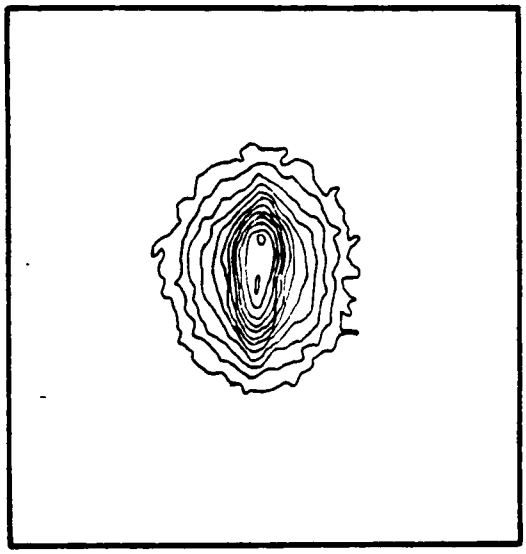

B

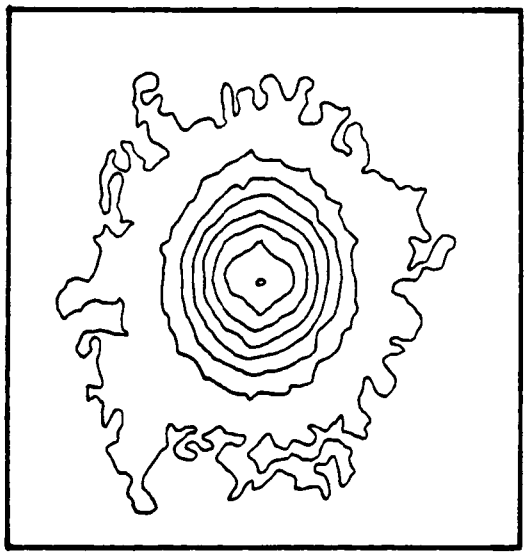

C

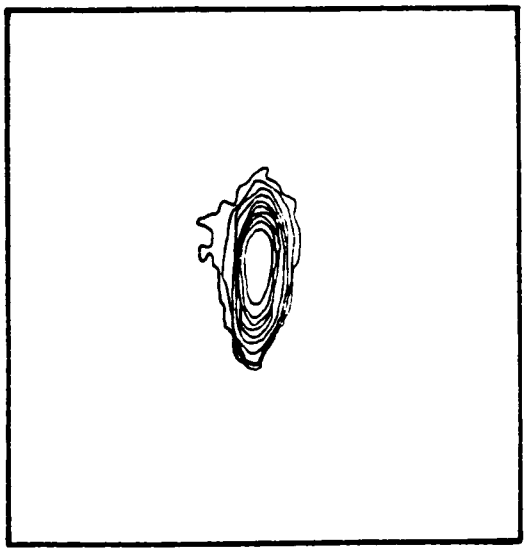

Figure 3.10. Contour scattering patterns for poly(methyl methacrylate). A) Normal geometry. B) Tilted geometry. C) Tilt corrected normal geometry.

A

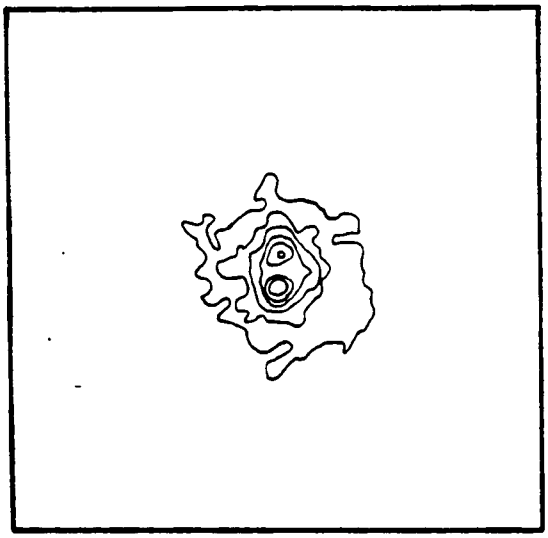

B

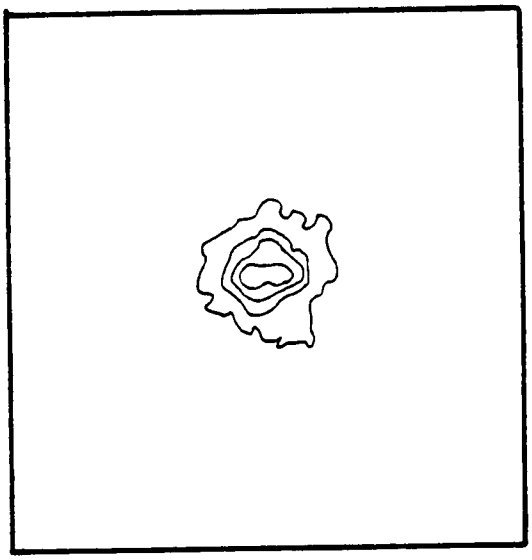

C

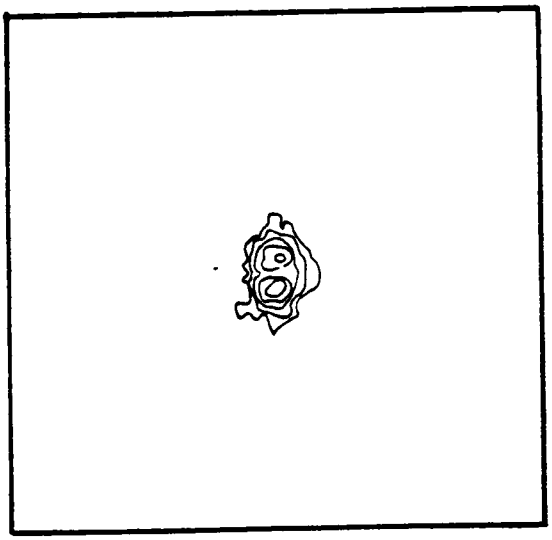

Figure 3.11. Contour scattering patterns for polycarbonate (120G). A) Normal geometry. B) Tilted geometry. C) Tilt corrected normal geometry.

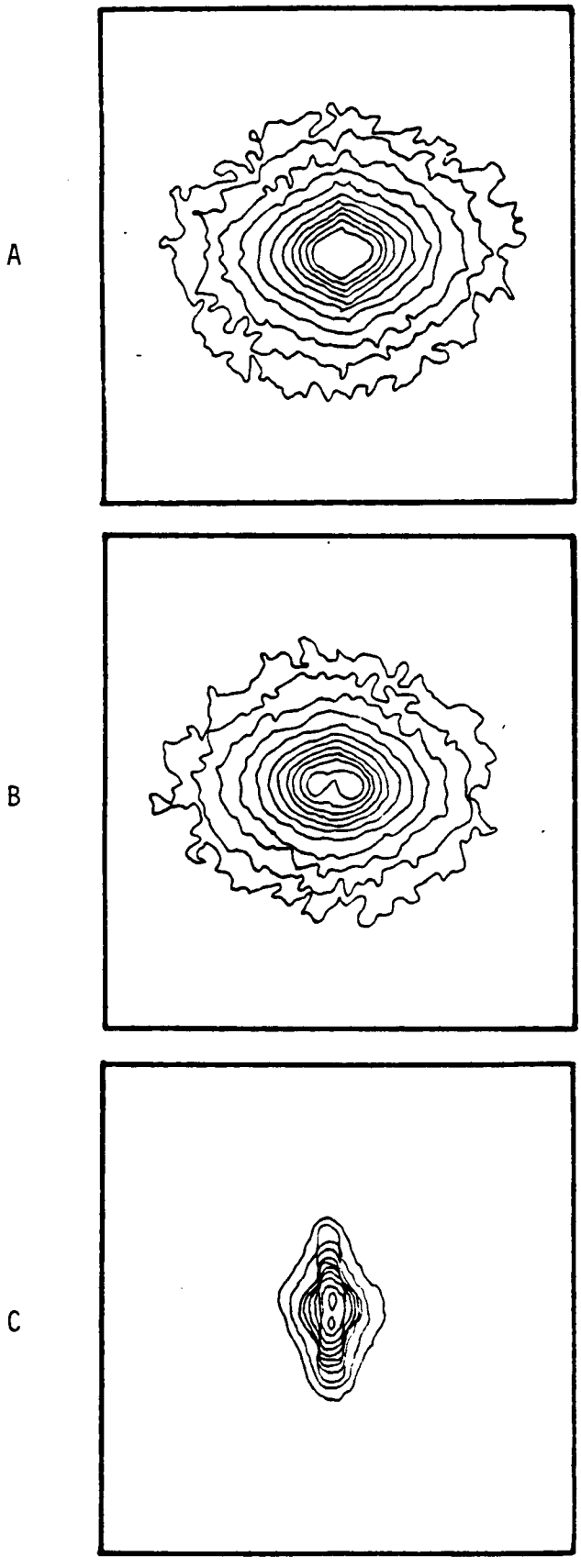
A
B
C

Figure 3.12. Contour scattering patterns for polycarbonate (100G). A) Normal geometry. B) Tilted geometry. C) Tilt corrected normal geometry.

A

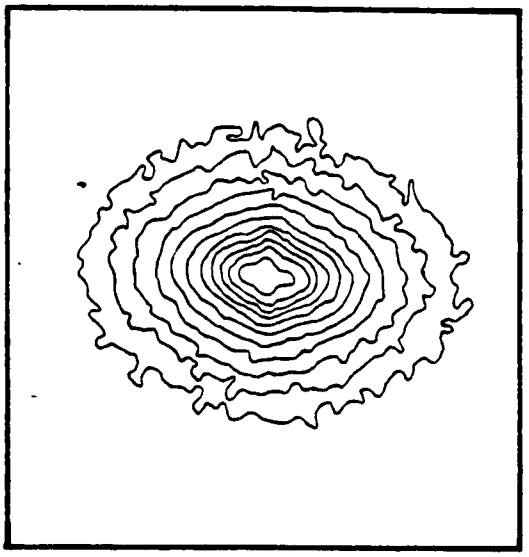

B

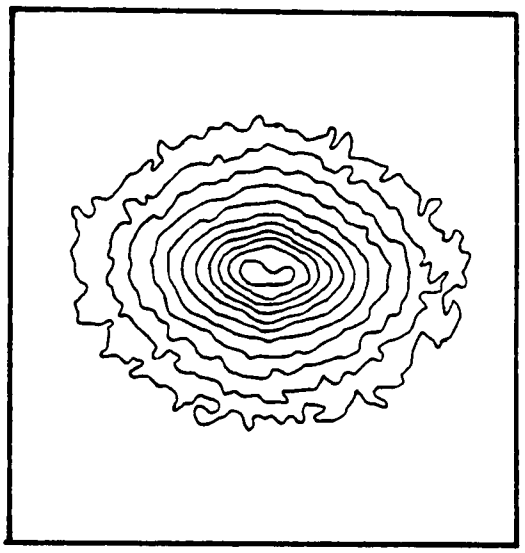

C

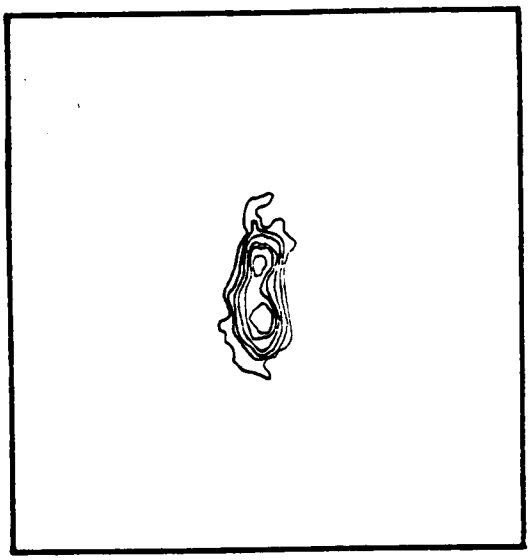

Figure 3.13. Contour scattering patterns for polycarbonate (130G). A) Normal geometry. B) Tilted geometry. C) Tilt corrected normal geometry.

A

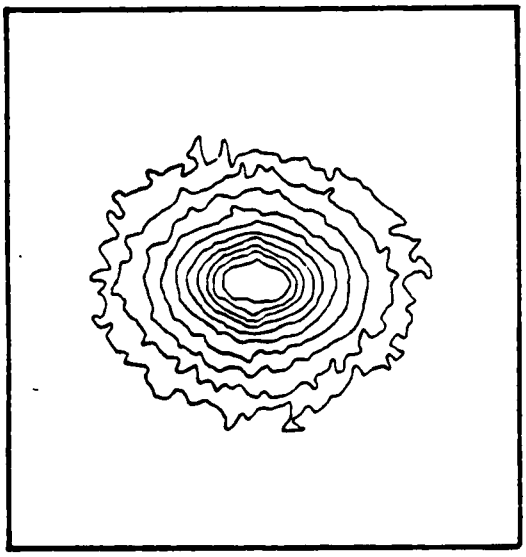

B

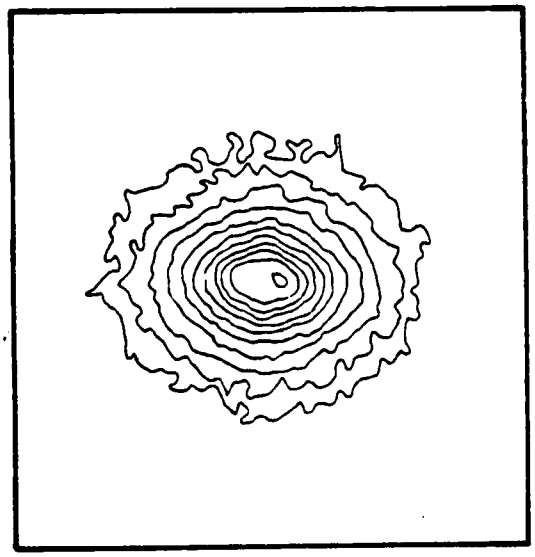

C

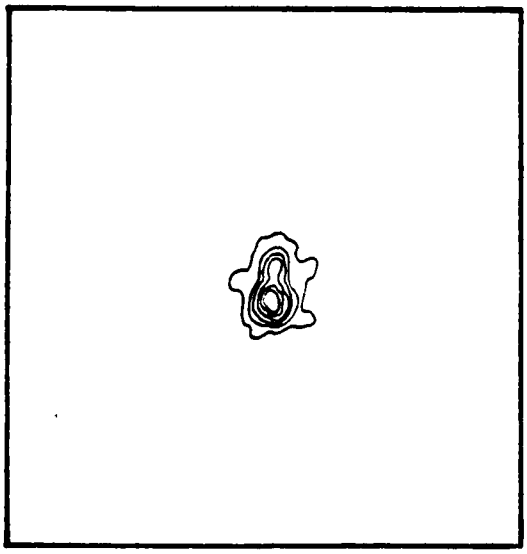

Figure 3.14. Contour scattering patterns for polysulfone (1700). A) Normal geometry. B) Tilted geometry. C) Tilt corrected normal geometry.

A

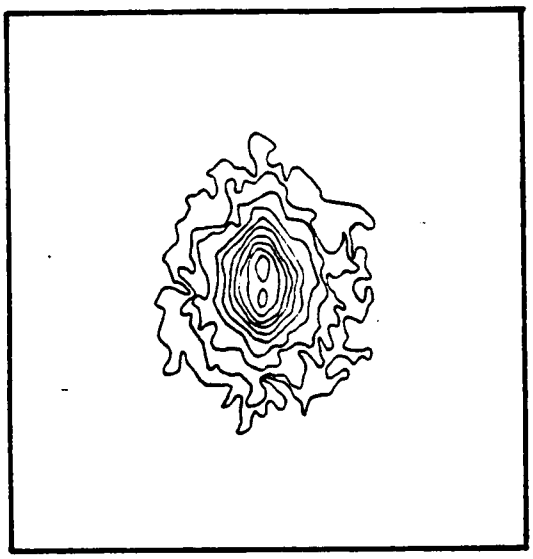

B

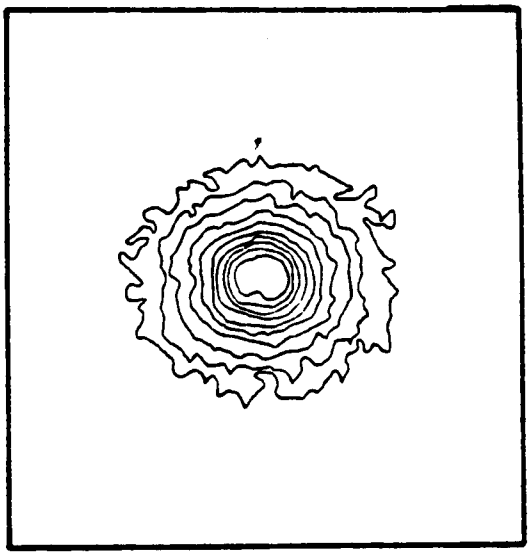

C

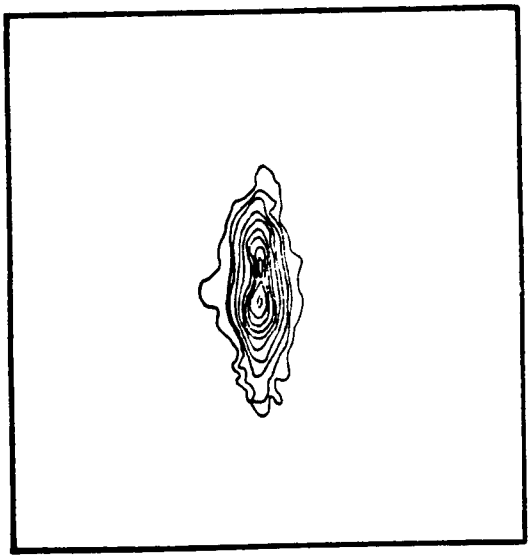

Figure 3.15. Contour scattering patterns for polysulfone (3500). A) Normal geometry. B) Tilted geometry. C) Tilt corrected normal geometry.

A

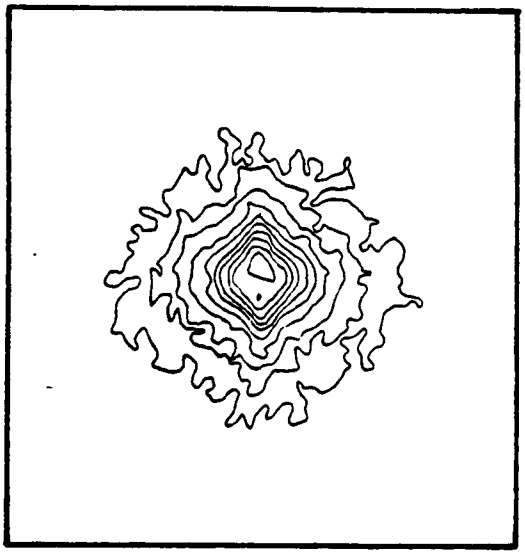

B

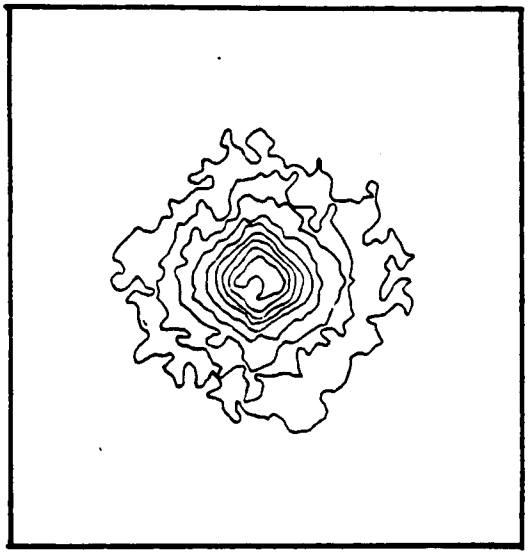

C

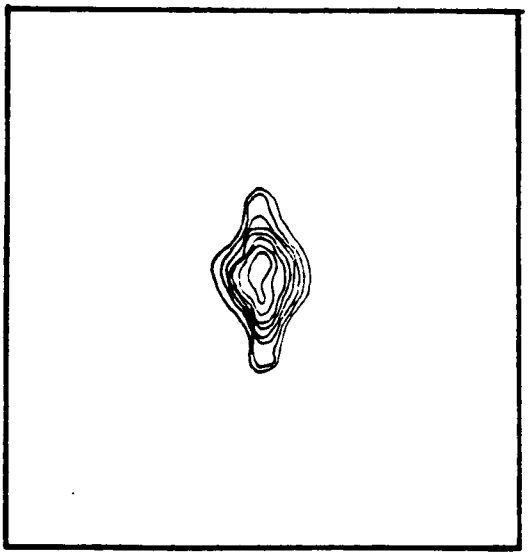

The surface scattering intensity as a function of scattering angle was obtained by averaging over a slice in the tensile axis for each of the tilt corrected scattering patterns. The intensity in the positive and negative scattering angles were averaged (assume centrally symmetric) to increase the statistical confidence. The surface and volume scattering correlation functions were calculated according to the algorithm of Tang (3-54) using the linear data described above. The averaged volume scattering intensity functions and corresponding volume correlation functions can be found in Figure 3.16 for polystyrene, Figure 3.17 for poly(methyl methacrylate), Figure 3.18 for polycarbonate, and Figure 3.19 for polysulfone. Likewise the averaged surface scattering intensity functions and their corresponding correlation functions can be found in Figure 3.20 for polystyrene, Figure 3.21 for poly(methyl methacrylate), Figure 3.22 for polycarbonate, and Figure 3.23 for polysulfone.

Using an isotropic random two phase model, the average chord length, l, for the volume scattering can be calculated as the negative inverse slope of the correlation function as r approaches zero. This procedure is performed in Figures 3.16 through 3.19 (page 151 through page 154). Similarly, using a Gaussian distribution model for the surface correlation, the average surface length can be calculated as the value of one when gamma(l) has a value of 1/e. This is performed in Figures 3.20 through 3.23 (page 155 through page 158). The values of l and tau computed for each material can be found summarized in Table 3.1 for each material.

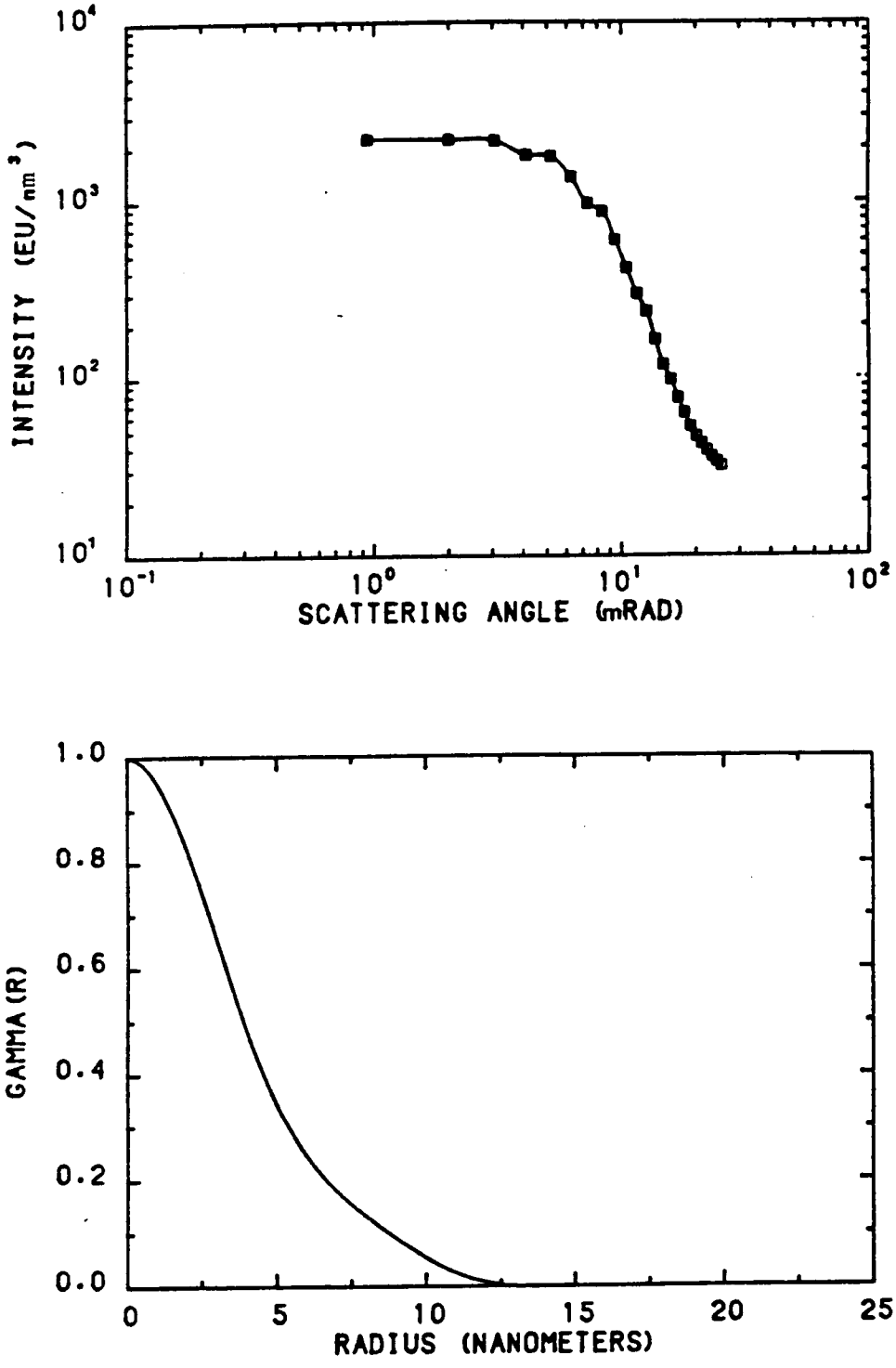

Figure 3.16. Volume scattering intensity and correlation functions for polystyrene (685D).

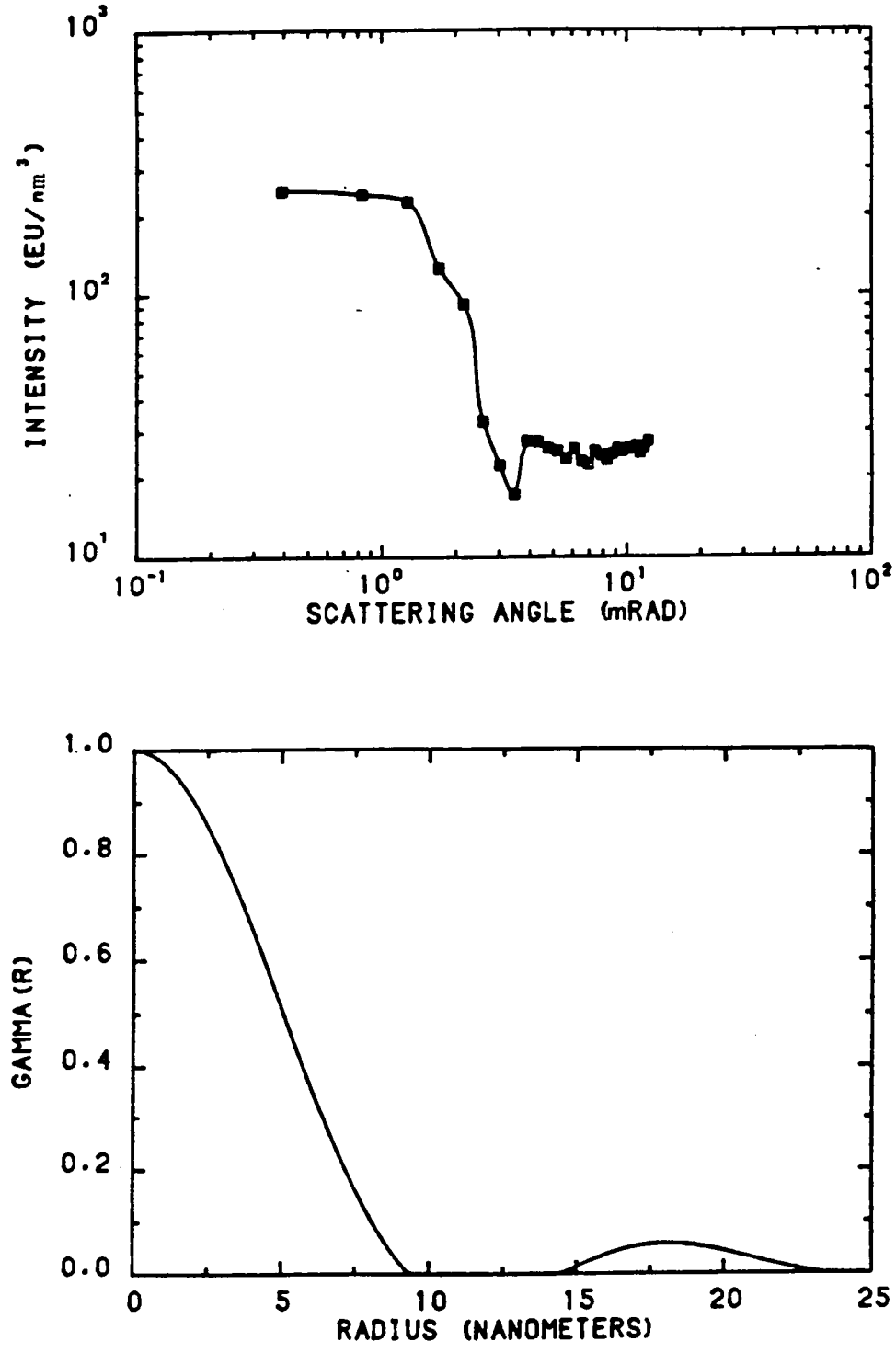

Figure 3.17. Volume scattering intensity and correlation functions for poly(methyl methacrylate) (2805).

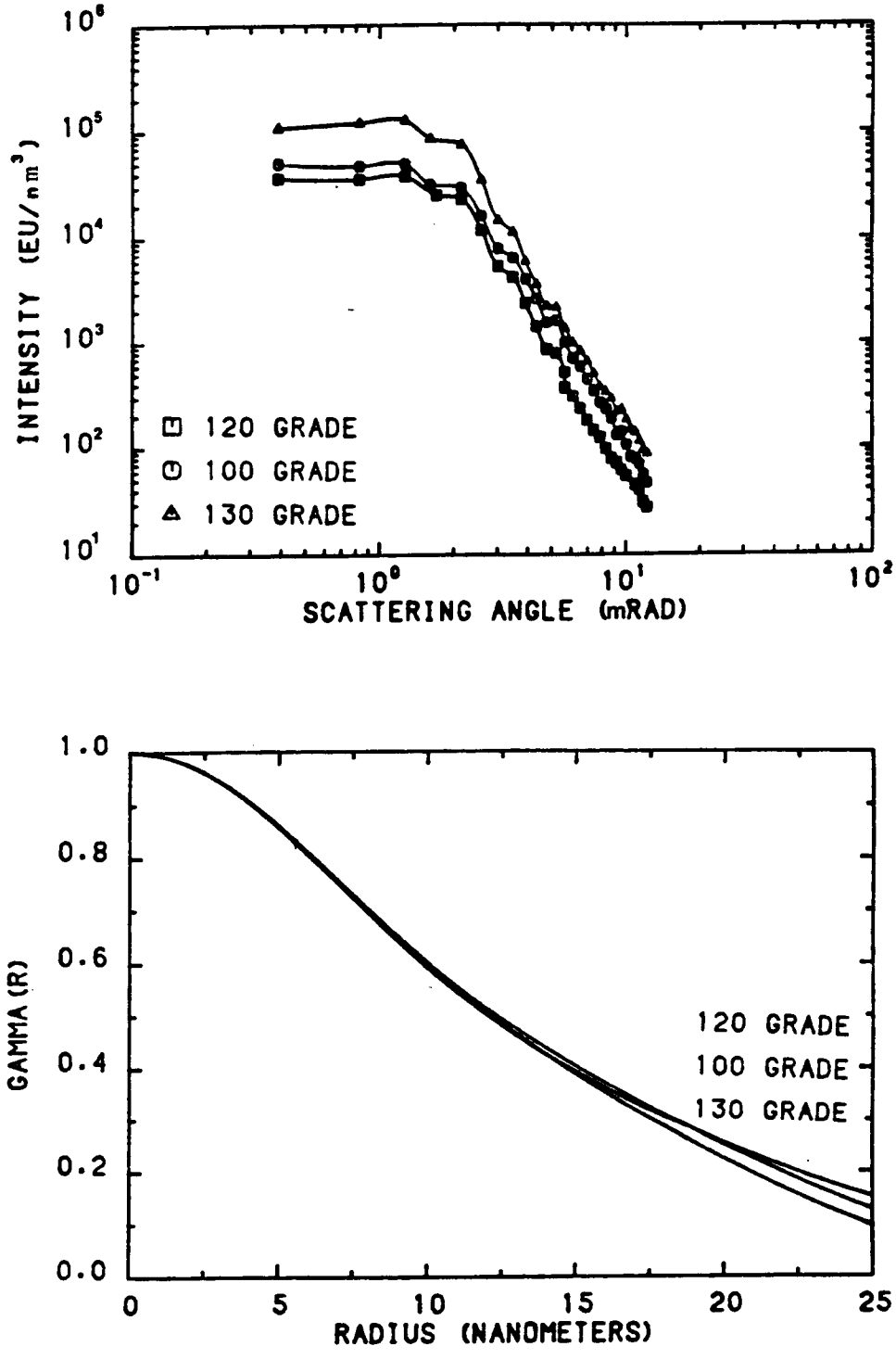

Figure 3.18. Volume scattering intensity and correlation functions for polycarbonates (120G, 100G, 130G).

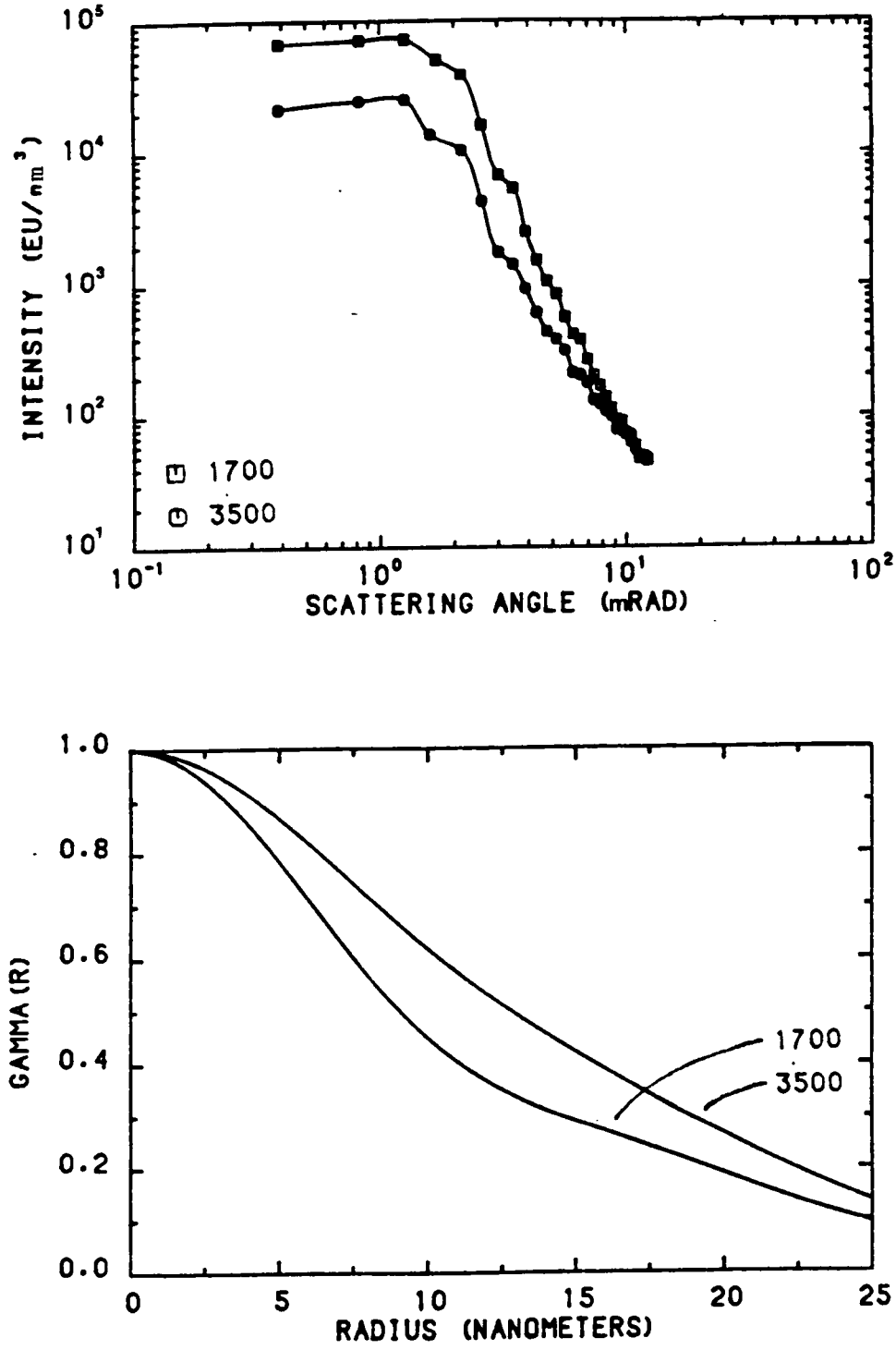

Figure 3.19. Volume scattering intensity and correlation functions for polysulfones (1700, 3500).

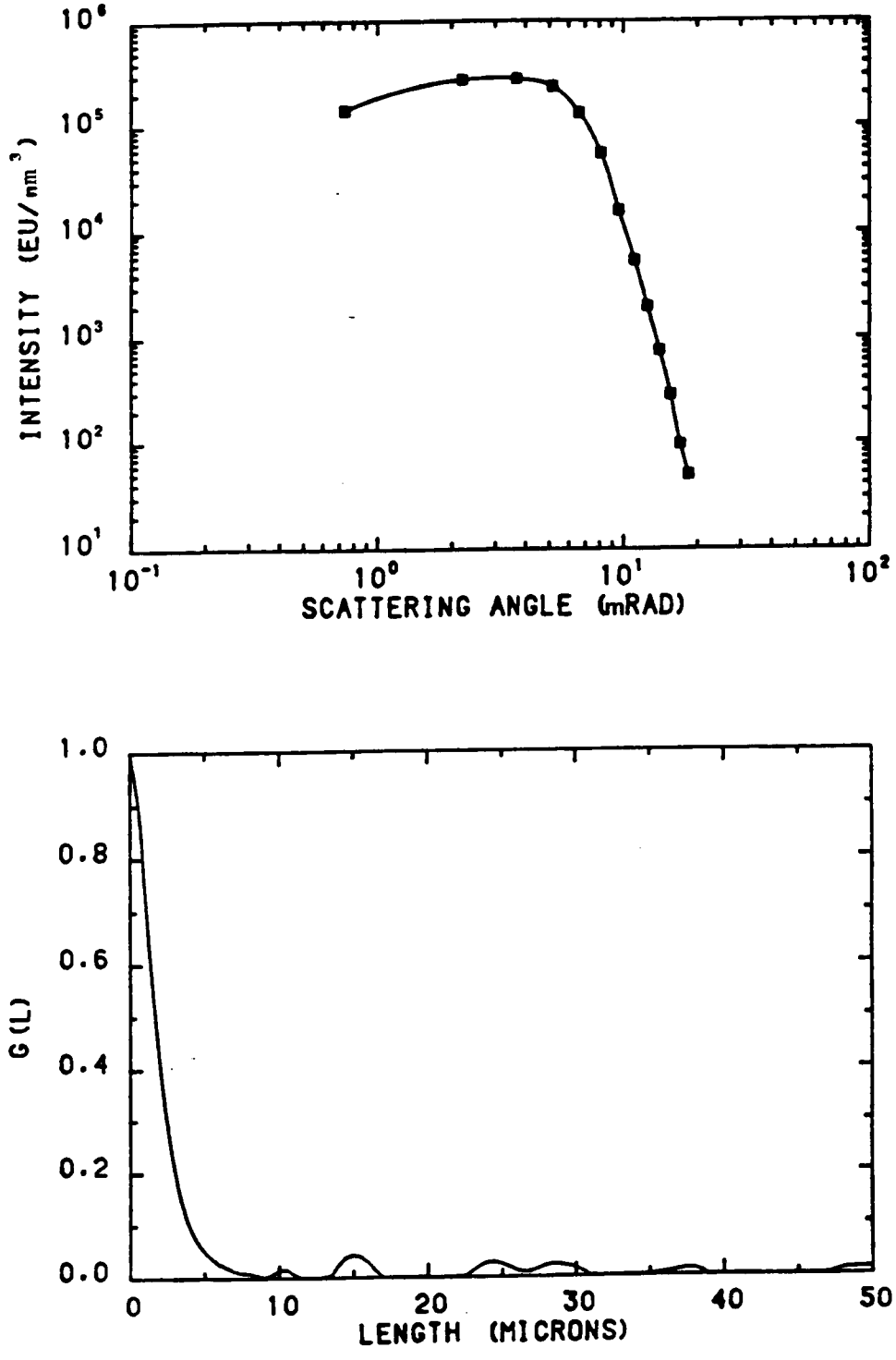

Figure 3.20. Surface scattering intensity and correlation functions for polystyrene (685D).

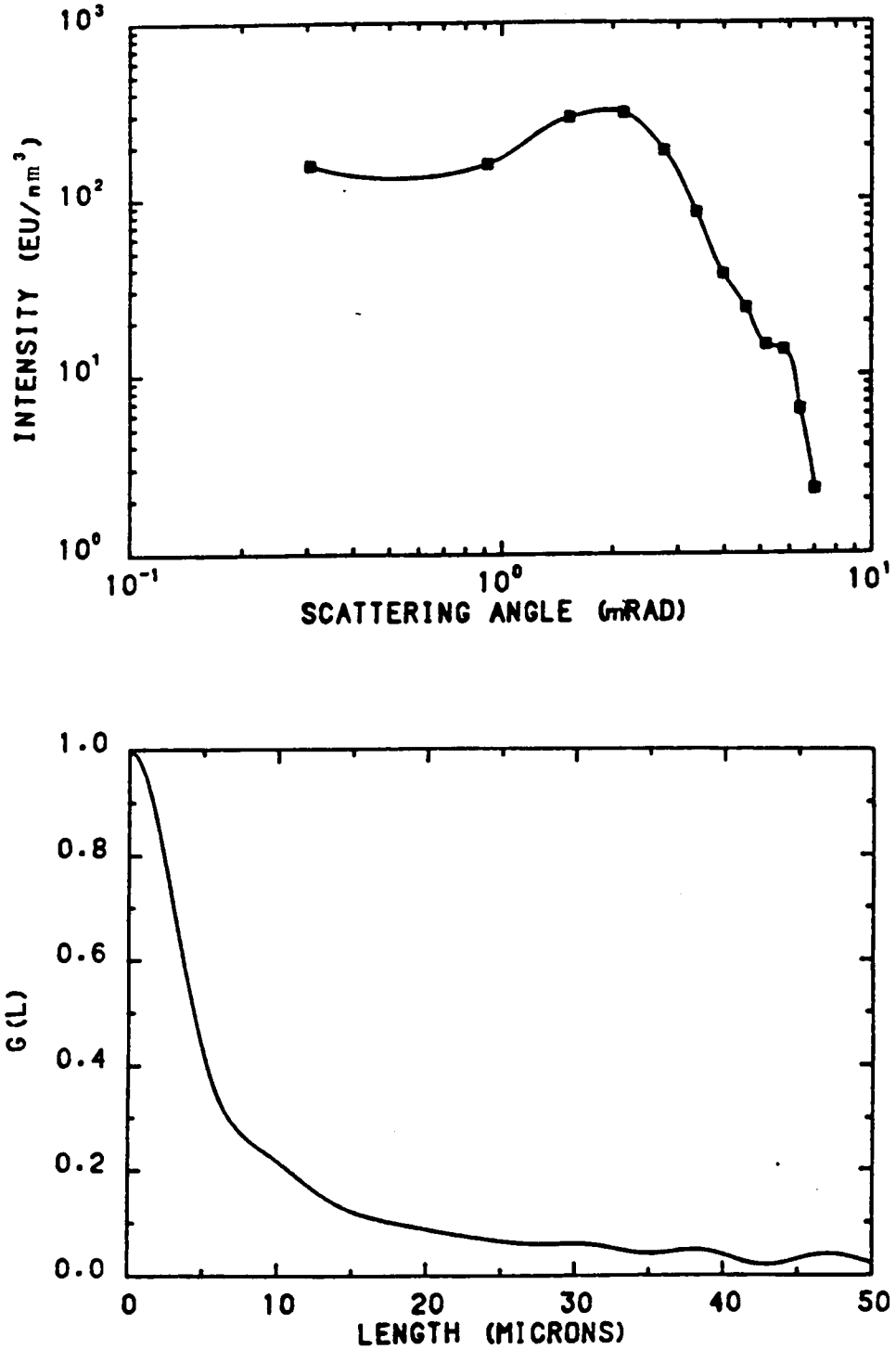

Figure 3.21. Surface scattering intensity and correlation functions for poly(methyl methacrylate) (2805).

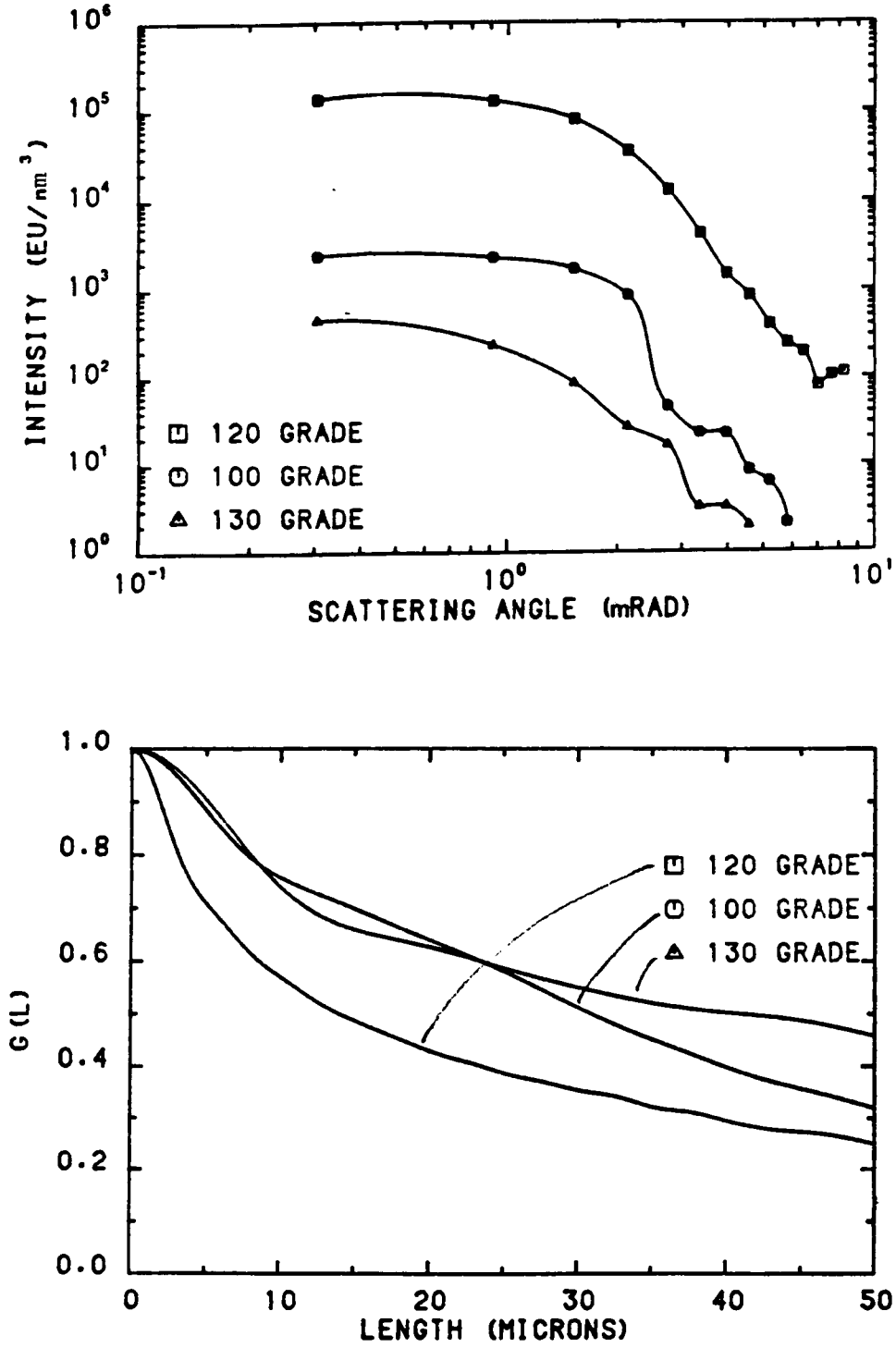

Figure 3.22. Surface scattering intensity and correlation functions for polycarbonates (120G, 100G, 130G).

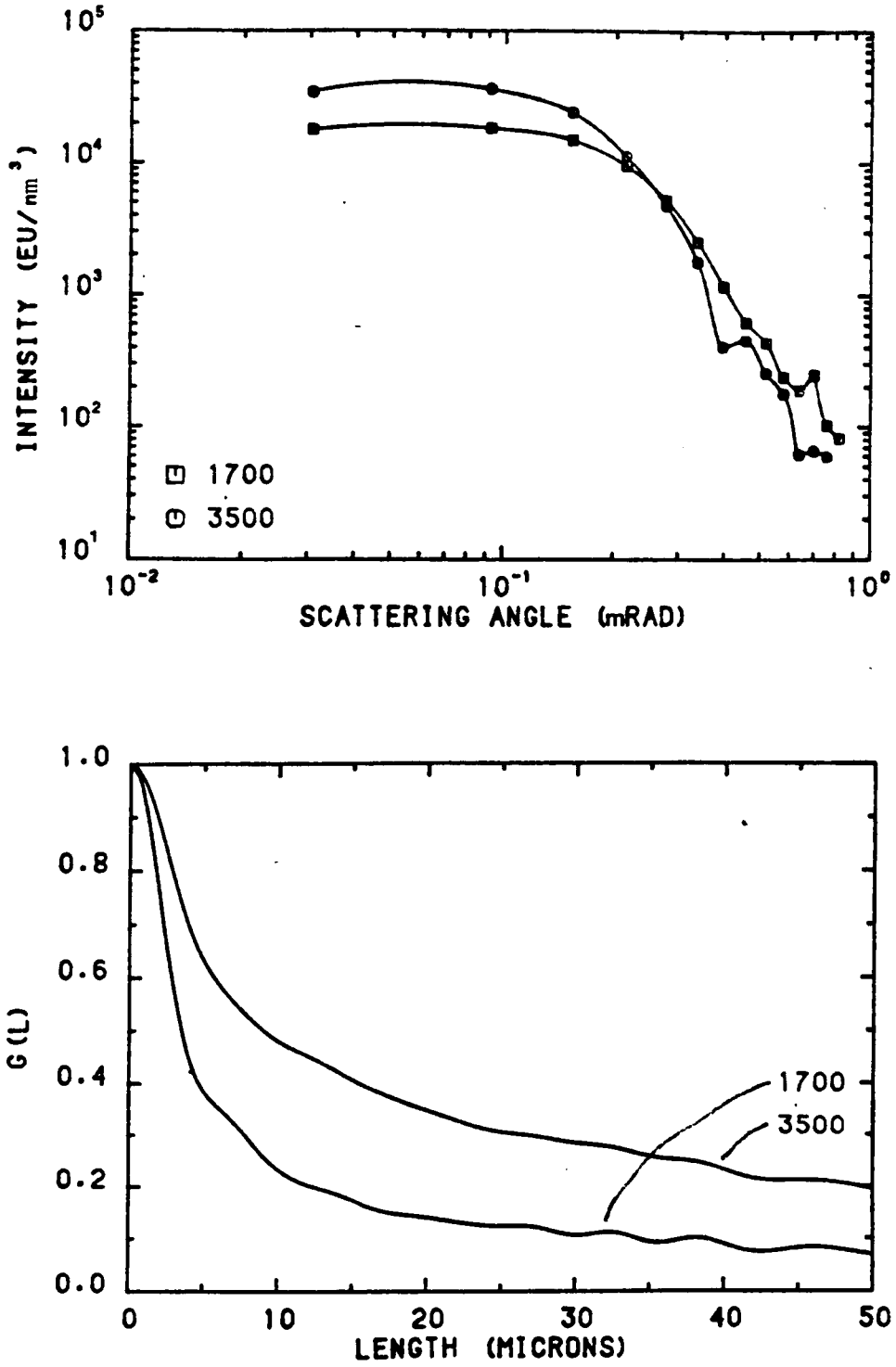

Figure 3.23. Surface scattering intensity and correlation functions for polysulfones (1700, 3500).

Table 3.1. Correlation dimensions from surface and volume SAXS.

Polymer	Surface Correlation length [microns]	Volume Correlation length [nanometers]
685D	2.2	27.4
2805	5.8	54.7
120G	28.3	212.
100G	43.7	207.
130G	70.0	213.
1700	5.5	222.
3500	18.1	231.

The invariants for surface and volume scattering were also calculated for each material in the tilted and tilt corrected scattering patterns using equation 3.14. A summary of the Ks and Kv values can be found in Table 3.2. The void fraction of the irradiated sample can be calculated using the volume invariant and the equation of Kratky and Milholic (3-80).

$$K_v = (\Delta\rho)^2 W_v(1 - W_v)V \qquad 3.22$$

where $(\Delta\rho)$, the electron density difference between polymer and void has to be calculated for each material. The volume of the irradiated sample is V, and Wv is the void fraction of the sample. The void fractions can also be found summarized in Table 3.2.

A third result of interest is the Hausdorff dimension of scattering entities as defined by the slope of the volume scattering intensity function in the high angle (Porod) region. Table 3.3 summarizes the slopes and Hausdorff dimensions of the volume scattering for all materials studied. All of the scattering functions yielded slopes in the range of negative three to negative four, which indicates that equation 3.16 can be used to describe the fractal geometry and scattering behavior of the crazed matter.

We now proceed from a presentation of scattering results to a more thoughtful discussion and interpretation of the results.

Table 3.2. Invariant analysis of surface and volume scattering.

Polymer	Ks [nm^3/m]	Kv [eu/nm^3]	$(\Delta\rho)^2$ [eu/cm^3]^2	Wv [%]
685D	1.0 E-3	3.1 E-3	0.302	1.07
2805	5.0 E-6	1.4 E-3	0.410	0.35
120G	3.9 E-5	0.8 E-3	0.398	0.21
100G	5.4 E-6	2.6 E-3	0.398	0.66
130G	4.5 E-7	1.5 E-3	0.398	0.39
1700	2.0 E-4	0.7 E-3	0.428	0.15
3500	1.4 E-4	0.2 E-3	0.428	0.06

Table 3.3. Fractal analysis of volume scattering from crazes.

Polymer	Porod Slope	Hausdorff Dimension
685D	-3.74	2.26
2805	-3.15	2.85
120G	-3.67	2.33
100G	-3.92	2.08
130G	-3.72	2.28
1700	-3.88	2.12
3500	-2.98	3.02

3.4.2. Interpretation of SAXS Results

There are three important categories of results presented in the previous section. They are the surface and volume correlation lengths, the surface and volume invariants and the Hausdorff dimension of the volume scattering component. Perhaps it is more convenient to discuss these results in reverse order.

The fact that the volume scattering intensity function with scattering angle scales in a power law to a slope between negative three and negative four, as shown in Table 3.3, indicates that a porous model for scattering centers is most appropriate. The corresponding Hausdorff dimension of these scatterers is between two and three. This observation is interpreted as scattering from a rough surface. Unfortunately there seems to be no correlation between molecular weight parameters and the Hausdorff dimension of the scattering matrix. However the fit of the porous scattering theory in itself provides more justification for the use of a void scattering concept for crazed materials. If on the other hand an aggregate model would have been more suitable, perhaps an interpretation of fibril scattering would be in order. But this is not the case and therefore the voided fraction of crazed matter in these materials is considered the discontinuous phase and the open celled foam model of craze morphology is reinforced (3-25). In this model the microvoids are defined by fibrils and interconnections well enough to respond independently to electromagnetic radiation (3-40).

Since the stress history of the glassy polymers is not quantified, it is dangerous to quantitatively compare the invariant values summarized in Table 3.2 (page 161) for trends between samples. However it may be instructive to compare the relative magnitudes of the surface and volume scattering invariants systematically for each sample. For example it is observed that these invariants are of the same order of magnitude for the polystyrene crazes, but the surface invariant is several orders of magnitude less than the volume invariant for the other samples. Polycarbonate seems to show the least surface generation relative to its volume fraction of voids. Furthermore the increase of molecular weight in polycarbonate seems to retard the generation of surfaces even more.

The vast difference in surface scattering power between crazes formed in different polymers sheds light on the question of how to interpret the origin of the reflection streak. This author has previously proposed (3-40) that reflection may occur off the regular interfaces between craze matter and bulk polymer, while Tang (3-54,3-55) proposed that the reflection occurs from the distribution of cracks in the crazed matter (3-2). Since both the polystyrene and polycarbonate samples were profusely crazed, both samples provide large ammounts of interfacial surface area. However, the polycarbonate scattering patterns consistently show orders of magnitude less reflected component. Thus, in light of the fact that polycarbonate has far superior ultimate properties it is more appropriate to model the reflection scattering as surface scattering

from crack-like defects contained in the craze matter. In other words, the observation of superior mechanical properties and the observation of less reflection from crack-like defects are self consistent.

A summary of the volume and surface scattering correlation distances of crazed matter is found in Table 3.1 (page 159). Possibly as a result of the use of relaxed (unloaded during SAXS) samples, the values obtained for polystyrene are about fifty percent smaller than those reported by Tang (3-54,3-55). However the correlation lengths for polycarbonate are at least an order of magnitude greater than the polystyrene lengths. For the case of surface scattering, this indicates that there are large distances between inhomogeneous crack defects. For the case of volume scattering, this indicates that weighted average lengths of fibril and void are larger for polycarbonate. The crazed poly(methyl methacrylate) showed a scaled intermediate behavior between that of polystyrene and polycarbonate. Interestingly, the polysulfone crazed matter showed volume chord lengths the same as polycarbonate, while the surface correlation length was closer to the poly(methyl methacrylate) behavior.

From the data presented in Tables 3.1 and 3.2 (page 159 and 161), a generalized craze morphology model can be proposed based on the preliminary model of Tang (3-54). Figure 3.24 shows this model pictorially. For the case of polystyrene, many crack-like defects exist (large Ks) and the distance between inhomogeneities is relatively small (low tau). It is implied that in a random sample the

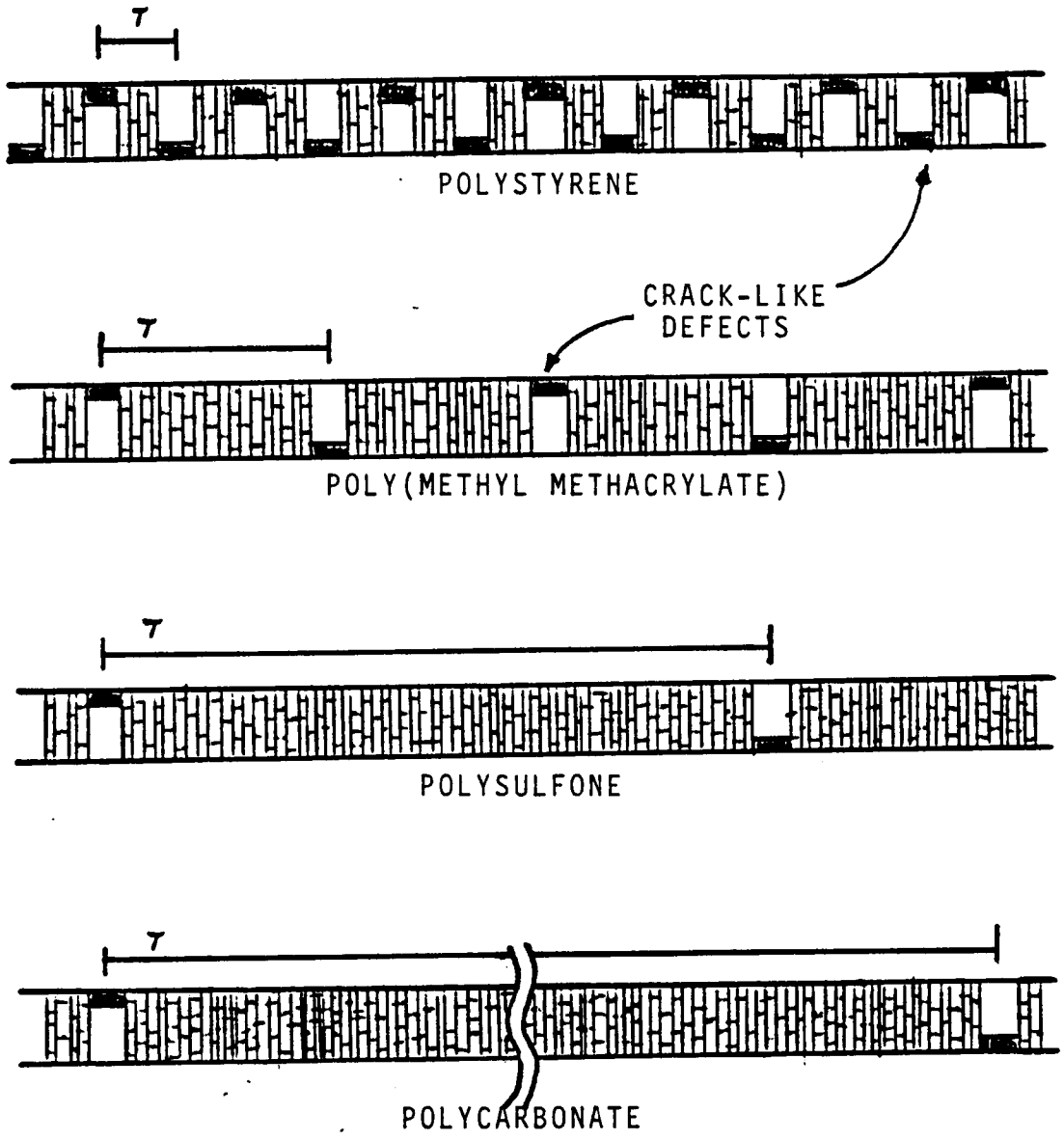

Figure 3.24. A generalized model for craze morphology.

probability of finding crazed matter which is extended the width of the craze is the same order of magnitude relative to the probability of finding relaxed material due to the action of the crack defect. In this model the relaxed craze material contains smaller void defects because the local stress which would extend the material is absent. Therefore the averaged chord length (l) is substantially affected by the large percentage of relaxed crazed material and the chord length is correspondingly low.

For the case of polycarbonate, few cracks exist as given by the magnitude of Ks and the distance between cracks is large (tau). It is implied that, in a random sample, the probability of finding crazed material affected by a crack defect is very low. Therefore, the overall averaged chord length (l) is not affected by a significant portion of relaxed crazed material. The values for (l) in polycarbonate and polysulfone are more indicative of the representative chord length of extended stress supporting crazed matter. The morphologies implied for poly(methyl methacrylate) and polysulfone are intended to display intermediate features between the extremes of polycarbonate and polystyrene.

CHAPTER IV

SUMMARY AND CONCLUSIONS

This work has provided a deeper understanding of the deformation characteristics of polymers in the glassy state. Stress-strain relationships have been modelled for pre-neck deformation, and craze morphology studies have been performed using small-angle x-ray scattering. As a result, a better understanding of the mechanical properties of glassy polymers has been gained.

In chapter two the combination of two rheological ideas resulted in a more satisfying theoretical analysis of viscoelasticity. That analysis is the generalization of a single Maxwell mechanical element (2-2) such that it will accomodate the more progressive notions of the behavior of monotonic decays in materials (2-33,2-35 through 2-41). Most of classical rheology is based on a mechanical element which dates back over 100 years. Therefore the mathematical properties and physical implications of that model are widely understood. Even so a single Maxwell element does not describe the behavior of a deforming viscoelastic solid, solution or melt because the real viscoelastic fluid responds as if it had a spectrum of time constants.

One idea which has been applied to viscoelasticity over the last five years attempts to broaden the characteristic time spectrum in a mathematical sense by including a power relationship for time in the exponential decay term (2-33). Such a relationship is called the

Williams-Watts (2-36) equation and it has been used successfully to model dielectric and magnetic as well as stress relaxation in materials. One major contribution of chapter two is to show how a classical viscoelastic model can be generalized to accomodate the Williams-Watts result for stress in the simple kinematics of constant strain. The mathematical power of the resulting integral model, which includes the deformation kinematics, is that it can then be solved for more complicated strain histories. The advantage this theory has over conventional integral models is that relationships for stress in terms of strain and time are obtained with two material parameters which are constant with respect to kinematics.

These constants, tau and n, are functions of the material and thermal conditions. Results obtained in this work however, indicate that molecular weight variables and thermal variables can produce rational variations in the model constants. For example, independent studies showed that tau scales to an Arrhenius equation for thermal variations in testing temperature (2-33,2-35). Further, it was shown here that a reduced molecular weight variable may help quantify material conditions for both tau and n. If future efforts can quantify these effects, then an important understanding of structure-property relationships in glassy materials would be reached.

It is further recommended that the generalized Maxwell model developed here be used to model stress-strain relationships in shear for polymer melts. It may be helpful to describe the flow behavior of viscoelastic fluids in various conduits.

In chapter three a fundamental understanding of the relative mechanical properties of several glassy polymers was gained by investigation of the morphology of crazes which are formed in the host glass. Studies of SAXS behavior of these crazed materials allow the determination of four independent parameters associated with the morphology (3-54,3-55). The surface and volume scattering invariants are proportional to the relative amount of surface area and volume discontinuities present in the sample. The surface and volume correlation distances are proportional to the distance between discontinuties in the sample. Typically the polycarbonates (including polysulfone) deform until stable necks form and the material is allowed to draw. Ultimate stresses and strains can exceed 70 megaPascals and 100 percent, respectively. SAXS studies reveal that crazes in these materials have relatively few crack-like defects. Conversely polystyrene (and to a lesser extent poly(methyl methacrylate)) is a brittle material at room temperature which will not form stable necks. Thus their ultimate stresses and strains reach only about 40 megaPascals and 2.5 percent, respectively, depending upon the molecular weight. SAXS studies revealed that their craze structure contains a relatively large number of crack-like defects. It is the relative proportion of these cracks which cause the crazed matter to be weakened and the material to be brittle.

Further SAXS studies of these materials should be performed using the on-line dynamic deformation sample holder at NCSASR (3-75,3-76). In this way, the structure development of inhomogeneous

deformations can be monitored during necking, drawing and fracture. In light of the fact that one cause of stress relaxation in these materials is the formation of large deformation zones, it would be interesting to determine if the dynamics and growth can be scaled to a Williams-Watts type of formulation.

LIST OF REFERENCES

LIST OF REFERENCES

2- 1) Han,C.D.,"Rheology in Polymer Processing," Acedemic Press, New York (1976)

2- 2) Maxwell,J.C., Phil. Trans. Roy. Soc., 157, 249 (1866)

2- 3) Boltzman,B., Sitzungber, Akad. Wiss. Wien., 70, 275 (1874)

2- 4) Zaremba,S., Bull. Acad. Cracovie, 594 (1903)

2- 5) Oldroyd,J.G., Proc. Roy. Soc. (London),A200, 523 (1950)

2- 6) Noll,W., Rat. Mech. Anal., 4, 13 (1955)

2- 7) White,J.L., and Metzner,A.B., J. Appl. Polym. Sci., 8, 1367 (1963)

2- 8) Williams,M.C., and Bird,R.B., Phys. Fluid, 5, 1126 (1962)

2- 9) Spriggs,S.E., and Bird,R.B., Ind. Chem. Fund., 4, 182 (1964)

2-10) Lodge,A.S., Trans. Faraday Soc., 52, 120 (1956)

2-11) Green,A.E., and Rivlin,R.S., Arch. Rat. Mech. Anal., 1, 1 (1957)

2-12) Coleman,B.D., and Noll,W., Arch. Rat. Mech. Anal., 6, 355 (1960)

2-13) Bernstein,B., Kersley,E.A. and Zappas,L.J., Trans. Soc. Rheo., 7, 931 (1963)

2-14) Bogue,D.C. and White,J.L., "Engineering Analysis of Non-Newtonian Fluids," NATO Agardograph 144 (1970)

2-15) Kuhn,W. and Grun,F., Kolloid-Z.,101, 248 (1942)

2-16) Whitfield,J.K. and Smith,C.W., Exp. Mech., 12, 72 (1972)

2-17) Dally,J.W. and Mulc,A., J. Appl. Mech., (1975)

2-18) Gurtman,G.A., Jenkins,W.C. and Tung,T.K., Douglass Report SM4T196 (1965)

2-19) Ward,I.M., "Mechanical Properties of Solid Polymers," John Wiley, New York (1979)

2-20) Hill,R., "The Mathematical Theory of Plasticity," Clarendon (1950)

2-21) Landau,H.G., Weiner,J.H. and Zwicky,E.E., J. Appl. Mech., 30, 297 (1960)

2-22) Naghdi,D.M. and Murch,S.A., J. Appl. Mech., 30, 321 (1963)

2-23) Crochet,M.J., J. Appl. Mech., 33, 327 (1966)

2-24) Brinson,H.F., Exp. Mech., 10, 72 (1970)

2-25) Brinson,H.F., Exp. Mech., 11, 467 (1971)

2-26) Brinson,H.F., Exp. Mech., 12, 130 (1972)

2-27) Brinson,H.F., "Deformation and Fracture of High Polymers," Plenum, 397 (1974)

2-28) Brinson,H.F. and DasGupta,A., Exp. Mech., 15, 458 (1975)

2-29) Reiner,M., "Advanced Rheology," Lewis, London (1971)

2-30) Brinson,H.F., Proc. Eur. Mech. Coll., 182, (1984)

2-31) Schapery,R.A., Polym. Eng. Sci., 9, 295 (1969)

2-32) Lou,Y.C. and Schapery,R.A., J. Comp. Mat., 33, 209 (1971)

2-33) Matsuoka,S., Polym. J., 17, 335 (1985)

2-34) Boyd,R.H., J. Polym. Sci. Phys. Ed., 16, 1227 (1978)

2-35) Matsuoka,S., Polym. Eng. Sci., 21, 907 (1981)

2-36) Williams,G. and Watts,D.C., Trans. Faraday Soc., 66, 80 (1970)

2-37) Ngai,K.L., Comm. Sol. St. Phys., 9, 127 (1979)

2-38) Ngai,K.L., Comm. Sol. St. Phys., 9, 141 (1980)

2-39) Rajagopal,A.K., Ngai,K.L., Rendell,R.W. and Teitler,S., J. Stat. Phys., 30, 285 (1983)

2-40) Ngai,K.L. and Rendell,R.W., Polymer Preprints, 23, 46 (1982)

2-41) Plazek,D.J., Ngai,K.L. and Rendell,R.W., Proc. IUPAC, 29 (1983)

2-42) Rendell,R.W., Lee,T.K. and Ngai,K.L., Proc. NATAS Conf. (1983)

2-43) Wylie,C.R. and Barrett,L.C., "Advanced Engineering Mathematics," McGraw-Hill, New York, 454 (1982)

2-44) Donald,A.M. and Kramer,E.J., MSC Report No. 4407 (1981)

2-45) Porter,R.S. and Johnson,J.E., Chem. Rev., 66, 1 (1966)

2-46) Agranof,J., ed., "Modern Plastics Encyclopedia," McGraw-Hill, New York, 60, 469-501 (1984)

2-47) Brinson,H.F., Proc. Eur. Mech. Coll., 182 (1984)

2-48) Agranof,J., ed., "Modern Plastics Encyclopedia," McGraw-Hill, New York, 60, 470-500 (1984)

2-49) Agranof,J., ed., "Modern Plastics Encyclopedia," McGraw-Hill, New York, 60, 564-577 (1984)

2-50) Agranof,J., ed., "Modern Plastics Encyclopedia," McGraw-Hill, New York, 60, 512-531 (1984)

2-51) Findley,W.N. and Worley,W.J., Proc. Soc. Exp. Stress Anal., 17, 5 (1959)

2-52) Burden,R.L., Faires,J.D. and Reynolds,A.C., "Numerical Analysis" Prindle, Weber and Schmidt, Boston, Mass (1981)

3- 1) Agranof,J., ed., "Modern Plastics Encyclopedia," McGraw-Hill, New York, 60, 495 (1984)

3- 2) Lauterwasser,B.D. and Kramer,E.J., Phil. Mag., 39, 469 (1979)

3- 3) Kambour,R.P., J. Polym. Sci. Macromol. Rev., 7, 1 (1973)

3- 4) Rabinowitz,S. and Beardmore,P., CRC Crit. Rev. Macro. Molec. Sci. (1972)

3- 5) Kausch,H.H., "Polymer Fracture," Springer-Verlag N.Y. (1978)

3- 6) Kambour,R.P. and Robertson,R., General Electric Report, 70-C-104 (1970)

3- 7) Sternstein,S.S. and Meyers,F., Macromol. Sci. Phys. ed., 88, 539 (1973)

3- 8) Sternstein,S.S., Ongchin,L. and Silverman,A., Appl. Poly. Symp., 7, 175 (1968)

3- 9) Kambour,R.P., J. Polym. Sci., 2, 4159 (1964)

3-10) LeGrand,D.G., J. Appl. Poly. Sci., 20, 1573 (1976)

3-11) Farrar,N.R. and Kramer,E.J., MSC Report No. 4267 (1981)

3-12) Sauer,J.A. and Hsiao,C.C., J. Appl. Phys., 21, 1071 (1950)

3-13) Sauer,J.A., Marin,J. and Hsiao,C.C., J. Appl. Phys., 20, 507 (1979)

3-14) Argon,A., Cohen,R., Zang,B. and Vandersande,J., J. Polym. Sci. Phys. Ed., 19, 253 (1981)

3-15) Behan,P., Bevis,M. and Hull,D., J. Mat. Sci., 78, 162 (1972)

3-16) Behan,P., Bevis,M. and Hull,D., Phil. Mag., 24, 1267 (1971)

3-17) Behan,P., Bevis,M. and Hull,D., Polymer, 14, 96 (1973)

3-18) Behan,P., Bevis,M. and Hull,D., Phil. Mag., 24 192 (1971)

3-19) Bevis,M. and Hull,D., J. Mat. Sci., 5, 983 (1970)

3-20) Bird,R.J., Mann,J., Pogany,G. and Rooney,G., Phil. Mag., 19, 307 (1966)

3-21) Haward,R.N. and Owen,D., J. Mat. Sci., 8, 1136 (1978)

3-22) Hoare,J. and Hull,D., Phil. Mag., 24, 443 (1971)

3-23) Hull,D., J. Mat. Sci., 5, 357 (1970)

3-24) Kambour,R.P., ACS Meeting (1962)

3-25) Kambour,R.P. and Holik,A.J., J. Polym. Sci., 1, 1393 (1969)

3-26) Murray,J. and Hull,D., J. Polym. Sci., 8, 1513 (1971)

3-27) Murray,J. and Hull,D., J. Polym. Sci., 7, 583 (1970)

3-28) Wellinghoff,S. and Baer,E., J. Appl. Sci. 22, 2025 (1978)

3-29) Kambour,R.P., J. Polym. Sci., 4, 319 (1966)

3-30) Guinier,A. and Fournet,G., "Small-Angle Scattering of X-Rays," John Wiley, N.Y. (1955)

3-31) Legrand,D.G., Kambour,R.P. and Haaf,W.R., J. Polym. Sci, 10, 1565 (1972)

3-32) Steger,T.R. and Neilson,L.E., J. Poly. Sci. Phys. Ed., 16, 613 (1978)

3-33) Haward,R.N. Ed., "The Physics of Glassy Polymers," John Wiley N.Y. (1974)

3-34) Fellers,J.F. and Chapman,T.F., J. Appl. Sci., 22, 1029 (1978)

3-35) Kambour,R.P., Polym. Eng. Sci., 8, 569 (1968)

3-36) Donald,A.M. and Kramer,E.J., Phil. Mag., A43, 857 (1981)

3-37) Donald,A.M. and Kramer,E.J., J. Mat. Sci., 18, 272 (1982)

3-38) Chan,T., Donald,A.M. and Kramer,E.J., J. Mat. Sci., 16, 676 (1981)

3-39) Fellers,J.F. and Kee,B.F., J. Appl. Polym. Sci., 18, 2355 (1974)

3-40) Westbrook,P.A., Masters Thesis, Univ. Tenn., (1982)

3-41) Brown,H.R., J. Polym. Sci. Phys. Ed., 21, 483 (1983)

3-42) Donald,A.M. and Kramer,E.J., MSC Report No. 4463 (1981)

3-43) King,P. and Kramer,E.J., J. Mat. Sci., 16, 1843 (1981)

3-44) Taylor,G., Proc. Roy. Soc., A201, 192 (1950)

3-45) Wellinghoff,S. and Baer,E., J. Macromol. Sci. Phys. Ed. B11, 367 (1975)

3-46) Pape,E. and Kreutz,W., Phil. Mag., 21, 451 (1968)

3-47) Westbrook,P.A., Fellers,J.F., Hendricks,R.W. and Lin,J.S., J. Polym. Sci., Phys. Ed., 21, 969 (1983)

3-48) Brown,H.R. and Kramer,E.J., J. Macromol. Sci. Phys. Ed., B19, 487 (1981)

3-49) Parades,E. and Fischer,E., Macromol. Chem., 180, 2707 (1979)

3-50) Parvin,M. and Williams,J., Polym. Eng. Sci., 21, 816 (1981)

3-51) Brown,H.R., Personal Communication (1982)

3-52) Westbrook,P.A., Fellers,J.F., Cakmak,M., Lin,J.S. and Hendricks,R.W., J. Polym. Sci. Phys. Ed., 21, 1913 (1983)

3-53) Halliday,D. and Resnick,R., "Fundementals of Physics," John Wiley, New York, 732 (1974)

3-54) Tang,M.Y., Ph.D. Dissertation, Univ. Tenn., (1984)

3-55) Tang,M.Y., Fellers,J.F. and Lin,J.S., J. Polym. Sci. Phys. Ed., 22, 2215 (1984)

3-56) Beaglehole,D. and Hunderi,O., Phys. Rev. B, 2, 309,321 (1970)

3-57) Elson,J.M. and Ritchie,R.H., Phys. Rev. B, 4, 4129 (1971)

3-58) Elson,J.M., Phys. Rev. B, 12, 2541 (1975)

3-59) Kroger,E. and Kretshmann,E., Z. Phys., 27, 1 (1970)

3-60) Elson,J.M. and Bennet,J.M., J. Opt. Sci. Am., 69, 31 (1979)

3-61) Elson,J.M., J. Opt. Sci. Am., 66, 682 (1976)

3-62) Porod,G., Kolloid-Z., 24, 83 (1951)

3-63) Mandlebrot,B., "The Fractal Geometry of Nature," Freemen San Fransisco (1982)

3-64) Schaefer,D.W., Martin,J.E., Wiltzius,P. and Cannell,D., Phys. Rev. Lett., 52, 2371 (1984)

3-65) Schaefer,D.W., Martin,J.E., Wiltzius,P. and Cannell,D., Prodeedings of the International Conference on Kinetics of Aggregation and Gelation, (1984)

3-66) Sinha,S., Freltoft,T. and Kjens,J., Proceedings of the International Conference on Kinetics of Aggregation and Gelation, (1984)

3-67) Weitz,D. and Huang,J.S., Proceedings of the International Conference on Kinetics of Aggregation and Gelation, (1984)

3-68) Bale,H. and Schmidt,P.W., Phys. Rev. Lett., 53, 596 (1984)

3-69) Brown,H.R., Ultramicroscopy, 7, 263 (1982)

3-70) Fellers,J.F. and Huang,D.C., J. Appl. Polym. Sci., 23, 2315 (1979)

3-71) Wool,R. and O'Connor,K., Polym. Eng. Sci., 21, 14 (1981)

3-72) Flory,P.J., "Principles of Polymer Chemistry," Cornell Press (1953)

3-73) Wendorff,J.H. and Fischer,E.W., Kolloid-Z., Polymere, 251 884 (1973)

3-74) Wendorff,J.H. and Fischer,E.W., Kolloid-Z., Polymere, 251 867 (1973)

3-75) Hendricks,R.W., J. Appl. Cryst., 11, 15 (1978)

3-76) Hendricks,R.W., Suehiro,S. and Lin,J.S., Bull. Am. Phys. Soc., 27, 357 (1982)

3-77) Luzzati,V., "X-Ray Optics and X-Ray Microanalysis," Patee,H.H., Cosslett,V.E. and Engstrom,A., Eds., Academic Press New York, (1963)

3-78) Pilz,I., J. Coll. Int. Sci., 30, 140 (1969)

3-79) Pilz,I. and Kratky,O., J. Coll. Int. Sci., 24, 211 (1967)

3-80) Kratky,O. and Milholic,G., J. Polym. Sci., 2, 449 (1963)

APPENDICES

APPENDIX A

MECHANICAL PROPERTIES

Table A.1. Instantaneous mechanical behavior of polycarbonate.

Percent Strain	Effective Modulus(GPa)	Fitted Stress(MPa)	Percent Error	a	E(GPa)
	120 GRADE			14.7	2.42
0.00	2.36	0.00	0.0		
0.50	2.36	12.0	1.6		
1.00	2.35	23.6	0.2		
1.50	2.30	34.5	0.0		
2.00	2.19	44.3	1.0		
2.50	2.10	52.6	0.5		
3.00	1.97	59.2	0.2		
3.50	1.85	63.8	0.9		
4.00	1.72	66.0	4.1		
4.50	1.50	65.8	7.8		
	100 GRADE			14.5	2.48
0.00	2.53	0.0	0.0		
0.50	2.53	12.3	2.4		
1.00	2.42	24.2	0.2		
1.50	2.35	35.4	0.0		
2.00	2.20	44.1	3.1		
2.50	2.14	53.4	1.3		
3.00	2.03	60.9	0.0		
3.50	1.92	67.1	1.5		
4.00	1.76	69.1	1.9		
4.50	1.62	70.0	3.7		
	130 GRADE			14.6	2.48
0.00	2.56	0.0	0.0		
0.50	2.56	12.3	3.8		
1.00	2.45	24.3	1.1		
1.50	2.36	35.5	0.0		
2.00	2.26	45.5	0.6		
2.50	2.14	53.6	1.0		
3.00	2.03	61.0	0.0		
3.50	1.91	66.0	1.1		
4.00	1.78	69.0	1.8		

Table A.2. Instantaneous mechanical behavior of polystyrene.

Percent Strain	Effective Modulus(GPa)	Fitted Stress(MPa)	Percent Error	a	E(GPa)
	S104			13.7	2.38
0.00	2.35	0.0	0.0		
0.15	2.35	3.57	1.4		
0.30	2.36	7.09	0.7		
0.45	2.36	10.7	0.0		
0.60	2.36	14.2	0.1		
0.75	2.36	17.7	0.4		
0.90	2.34	21.1	0.0		
1.05	2.33	24.5	0.1		
1.20	2.33	27.8	0.5		
1.35	2.31	31.1	0.4		
1.50	2.26	34.2	0.8		
1.65	2.24	37.3	1.1		
	685D			21.8	2.46
0.00	2.53	0.0	0.0		
0.15	2.53	3.79	2.7		
0.30	2.49	7.35	1.4		
0.45	2.44	10.9	0.0		
0.60	2.40	14.5	1.0		
0.75	2.39	18.0	0.5		
0.90	2.37	21.3	0.0		
1.05	2.30	24.5	0.1		
1.20	2.30	27.6	0.4		
1.35	2.28	30.4	1.2		
1.50	2.25	33.1	1.9		
1.65	2.23	35.6	3.4		
1.80	2.21	37.8	5.0		
1.95	2.19	39.8	6.2		
2.10	2.10	41.6	5.8		

Table A.3. Instantaneous mechanical behavior of polysulfone.

Percent Strain	Effective Modulus(GPa)	Fitted Stress(MPa)	Percent Error	a	E(GPa)
	P1700			14.2	3.42
0.00	3.43	0.0	0.0		
0.50	3.43	16.9	1.1		
1.00	3.40	33.4	1.9		
1.50	3.25	48.9	0.0		
2.00	3.14	62.8	0.1		
2.50	2.98	74.9	0.8		
3.00	2.82	84.8	0.0		
3.50	2.68	92.4	2.0		
	P3500			14.2	3.45
0.00	3.36	0.0	0.0		
0.50	3.36	17.6	4.8		
1.00	3.36	33.7	3.6		
1.50	3.38	50.8	0.0		
2.00	3.24	65.3	0.9		
2.50	3.10	77.9	0.7		
3.00	2.94	88.3	0.0		
3.50	2.76	95.8	0.8		
4.00	2.57	101.	2.1		

Table A.4. Instantaneous mechanical behavior of poly(methyl methacrylate).

Percent Strain	Effective Modulus(GPa)	Fitted Stress(MPa)	Percent Error	a	E(GPa)
	2805			15.5	2.40
0.00	2.46	0.0	0.0		
0.50	2.46	11.9	3.6		
1.00	2.33	23.3	0.2		
1.50	2.25	33.9	0.0		
2.00	2.16	43.3	0.1		
2.50	2.02	51.2	1.0		
3.00	1.91	57.2	0.0		
3.50	1.78	61.3	1.4		

Table A.5. Rate dependent mechanical behavior of polystyrene (S104).

	0.04 min^{-1}		0.004 min^{-1}		0.0004 min^{-1}	
Percent Strain	Measured Stress (MPa)	Percent Error	Measured Stress (MPa)	Percent Error	Measured Stress (MPa)	Percent Error
0.00	0.0	0.0	0.0	0.0	0.0	0.0
0.15	3.66	0.0	3.25	3.6	2.65	19.0
0.30	6.71	0.0	6.61	1.2	5.18	17.0
0.45	10.1	0.0	9.85	0.6	8.03	19.0
0.60	13.3	0.0	13.1	1.2	10.7	15.0
0.75	16.6	0.0	16.1	0.5	13.7	13.0
0.90	19.7	0.0	18.8	1.8	16.2	13.0
1.05	22.8	0.0	21.6	2.1	18.9	11.0
1.20	26.1	0.0	24.2	4.0	21.5	12.0
1.35	29.0	0.0	26.9	4.1	23.9	12.0
1.50	31.6	0.0	29.5	3.3	26.5	9.7
1.65	34.3	0.0	32.1	3.0	29.0	8.7

Table A.6. Rate dependent mechanical properties of polystyrene (685D).

	$0.04\ min^{-1}$		$0.004\ min^{-1}$		$0.0004\ min^{-1}$	
Percent Strain	Measured Stress (MPa)	Percent Error	Measured Stress (MPa)	Percent Error	Measured Stress (MPa)	Percent Error
0.00	0.0	0.0	0.0	0.0	0.0	0.0
0.15	3.44	0.0	3.30	1.2	3.22	0.5
0.30	6.71	0.0	6.14	4.0	6.13	1.4
0.45	9.81	0.0	9.19	3.1	8.98	0.9
0.60	12.8	0.0	12.3	0.0	11.9	0.7
0.75	15.9	0.0	15.1	1.4	14.6	0.1
0.90	18.9	0.0	17.7	2.7	17.3	0.1
1.05	21.6	0.0	20.6	0.8	19.3	0.5
1.20	24.4	0.0	23.3	0.4	22.5	0.9
1.35	27.1	0.0	26.2	0.5	25.1	1.3
1.50	29.6	0.0	28.8	1.3	28.0	3.4
1.65	32.3	0.0	31.4	1.3	30.3	2.7
1.80	34.8	0.0	33.8	1.0	32.9	3.3
1.95	37.1	0.0	35.5	0.3	34.4	1.8
2.10	38.5	0.0	37.0	0.3	35.9	2.5

Table A.7. Rate dependent mechanical behavior of polycarbonate (120G).

	0.04 min^{-1}		0.004 min^{-1}		0.0004 min^{-1}	
Percent Strain	Measured Stress (MPa)	Percent Error	Measured Stress (MPa)	Percent Error	Measured Stress (MPa)	Percent Error
0.00	0.0	0.0	0.0	0.0	0.0	0.0
0.50	11.1	0.0	11.0	0.2	10.6	0.6
1.00	22.1	0.0	21.4	1.6	20.3	4.3
1.50	32.3	0.0	31.0	2.3	29.7	4.1
2.00	40.9	0.0	39.2	2.4	37.6	4.2
2.50	48.7	0.0	47.3	0.9	44.8	3.9
3.00	55.0	0.0	53.2	1.4	50.6	3.9
3.50	60.3	0.0	58.0	1.7	55.1	4.4
4.00	63.9	0.0	61.0	2.5	58.7	3.8
4.50	66.1	0.0	64.0	1.0	61.0	3.3

Table A.8. Rate dependent mechanical behaviior of polycarbonate (100G).

	0.04 min^{-1}		0.004 min^{-1}		0.0004 min^{-1}	
Percent Strain	Measured Stress (MPa)	Percent Error	Measured Stress (MPa)	Percent Error	Measured Stress (MPa)	Percent Error
0.00	0.0	0.0	0.0	0.0	0.0	0.0
0.50	11.4	0.0	11.3	1.6	11.0	1.5
1.00	21.6	0.0	21.4	1.1	20.7	0.4
1.50	31.5	0.0	30.7	0.4	29.9	0.6
2.00	39.2	0.0	38.5	0.7	37.6	0.9
2.50	47.3	0.0	45.9	0.7	45.1	0.4
3.00	54.0	0.0	52.5	0.3	51.5	0.6
3.50	59.3	0.0	57.1	1.3	55.6	1.1
4.00	62.1	0.0	59.8	1.4	58.5	0.8
4.50	64.1	0.0	62.3	0.4	60.6	0.3

Table A.9. Rate dependent mechanical properties of polycarbonate (130G).

	0.04 min^{-1}		0.004 min^{-1}		0.0004 min^{-1}	
Percent Strain	Measured Stress (MPa)	Percent Error	Measured Stress (MPa)	Percent Error	Measured Stress (MPa)	Percent Error
0.00	0.0	0.0	0.0	0.0	0.0	0.0
0.50	11.0	0.0	10.7	0.9	10.6	1.1
1.00	20.9	0.0	20.9	2.1	20.7	3.7
1.50	30.2	0.0	30.1	2.2	30.0	4.3
2.00	38.5	0.0	38.3	2.4	38.3	4.8
2.50	45.3	0.0	45.1	2.0	44.8	3.9
3.00	51.5	0.0	51.1	1.7	50.4	3.1
3.50	56.2	0.0	55.7	1.7	54.6	2.4
4.00	59.7	0.0	59.0	1.4	57.0	0.8

Table A.10. Rate dependent mechanical behavior of polysulfone (1700).

	$0.04\ min^{-1}$		$0.004\ min^{-1}$		$0.0004\ min^{-1}$	
Percent Strain	Measured Stress (MPa)	Percent Error	Measured Stress (MPa)	Percent Error	Measured Stress (MPa)	Percent Error
0.00	0.0	0.0	0.0	0.0	0.0	0.0
0.50	13.6	0.0	13.4	0.4	13.3	0.5
1.00	26.9	0.0	26.1	1.7	25.6	2.5
1.50	38.5	0.0	38.0	0.5	37.6	0.2
2.00	49.5	0.0	48.7	0.4	48.2	0.2
2.50	58.4	0.0	57.7	0.2	57.4	0.8
3.00	66.6	0.0	65.7	0.6	65.4	0.7
3.50	73.8	0.0	72.8	0.8	71.7	1.2

Table A.11. Rate dependent mechanical behavior of polysulfone (3500).

	0.04 min^{-1}		0.004 min^{-1}		0.0004 min^{-1}	
Percent Strain	Measured Stress (MPa)	Percent Error	Measured Stress (MPa)	Percent Error	Measured Stress (MPa)	Percent Error
0.00	0.0	0.0	0.0	0.0	0.0	0.0
0.50	12.7	0.0	12.4	1.4	12.3	0.7
1.00	25.3	0.0	24.9	0.4	24.7	0.2
1.50	38.2	0.0	37.1	1.8	36.6	2.0
2.00	48.6	0.0	47.4	1.4	47.1	0.9
2.50	58.0	0.0	56.8	0.8	56.5	0.3
3.00	66.0	0.0	65.2	0.1	64.9	0.5
3.50	72.4	0.0	71.0	0.5	69.6	0.9
4.00	76.5	0.0	75.8	1.2	75.2	1.9

Table A.12. Rate dependent mechanical behavior of poly(methyl methacrylate) (2805).

	0.04 min^{-1}		0.004 min^{-1}		0.0004 min^{-1}	
Percent Strain	Measured Stress (MPa)	Percent Error	Measured Stress (MPa)	Percent Error	Measured Stress (MPa)	Percent Error
0.00	0.0	0.0	0.0	0.0	0.0	0.0
0.50	11.9	0.0	11.8	0.7	11.1	3.3
1.00	22.5	0.0	22.1	0.1	21.6	0.4
1.50	32.5	0.0	31.8	0.5	31.2	0.2
2.00	41.4	0.0	40.5	0.1	40.0	1.4
2.50	48.4	0.0	47.8	0.9	47.1	2.2
3.00	54.6	0.0	53.6	0.4	52.9	2.0
3.50	59.3	0.0	58.1	0.1	57.1	1.5

APPENDIX B

COMPUTER PROGRAMS

```
c*************************************************************************c
c                                                                         c
c  Programmer: Paul Westbrook                                             c
c                                                                         c
c       The following program calculates theoretical stress strain        c
c  curves for glassy polymers.  The program inputs a known stress-        c
c  strain curve at a specified rate of deformation, then calculates       c
c  new stress-strain behavior at another specified rate of deforma-       c
c  tion.  The relaxation behavior is calculated from Equation 2.17        c
c  using a generalized Maxwell model.  The material parameters are        c
c  also input.  The algorithm further compares the theoretical pre-       c
c  diction for stress with experimentally determined stress-strain        c
c  behavior.  Lastly, the theoretical instantaneous deformation           c
c  behavior is fit to both a cosine and a cosine squared impirical        c
c  fit (Equation 2.12) and the model parameters are output.               c
c                                                                         c
c               Variables:                                                c
c                  TISTRE: Theoretical instantaneous stress               c
c                  TSTRES: Theoretical stress                             c
c                  ERROR : Theoretitical error from experiment            c
c                  STIFF : Secant modulus                                 c
c                  TIME  : Laboratory time                                c
c                  DTIME : Deborah number (see Equation 2.20)             c
c                  RELAX : Relaxation factor                              c
c                  STRAIN: Sample strain                                  c
c                  STRESS: Experimentally determined stress               c
c                  PISTRE: Fitted instantaneous stress                    c
c                  ERRORI: Error of instantaneous stress fit              c
c                  FISTRE: Fitted instantaneous stress                    c
c                  TAU   : Relaxation element time constant               c
c                  EX    : Relaxation element shape factor                c
c                                                                         c
c*************************************************************************c
c
c
      DIMENSION TISTRE(15), TSTRES(15,3), ERROR(15,3), STIFF(15)
      DIMENSION TIME(15,3), DTIME(15,3), RELAX(15,3), STRAIN(15)
      DIMENSION STRESS(15,3), PISTRE(15), ERRORI(15), FISTRE(15)
c
c  Input model parameters, number of data points and then experimental
c  elapsed times.  The Deborah number is calculated for each time and
c  the strains are incremented at one half percent.
c
      READ (20,*) EX, TAU, NTIME
      DO 100 I=1, NTIME
            READ (20,*) (TIME(I,J), J=1,3)
            DO 150 J=1,3
                  DTIME(I,J)=(TIME(I,J)/TAU)**EX
150         CONTINUE
            STRAIN(I)=0.0050*FLOAT(I-1)
100   CONTINUE
```

```
c
c  The relaxation factor is calculated for each Deborah number.
c
        DO 200 I=1, NTIME
                DO 250 J=1,3
                        STIME=DTIME(I,J)
                        CALL SIMPSO(STIME, EX, ANS)
                        RELAX(I,J)=ANS
 250            CONTINUE
 200    CONTINUE
c
c  The experimentally observed stresses are input for each deformation
c  rate.
c
        DO 120 I=1,NTIME
                READ(22,*) STRESS(I,1), STRESS(I,2), STRESS(I,3)
 120    CONTINUE
c
c  The instantaneous stresses are calculated from the fastest
c  deformation rate by dividing by the appropriate relaxation factor.
c  Then the theoretical stresses are calculated by multiplying the
c  theoretical instantaneous stress by the appropriate relaxation
c  factor.
c
        DO 300 I=1,NTIME
                TISTRE(I)=STRESS(I,1)/RELAX(I,1)
                DO 350 J=1,3
                        TSTRES(I,J)=TISTRE(I)*RELAX(I,J)
                        IF (I.EQ.1) ERROR(I,J)=0.0
                        IF (I.EQ.1) GO TO 350
                        ERROR(I,J)=(TSTRES(I,J)/STRESS(I,J)-1.0)*100.
 350            CONTINUE
 300    CONTINUE
c
c  Output the results of rate dependent stress-strain curves and
c  compare to experiment.
c
        ER=2.0
        DO 400 J=1,3
                ER=ER/10.0
                WRITE(21,1) ER
                WRITE(21,2)
                WRITE(21,3)
                WRITE(21,4)(STRAIN(I),STRESS(I,J),TSTRES(I,J),
     C          ERROR(I,J), TIME(I,J), I=1,NTIME)
                WRITE(21,5)
 400    CONTINUE
c
c  Calculate stiffnesses as a function of strain for the instantaneous
c  deformation case.
c
```

```
      DO 500 I=2,NTIME
             STIFF(I)=TISTRE(I)/STRAIN(I)
500   CONTINUE
      STIFF(1)=STIFF(2)
      A=8.1
c
c  Fit the stiffnesses to a cosine model.  The results of this fit are
c  not discussed in the text because the cosine squared fit works
c  better.
c
      DO 600 I=1,50
             AA=ACOS(COS(A*STRAIN(4))*TISTRE(7)*STRAIN(4)/
     C       (TISTRE(4)*STRAIN(7)))/STRAIN(7)
             DIFFER=ABS(AA-A)
             A=AA
             IF (DIFFER.LT.0.001) GO TO 601
600   CONTINUE
      WRITE(21,6)
601   WRITE(21,66)
      WRITE(21,7)
      DO 700 I=1,NTIME
             WRITE(21,8) STRAIN(I), STIFF(I), TISTRE(I)
700   CONTINUE
      WRITE(21,5)
      E=TISTRE(4)/(COS(A*STRAIN(4))*STRAIN(4))
      WRITE(21,9) A
      WRITE(21,10) E
      DO 800 I=1,NTIME
             PISTRE(I)=COS(A*STRAIN(I))*E*STRAIN(I)
             IF (I.EQ.1) ERRORI(I)=0.0
             IF (I.EQ.1) GO TO 800
             ERRORI(I)=(PISTRE(I)/TISTRE(I)-1.0)*100.0
800   CONTINUE
      WRITE(21,11)
      WRITE(21,12)
      WRITE(21,13)(STRAIN(I),TISTRE(I),PISTRE(I),ERRORI(I),
     C  I=1,NTIME)
      YSTRAI=0.04
      TEMP=YSTRAI*A
      DO 900 I=1,50
             TEMP2=ATAN(1.0/TEMP)
             DIFFER=ABS(TEMP2-TEMP)
             TEMP=TEMP2
             IF (DIFFER.LT.0.0001) GO TO 901
900   CONTINUE
      WRITE(21,14)
901   YSTRAI=TEMP/A
      YSTRES=COS(A*YSTRAI)*YSTRAI*E
      WRITE(21,15) YSTRES
      WRITE(21,16) YSTRAI
```

```
c
c  Fit the instantaneous stiffnesses to a cosine squared model (see
c  Equation 2.12).  The fourth and seventh stresses are used as nodes
c  in the simultaneous solution of two equations.
c
        B=8.1
        DO 650 I=1,50
                BB=ACOS(((COS(B*STRAIN(4))**2.0)*TISTRE(7)*STRAIN(4)/
     C          (TISTRE(4)*STRAIN(7)))**0.5)/STRAIN(7)
                DIFFER=ABS(BB-B)
                B=BB
                IF (DIFFER.LT.0.001) GO TO 651
 650    CONTINUE
        WRITE(21,6)
c
c  Calculate the fitted modulus parameter.
c
 651    EE=TISTRE(4)/((COS(B*STRAIN(4))**2.0)*STRAIN(4))
        WRITE(21,5)
        WRITE(21,17)B
        WRITE(21,18)EE
c
c  Calculate the fitted instantaneous stresses and compare to
c  experimental values.
c
        DO 850 I=1,NTIME
                FISTRE(I)=(COS(B*STRAIN(I))**2.0)*EE*STRAIN(I)
                IF (I.EQ.1) ERRORI(I)=0.0
                IF (I.EQ.1) GO TO 850
                ERRORI(I)=(FISTRE(I)/TISTRE(I)-1.0)*100.0
 850    CONTINUE
c
c  Output the results of cosine squared fit.
c
        WRITE(21,11)
        WRITE(21,12)
        WRITE(21,13)(STRAIN(I),TISTRE(I),FISTRE(I),ERRORI(I),
     C  I=1,NTIME)
        YYSTRA=0.04
        TTEMP=YYSTRA*B
c
c  Determine the expected yield strain through a recursive relation
c  (see Equation 2.19).
c
        DO 950 I=1,50
                TTEMP2=ATAN(0.5/TTEMP)
                DIFFER=ABS(TTEMP2-TTEMP)
                TTEMP=TTEMP2
                IF (DIFFER.LT.0.00001) GO TO 951
 950    CONTINUE
```

```
c
c  Output the yield values.
c
        WRITE(21,14)
        WRITE(5,*) TTEMP
 951    YYSTRA=TTEMP/B
        YYSTRE=((COS(B*YYSTRA))**2.0)*YYSTRA*EE
        WRITE(21,15) YYSTRE
        WRITE(21,16) YYSTRA
        STOP
   1    FORMAT(' FOR A RATE OF',F6.3,' INCHES PER MINUTE',/)
   2    FORMAT( 16X,'MEASURED',7X,'THEORETICAL',4X,'PERCENT')
   3    FORMAT(' STRAIN',9X,'STRESS',9X,'STRESS',9X,'ERROR',15X,'TIME')
   4    FORMAT( 5G15.8)
   5    FORMAT('1')
   6    FORMAT(' ***COSINE FIT ITERATION EXCEEDS FIFTY***',//)
  66    FORMAT(16X,'EFFECTIVE',6X,'INSTANTANEOUS')
   7    FORMAT(' STRAIN',9X,'MODULUS',8X,'STRESS')  .
   8    FORMAT( 3G15.8)
   9    FORMAT(' COSINE FIT PARAMETER EQUALS',F15.8)
  10    FORMAT(' FITTED MODULUS PARAMETER EQUALS  ',F15.8,//)
  11    FORMAT(16X,'INSTANTANEOUS',2X,'FITTED',9X,'PERCENT')
  12    FORMAT(' STRAIN',9X,'STRESS',9X,'STRESS',9X,'ERROR')
  13    FORMAT( 4G15.8)
  14    FORMAT(' ***YIELD ITERATION EXCEEDS FIFTY***')
  15    FORMAT(//,' PREDICTED YIELD STRESS EQUALS',F15.8,' PSI')
  16    FORMAT(' PREDICTED YIELD STRAIN EQUALS',F15.8)
  17    FORMAT(' COSINE SQUARE FIT PARAMETER EQUALS',F15.8)
  18    FORMAT(' MODULUS FIT PARAMETER EQUALS  ',F15.8)
        END
```

```
c
c  Subroutine SIMPSO integrates the relaxation element of Equation 2.17
c  by a compounded Simpson's rule.
c
        SUBROUTINE SIMPSO(DTIME, EX, ANS)
c
c  Divide interval up into eight subintervals.
c
        DIV=16.0
        NOSIM=8
        AREA=0.0
        WIDTH=DTIME/DIV
        IF (DTIME.EQ.0.0) GO TO 100
```

```
c
c  Evaluate equations of condition and sum up the areas.
c
        DO 100 I=1,NOSIM
                TL=2.0*FLOAT(I-1)*WIDTH
                TR=2.0*FLOAT(I)*WIDTH
                TM=(TL+TR)/2.0
                FL=((TL/DTIME)**EX)*EXP(TL-DTIME)
                FM=((TM/DTIME)**EX)*EXP(TM-DTIME)
                FR=((TR/DTIME)**EX)*EXP(TR-DTIME)
                A=(WIDTH/3.0)*(FL+4.0*FM+FR)
                AREA=AREA+A
 100    CONTINUE
c
c  Return the value of the integral.
c
        ANS=1.0-AREA
        RETURN
        END
```

```
c*************************************************************************c
c                                                                         c
c  Programmer: Paul Westbrook                                             c
c                                                                         c
c       The following program calculates the material parameters          c
c  Tau and N for the Williams-Watts relaxation equation (see              c
c  Equations 2.10 and 2.11).  The program works in an interactive         c
c  mode where the user inputs N and a step size and a number of           c
c  steps.  The computer then calculates an optimum Tau for the best       c
c  fit of the data for each N in the spectrum specified by the user.      c
c  A fit parameter which is the correlation coefficient of the fit        c
c  is output to the screen for each N.  The user attempts to              c
c  optimise the fit for his choice of N.  Finally, the program            c
c  calculates Tau for the optimum N chosen by the user.                   c
c  The program uses relaxation data at three different times in           c
c  order to calculate Tau and N.  In this work, data at times 0.01,       c
c  1.00 and 100.0 minutes were used.                                      c
c                                                                         c
c               Variables:                                                c
c                  T     : Time of relaxation data                        c
c                  R     : Force at time T                                c
c                  RESID : Residuals in fit determination                 c
c                                                                         c
c*************************************************************************c
c
c
        IMPLICIT DOUBLE PRECISION (A-H,O-Z)
        DIMENSION T(3), R(3)
c
c  Input relaxation data points.
c
        READ (20,*) (T(I), I=1,3)
        READ (20,*) (R(I), I=1,3)
        DO 110 I=1,3
                R(I)=-ALOG(R(I))
 110    CONTINUE
 900    WRITE (5,1)
   1    FORMAT(' INPUT EXPONENT, STEP SIZE, AND NUMBER OF STEPS (*).')
        READ  (5,*) EX, DELTA, NSTEPS
c
c  Calculate fit parameters for each N specified by incrementation.
c
        DO 100 I=1,NSTEPS
                RESID= (T(2)**EX-T(1)**EX)/(T(3)**EX-T(1)**EX)
                RESID= RESID-(R(2)-R(1))/(R(3)-R(1))
                WRITE (5,*) EX, RESID
                EX=EX-DELTA
 100    CONTINUE
        WRITE (5,2)
   2    FORMAT(' ANOTHER SCAN (YES=1)?')
        READ  (5,*) IANS
```

```
      IF    (IANS.EQ.1)       GO TO 900
c
c  When search is complete, calculate Tau for optimum N determined
c  above.
c
      WRITE (5,3)
   3  FORMAT(' INPUT DESIRED EXPONENT')
      READ  (5,*) DEX
      TAU= (T(2)**DEX-T(1)**DEX)/(R(2)-R(1))
      TAU= TAU**(1.0/DEX)
      WRITE (5,4) DEX, TAU
   4  FORMAT(' N=',F15.12,/,' TAU=',G25.13)
      STOP
      END
```

VITA

The author, Paul A. Westbrook, was born in Cleveland, Ohio on January 18, 1958. He attended elementary schools in Cleveland and Oak Ridge, Tennessee, where he moved in 1966. Upon graduation from Oak Ridge High School in 1976, he enrolled at The University of Tennessee, Knoxville. After graduating with honors in 1981 with a B.S. degree in Chemical Engineering, he was awarded a research assistantship in the Polymer Engineering program at the same university. After receiving a Master's degree in August 1982, he continued his education at the doctoral level in the same department. On December 17, 1983 the author married Margaret Elizabeth Oswalt of Memphis, Tennessee. Upon graduation from The University of Tennessee in August 1985 with a Ph.D. in Materials Science, the author will become employed with Shell Development Company in Houston Texas.